2 Mic

NATIONAL AERONAUTICS AND SPACE ADMINISTRATION

Technical Report 32-1588

Analysis of Transient Heat Flow to Thick-Walled Plates and Cylinders

W. B. Powell

(NASA-CR-136226) ANALYSIS OF TRANSIENT HEAT FLOW TO THICK-WALLED PLATES AND CYLINDERS (Jet Propulsion Lab.) 73 p HC $5.75 CSCL 20M

N74-12576

Unclas

G3/33 23610

JET PROPULSION LABORATORY
CALIFORNIA INSTITUTE OF TECHNOLOGY
PASADENA, CALIFORNIA

December 1, 1973

NATIONAL AERONAUTICS AND SPACE ADMINISTRATION

Technical Report 32-1588

Analysis of Transient Heat Flow to Thick-Walled Plates and Cylinders

W. B. Powell

JET PROPULSION LABORATORY
CALIFORNIA INSTITUTE OF TECHNOLOGY
PASADENA, CALIFORNIA

December 1, 1973

I

Prepared Under Contract No. NAS 7-100
National Aeronautics and Space Administration

Preface

The work described in this report was performed by the Propulsion Division of the Jet Propulsion Laboratory.

PRECEDING PAGE BLANK NOT FILMED

Acknowledgment

The author wishes to acknowledge the contributions of Gregory J. Nunz and Charles H. Dodge in formulating and carrying out the computer solution of the curved-plate transient heat transfer problem, and of Robert W. Riebling for his perceptive and helpful suggestions during the writing of this report.

Contents

Tables

Contents (contd)

Tables (contd)

Contents (contd)

Tables (contd)

Figures

Contents (contd)

Figures (contd)

Contents (contd)

Figures (contd)

Contents (contd)

Figures (contd)

Users' Guide to Tables and Figures

Many of the tables and figures in this report have almost identical titles, which differ only in the values of the parameters (L/R_i, x/L, Fo, Bi) which define the conditions to which the tabulated or plotted values apply. To aid the reader in selecting the appropriate table or figure within these look-alike title groups, the following tabulations by groups and parameter variations are presented.

The table number groups are as follows:

Table title	Parameter value		Table number
	L/R_i	x/L	
Temperature ratio vs Fourier and Biot Numbers	0	0	2
	0	0.55	3
	0.214	0.55	4
	0.540	0.55	5
	0.893	0.55	6
	1.303	0.55	7
	0	1.00	8
	0.214	1.00	9
	0.540	1.00	10
	0.893	1.00	11
	1.303	1.00	12
Heat flux ratio vs Fourier and Biot Numbers	0	0	13
	0	0.55	14
	0.214	0.55	15
	0.540	0.55	16
	0.893	0.55	17
	1.303	0.55	18
	0	1.00	19
Rate of temperature rise vs Fourier and Biot Numbers	0	0	20
	0	0.55	21
	0	1.00	22
Ratio of temperature rise to rate of temperature rise vs Fourier and Biot Numbers	0	0.55	23
	0.214	0.55	24
	0.540	0.55	25
	0.893	0.55	26
	1.303	0.55	27

The figure number groups are as follows:

Figure title	Parameter value		Figure number
	L/R_i	x/L	
Temperature ratio vs Fourier and Biot Numbers	0	0	3
	0	0.55	4
	0.214	0.55	5
	0.540	0.55	6
	0.893	0.55	7
	1.303	0.55	8
	0	1.00	9
	0.214	1.00	10
	0.540	1.00	11
	0.893	1.00	12
	1.303	1.00	
Heat flux ratio vs Fourier and Biot Numbers	0	0	14
	0	0.55	15
	0.214	0.55	16
	0.540	0.55	17
	0.893	0.55	18
	1.303	0.55	19
	0	0.57	20
	0	1.00	21
Ratio of temperature rise to rate of temperature rise vs Fourier and Biot Numbers	0	0	22
	0	0.55	23
	0.214	0.55	24
	0.540	0.55	25
	0.893	0.55	26
	1.303	0.55	27
	0	1.00	28

Figure title	Parameter value		Figure number
	Fo	x/L	
Crossplot of temperature ratio vs curvature ratio and Biot number	0.60	0.55	31
	0.80	0.55	32
	1.00	0.55	33
	1.20	0.55	34
	1.40	0.55	35
	0.60	1.00	36
	0.80	1.00	37
	1.00	1.00	38
	1.20	1.00	39
	1.40	1.00	40

Table title	Parameter value		Table number
	Fo	x/L	
Crossplot of ratio of temperature rise to rate of temperature rise vs curvature ratio and Biot number	0.60	0.55	41
	0.80	0.55	42
	1.00	0.55	43
	1.20	0.55	44
	1.40	0.55	45

Abstract

A methodology is described for the analysis of a transient temperature measurement made in a flat or curved plate subjected to convective heat transfer, such that the surface heat flux, the hot-gas temperature, and the gas heat transfer coefficient can be determined. It is shown that if the transient temperature measurement is made at a particular point located nearly midway in the thickness of the plate there is an important simplification in the data analysis process, in that the factor relating the surface heat flux to the measured rate of rise of temperature becomes invariant for a Fourier Number above 0.60 and for all values of the Biot Number. Parameters are derived, tabulated, and plotted which enable straightforward determination of the surface heat flux, the hot-gas temperature, and the gas heat transfer coefficient from the measured time, the interior temperature of the plate, the rate of rise of temperature, the plate thickness and curvature, and the mean thermal properties of the plate material at the test temperature. It is shown that OFHC copper is the preferred material for experimental determination of heat transfer parameters using the described methodology.

The design and method of fabricating and installing a "thermocouple plug" which enable measurement of the temperature at an internal position within a plate with a minimum of thermal disturbance are described.

The surface heat flux is determined with an uncertainty the same as the uncertainty in the measured rate of rise of temperature and in the mean physical properties of the material. The determination of the hot-gas temperature and the gas heat transfer coefficient involves an uncertainty which is several times the uncertainty of the experimental data.

Analysis of Transient Heat Flow to Thick-Walled Plates and Cylinders

I. Introduction

Many rocket motor and other heat transfer problems approximate the conditions of the classical analysis of transient heat flow to an infinite slab or cylinder.

The development of the analytical expression for the transient temperature distribution in an infinite slab due to the convective heat flux corresponding to a sudden change in the temperature of the surroundings is given by Kreith (Ref. 1) and other authors. In the nomenclature of this report, this expression is

$$\left[\frac{(T_x - T_g)}{(T_0 - T_g)}\right] = 2\sum_{n=1}^{\infty} \exp(-\delta_n^2 Fo) \frac{\sin \delta_n \cos \delta_n \left(\frac{x}{L}\right)}{(\delta_n + \sin \delta_n \cos \delta_n)} \tag{1}$$

where a plate of thickness L and uniform temperature T_0 is subjected suddenly at $t = 0$ to convective heat transfer on one surface ($x/L = 1$) from a fluid of temperature T_g having a boundary heat transfer coefficient h, as in Figs. 1 and 2, for a flat plate and a curved plate, respectively. The back side of the plate ($x/L = 0$) is assumed to be insulated. The physical properties of the plate material (ρ, c_p, k) are assumed constant over the range of temperatures encountered.

The parameter δ_n is a root of the transcendental equation

$$\cot \delta_n = \frac{\delta_n}{B_i} \qquad \text{(See Table 1)} \tag{2}$$

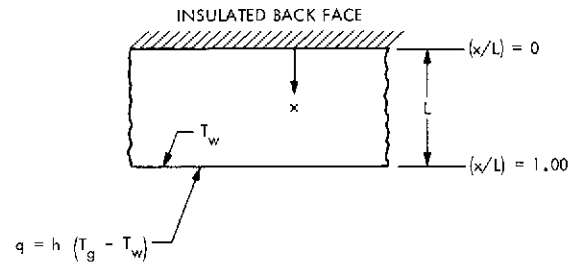

Fig. 1. Coordinate system for convective heat transfer to flat plate

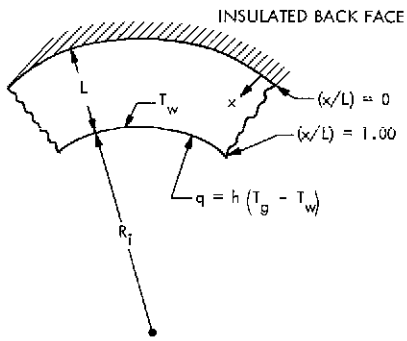

Fig. 2. Coordinate system for convective heat transfer to curved plate

Thus the dimensionless temperature distribution ratio is a function of the location within the plate, given by x/L, and of the two dimensionless parameters

$$Fo = \frac{\alpha t}{L^2} \tag{3}$$

and

$$Bi = \frac{hL}{k} \tag{4}$$

where

$$\alpha = \frac{k}{\rho c_p} \tag{5}$$

Inspection of Eqs. (1–5) shows that, with respect to most rocket motor problems, where the initial temperature and the physical properties are known, the temperature–time relationship within the plate is a function of two unknowns: the external gas temperature T_g and the gas heat transfer coefficient h. Therefore, in principle, two pieces of information, such as wall temperatures at two different times or places, or wall temperature and corresponding rate of change of temperature with time at a given time, are sufficient to enable determination of those two unknowns and thus permit complete solution of the problem, as is shown in subsequent sections of this report.

In this report, Eq. (1) is used as a basis to develop equations, charts, and methods which enable determination of the heat flux to the surface of a flat plate, the external gas convective heat transfer driving temperature, and the gas heat transfer coefficient from transient temperature measurements made on the surface of or within the heated plate. In the process of developing these methods, it was found that if the transient temperature measurement is made at a particular location within the flat plate ($x/L = 0.57$), the heat flux to the surface of the plate can be determined independently of the value of the Biot Number

$$Bi = \frac{hL}{k}$$

as long as the Fourier Number

$$Fo = \frac{\alpha t}{L^2}$$

is higher than approximately 0.60. This "direct" determination of the heat flux may be all that is required in the way of data analysis in many instances, and it also simplifies the procedure for determination of the gas driving temperature and heat transfer coefficient.

A digital computer solution of transient heat flow to a series of thick-walled cylinders enabled determination of dimensionless temperature-response factors corresponding to those obtained from the flat plate analysis. This enabled extension of the methodology developed herein to the solution of transient heat flow problems involving curved plates.

The charts and procedures presented here can be used in the analysis of rocket motor and other heat transfer problems which approximate the analytical assumption of abrupt initiation of convective heat transfer to a flat or curved plate that has constant physical properties and that is initially at a known uniform temperature. Separate appendices detail (1) the techniques developed for fabrication and installation of "thermocouple plugs" enabling relatively undisturbed measurement of the temperature at a specified point within the interior of a thick plate or cylindrical wall, (2) the problems involved in selecting metallic materials suitable for use in conducting transient heat transfer tests, and (3) the solution of a typical transient heat transfer problem.

II. Development of Equations for Transient Heat Flow in Flat Plates

The equations used in developing the heat transfer analysis procedures described herein are obtained by operating on Eq. (1) and by appropriately combining the resulting equations with themselves and with the

basic equations for convective and conductive heat flux. These latter equations are:

$$\text{(Convection)} \quad q = h\,(T_g - T_w) \tag{6}$$

$$\text{(Conduction)} \quad q = +k\left(\frac{dT_x}{dx}\right)_{(x/L)=1.00} \tag{7}$$

(note that x is negative in proceeding from the heated surface to the interior of the plate, using the coordinate system shown in Fig. 1).

A temperature ratio expressed in terms of the temperature rise from the initial temperature of the plate can be obtained by a transformation of Eq. (1):

$$\left[\frac{(T_x - T_0)}{(T_g - T_0)}\right] = \left\{1 - \left[\frac{(T_x - T_g)}{(T_0 - T_g)}\right]\right\} = \left[1 - 2\sum_{n=1}^{\infty} \exp\left(-\delta_n^2 Fo\right) \frac{\sin\delta_n \cos\delta_n \left(\frac{x}{L}\right)}{(\delta_n + \sin\delta_n \cos\delta_n)}\right] \tag{8}$$

Equation (8) can be differentiated with respect to x and t respectively to obtain

$$\left(\frac{dT_x}{dx}\right) = 2\,(T_g - T_0)\frac{1}{L}\sum_{n=1}^{\infty} \delta_n \exp\left(-\delta_n^2 Fo\right) \frac{\sin\delta_n \sin\delta_n \left(\frac{x}{L}\right)}{(\delta_n + \sin\delta_n \cos\delta_n)} \tag{9}$$

$$\left(\frac{dT_x}{dt}\right) = 2\,(T_g - T_0)\frac{\alpha}{L^2}\sum_{n=1}^{\infty} \delta_n^2 \exp\left(-\delta_n^2 Fo\right) \frac{\sin\delta_n \cos\delta_n \left(\frac{x}{L}\right)}{(\delta_n + \sin\delta_n \cos\delta_n)} \tag{10}$$

Equations (8) and (10) are analytical expressions for a temperature difference and a temperature derivative which can be measured with respect to time. The measurable quantities are seen to depend functionally on $(T_g - T_0)$, δ_n, α, Fo, and x/L. When the definitions of these quantities are considered, Eqs. (8) and (10) are seen to relate the measurable quantities T_x, dT_x/dt, and t to the primary variables T_g and h, and to the known constants T_0, ρ, c_p, k, x, and L.

It is of interest to see if Eqs. (6–10) can be manipulated and combined to obtain useful expressions in only one independent variable, or expressions which have particular properties that make them especially useful in the analysis and solution of transient heat transfer problems. Two such expressions are presented below.

First, Eqs. (7), (9), and (10) can be combined to produce an expression for a heat flux ratio, which turns out to be a function of only Fo, Bi, and the location x/L at which the rate of change of temperature with time is measured. Thus,

$$\frac{q}{\rho c_p L\left(\frac{dT_x}{dt}\right)} = \frac{\sum_{n=1}^{\infty} \delta_n \exp\left(-\delta_n^2 Fo\right) \frac{\sin^2\delta_n}{(\delta_n + \sin\delta_n \cos\delta_n)}}{\sum_{n=1}^{\infty} \delta_n^2 \exp\left(-\delta_n^2 Fo\right) \frac{\sin\delta_n \cos\delta_n \left(\frac{x}{L}\right)}{(\delta_n + \sin\delta_n \cos\delta_n)}} \tag{11}$$

This heat flux ratio eliminates the variable T_g, but only at the expense of introducing a new variable, the surface heat flux q. This ratio turns out to be useful because of a specific property, which will be described later.

Finally, as a last step in the formulation of the analytical expressions, Eqs. (8) and (10) can be combined to obtain the ratio of temperature rise to rate of temperature rise. Thus

$$\frac{2\alpha}{L^2}\frac{(T_x - T_0)}{\left(\frac{dT_x}{dt}\right)} = \frac{\left[1 - 2\sum_{n=1}^{\infty} \exp\left(-\delta_n^2 Fo\right) \frac{\left(\sin\delta_n \cos\delta_n \frac{x}{L}\right)}{(\delta_n + \sin\delta_n \cos\delta_n)}\right]}{\sum_{n=1}^{\infty} \delta_n^2 \exp\left(-\delta_n^2 Fo\right) \frac{\sin\delta_n \cos\delta_n \left(\frac{x}{L}\right)}{(\delta_n + \sin\delta_n \cos\delta_n)}} \tag{12}$$

This ratio does not contain the $(T_g - T_0)$ term which was present in the original expressions, and it does not introduce any new variables. Thus it attains the objective of formulating an expression which gives the ratio of two measurable quantities in terms of only one independent variable, the gas heat transfer coefficient h.

III. Discussion of Analytical Results

The dimensionless functions of Fo, Bi, and x/L given by Eqs. (8), (10), (11), and (12) have been calculated and are included in Tables 2–27 of this report.[1] The dimensionless functions given by Equations (8), (11), and (12) have been plotted, based on the above-mentioned tabulated data, and are included in Figs. 3–28 of this report.[1] In each case, the tables and graphs cover a range of Fourier Number and Biot Number and are presented for the heated surface of the plate, for the insulated back surface of the plate, and for a location near the middle of the plate thickness.

Figures 9 and 3 give the temperature rise as a fraction of $(T_g - T_0)$ at the heated surface and at the insulated back surface of a flat plate respectively. The temperature ratio is plotted as a function of Fo for several values of Bi. Figure 9 shows that the heated surface temperature increases with time and that the temperature rises more rapidly for plates made of material having a low thermal conductivity.[2] Figure 3 shows a similar behavior at the back surface of the plate, except that there is a time lag before any temperature change occurs at the back surface, and at any given time the temperature rise at the back surface is much less than the temperature rise at the heated surface. Figure 4 shows that the response at a position 55% of the thickness of the plate (measured inward from the back surface of the plate, see Fig. 1), is intermediate between the response at the front and back surfaces. (The reason for the choice of the 55% position will be explained in the next paragraphs.)

Figures 21 and 14 give the ratio of the heated surface heat flux to the rate of change of temperature at the heated surface and at the insulated back surface, respectively, of a flat plate. These curves show that, for a given Biot Number, the heat flux ratio does not vary with Fo for Fourier Numbers above $Fo \simeq 0.60$. Further, it is noted that when referenced to the rate of rise of the temperature at the heated surface, the values of the heat flux ratio are more than unity, and increase with increasing Bi, see Fig. 21.

When the heat flux ratio is referenced to the rate of rise of temperature at the back surface of the plate, the values of the ratio are less than unity, and decrease with increasing Bi, see Fig. 14. This "mirror image" behavior led to speculation that there might be a "neutral plane" position for temperature measurement such that the corresponding heat flux ratio would be independent of *both* Fo and Bi. Accordingly, the heat flux ratio was calculated for several assumed interior reference temperature measurement positions, and it was found that the heat flux ratio for a flat plate did indeed converge on unity for all Bi and for $Fo \geq 0.60$ when the rate of change of temperature was measured at a position 57% of the thickness inward from the back surface ($x/L = 0.57$). This is shown in Fig. 20.

For various practical reasons, it was decided to use the 55% position ($x/L = 0.55$) as a standard location for measuring temperatures in the interior of a heated wall.[3] Figure 19 shows the heat flux ratio referenced to $x/L = 0.55$; the heat flux ratio is very close to unity at low Bi, and has only decreased to 0.98 when $Bi = 5.0$.

The dimensionless ratio of the temperature rise to the rate of temperature rise for a flat plate, as given by Eq. (11), is plotted on Figs. 28, 23, and 22, corresponding to temperature measurements made at the heated surface, at $x/L = 0.55$, and at the insulated back surface, respectively. These plots are of interest because both of the coordinates are dimensionless ratios which can be evaluated from experimental data and known thermal properties. This makes possible the direct determination of the Biot Number by interpolation between the lines on the graphs once the appropriate temperature response data has been measured. And once the value of Bi corresponding to a given set of data has been determined, it is an easy task to evaluate the gas heat transfer coefficient h and then the effective gas recovery temperature T_g, and the surface heat flux.

IV. Transient Heat Flow in Thick-Walled Cylinders

The problem of transient heat flow in a thick-walled cylinder is physically similar to that of transient heat flow

[1]The tables and figures are presented in groups which include results from both flat plate and curved plate calculations. The flat plate results are identified as corresponding to $L/R_i = 0$. The means by which the curved plate data were calculated are described in a later section of this report.

[2]Note that Fo is a linear function of time, and that Bi is inversely proportional to thermal conductivity.

[3]The extension to curved plates of the flat plate analysis just described is given in a following section of this report. Since the mean location of the "neutral plane" for curved plates having a wide range of thickness ratios seemed to be near $x/L = 0.55$, it was decided to use this value for the flat plates too, so that the two analyses would be on a common basis.

in a flat plate, except that the mathematical equations are more complicated. Charts giving the temperature rise ratio at the surfaces of, and at several positions within, a thick curved wall are given in Refs. 1 and 2; however, the dimensionless parameters used in the analyses leading to these charts are different from those used in the JPL work described herein. The analyses and charts are presented only for the temperature rise ratios and do not extend to the heat flux ratio and the rate of temperature rise ratio developed in the JPL work. Thus the material in Refs. 1 and 2 is not directly applicable to an attempt to extend the methods developed in Sections I–III of this report for the analysis of transient heat flow in flat plates to the analysis of transient heat flow in thick-walled cylinders.

It was hypothesized, following the flat plate analysis, that similar results might be obtained for a thick-walled cylinder (representing a section of a combustion chamber) if the additional curvature parameter L/R_i could be accounted for in a convenient manner. In order to test this hypothesis, and because they had immediate need for specific results, Nunz and Dodge at JPL (Ref. 3) used a thermal network simulation digital computer program to compute the temperature distribution and heat flux within a series of thick-walled cylinders heated from the inside by a hot gas having a constant temperature and heat transfer coefficient. The nodal map consisted of many elements within a pie-shaped segment of the cylinder, insulated on both sides.

The thick-walled cylinder problem was solved for a series of curvature parameter values, $L/R_i = 0.214$, 0.540, 0.893, and 1.303, and the results were tabulated and plotted to show the same parameters and temperature response ratios that had been previously developed for the flat plate, which corresponds to the curvature parameter $L/R_i = 0$.

It was found that for the thick-walled cylinders there was again a unique location (at the approximate midwall position) where the heat flux was directly related to the rate of rise of temperature at the location, and independent of the Biot Number and the Fourier Number, except that this time the constant of proportionality was a function of the curvature parameter L/R_i (Figs. 29 and 30).

The location of the "neutral" position within the curved wall, where the Biot Number dependence of the heat transfer ratio disappeared, varied from $x/L = 0.57$ at $L/R_i = 0$ to $x/L = 0.53$ at $L/R_i = 1.30$. It was arbitrarily decided, as previously mentioned, to use $x/L = 0.55$ as a common "neutral position" for both flat and curved plates, thus effectively suppressing what could have been a complicating, though minor, extra variable in the solution of curved plate transient heat flow problems. The heat flux ratio at the $x/L = 0.55$ neutral position is shown as a function of plate curvature L/R_i, in Fig. 30; this figure also shows the minor variation with Bi caused by using an arbitrary fixed location for the neutral position. That the finite-difference, computer-model-derived thick-walled cylinder results are consistent with the analytically derived flat plate results is indicated by the fact that the heat flux ratio varies smoothly from the curved plate values to the flat plate value on Figs. 30–40.

The values of the temperature ratio, the heat flux ratio, and the temperature rise to rate of temperature rise ratio for the curved plates are given in Tables 2–27. The corresponding curves are shown in Figs. 3–28.

In order to assist the user working with transient heat flow problems involving curved plates having curvature ratios L/R_i other than those for which the present calculations were performed, a series of cross plots was made. Figures 31–40 give the temperature ratio

$$\frac{T_x - T_o}{T_g - T_o}$$

as a function of L/R_i and Bi for fixed values of Fo, with the temperature measurement position at $x/L = 0.55$ and 1.00.

The heat flux ratio for temperature measurement at $x/L = 0.55$ is given as a function of L/R_i for $Fo \geq 0.60$ and for Bi between 0.05 and 5.0 in Fig. 30.

The temperature rise to rate of temperature rise ratio for temperature measurement at $x/L = 0.55$ is given vs curvature ratio L/R_i for fixed values of Fo in Figs. 41–45.

V. Solution of Transient Heat Flow Problems

The analysis and curves developed thus far can be applied to practical heat transfer problems which approximate the conditions of the analysis. The two types of application which are possible are discussed separately below.

A. Prediction

If the hot gas temperature and the gas heat transfer coefficient are known, then the temperature of the plate and the heat transfer to its surface can be determined directly as a function of time. It is presumed that the plate is of such a material that over the temperature range of interest the thermal properties do not vary much from their mean values, that the plate is initially at a known uniform temperature, and that the imposition of convective heat flux from the hot gas is instantaneous.

As described previously, Eq. (8) gives the flat plate temperature ratio at a given time as a function of T_g and h, and of the known constants T_0, ρ, c_p, k, x, and L. Thus, with T_g and h specified, the temperature ratio at any desired time can be calculated. Graphically, the temperature ratio for the heated surface, $x/L = 1.00$, of the flat plate is read from Fig. 9, and the heated surface temperature is obtained from this ratio and the other known temperatures. The surface heat flux is then calculated using Eq. (6). For curved plates, the procedure is exactly the same, except that the curvature ratio must be accounted for by using Figs. 10–13 or Figs. 36–40.

The prediction procedure described above is useful in estimating the transient heat flux and wall temperature rise which will be experienced when a flat or curved plate of finite thickness is suddenly subjected to convective heating. A typical example is the operation of a rocket motor with an uncooled combustion chamber, primarily for the purpose of determining propellant performance characteristics. Here the methodology above can be used to estimate the allowable test duration (limited by the temperature rise of the interior surface of the combustion chamber) and to estimate the heat-loss correction that should be used in correlating the propellant performance measured under the test conditions with the ideal thermodynamic performance of the propellant.

The detailed steps to be followed in making a temperature and heat flux prediction are summarized for the reader's convenience in Procedure I (Section VI).

B. Data Analysis

A useful application of the analysis and charts developed herein is in the solution of the inverse problem: the determination from measured data (temperature vs time within a plate) of the heat transfer rate, the gas heat transfer coefficient, and the effective gas recovery temperature, for the case of instantaneous application of convective heat transfer to a plate at an initially known uniform temperature.

Many actual transient heat transfer systems from which data may be obtained closely approximate the conditions described above; typical is the operation of a rocket motor with an uncooled thrust chamber and/or nozzle wall.[4] In the actual operation of a rocket motor there is usually a short initial period, during which propellant flow and combustion chamber pressure are increasing, before fully developed convective heat transfer conditions are established. Thus it is sometimes desirable to "refine" the actual test data to establish an effective starting time for the fully developed convective heat transfer process. After this step, the refined temperature vs time data can be used to obtain the corresponding values of the heat flux, the gas temperature, and the heat transfer coefficient by a procedure which will be developed below.

The analytical solutions for transient heat flow in a flat plate, Eqs. (8) and (10), show that the temperature rise and the rate of temperature rise at a given time are functions of the primary variables T_g and h, and of the known constants of the system. The inverse problem is to solve for T_g and h as unknowns. By the rules of algebra, there must be as many independent equations in the unknowns as there are unknowns to be solved for; thus two independent equations in T_g and h must be written in order to solve for T_g and h. These equations are obtained, in principle, by substituting two measured values of temperature rise, and/or rate of temperature rise, at known times and locations into Eq. (8) and/or (10).

In this particular case, when Eq. (12) is formed as the ratio of Eqs. (8) and (10), the variable T_g is eliminated; thus Eq. (12) is a single equation using both of the pieces of experimental data, but involving only h as an unknown. The solution of the simultaneous equations, Eqs. (8) and (10), or of Eq. (12) alone, would be very difficult, so equivalent graphical procedures have been developed, based on calculated and plotted values of the temperature ratio, the heat flux ratio, and the temperature rise to rate of temperature rise ratio. These equivalent graphical procedures require as input the same two consistent sets of experimental data as would the inverse analytical solution. The graphical procedures are equally applicable to curved plate problems if the curvature ratio is accounted for as an additional parameter.

[4]The application of cylindrical curved plate analytical results to a conical nozzle is discussed in Appendix C.

From the nature of the experimental transient heat transfer problem, it is clear that the inverse solution will be defined best by data taken at a time sufficiently far into the test that the startup perturbation has been "lost" and the temperature rise is high enough to be accurately measured. Inspection of the analytical temperature response curves (Figs. 3–13) and the analytical heat flux ratio curves (Figs. 14–21) indicates that the data should be taken at a time corresponding to $Fo \geq 0.60$ and probably does not need to be taken at a time later than that corresponding to $Fo = 2.0$, providing that this latter time is long compared to the startup perturbation time. (In the latter part of Section VII, it is shown that it is desirable to take the data at Fo of 1.5 to 2.0 or more to obtain the best accuracy in determining heat transfer coefficient and gas temperature.)

While two temperatures measured at the same place at different times or two temperatures at different locations measured at the same time would satisfy the need for two consistent sets of data, it is clear that a temperature rise and the corresponding rate of temperature rise measured at a single point at a time corresponding to $0.60 \leq Fo \leq 2.0$ would be the optimum data set for solution of the inverse problem, both from the standpoint of data measurement considerations and because the criteria requiring a consistent data pair at the latest possible point in time is best satisfied.

For the reasons above, the discussion of data analysis procedures herein will be confined to methods of handling a data-set composed of temperature rise and rate of temperature rise evaluated at the same place and at the same instant in time.

As a practical matter, the temperature at the insulated back surface of a heated plate generally has too slow and too low a response to provide data acceptable for inverse analysis purposes. The temperature at the middle of the plate has adequate response and is quite suitable for analysis purposes. The temperature at the heated surface of the plate would also be satisfactory, except that it is difficult to measure accurately, both because the temperature may rise beyond the limit of calibration of the sensing element and, more important, because it is extremely difficult to insert a thermal sensor in such a manner as to measure a heated-surface temperature without disturbing the temperature field in the region in which the measurement is made. For these reasons, the midwall temperature measurement position appears to be optimum and is recommended for transient heat flow investigations using the methodology and procedures described in this report.[5]

In Section III, the simplifications to be realized from measuring the temperature at the midplate position ($x/L = 0.55$) were discussed; and as a result of this, figures were prepared to enable data analysis when the temperature data were obtained at this specific position.[6]

A procedure by which the measured data of temperature rise and rate of temperature rise at a given time can be used to determine the hot gas temperature and heat transfer coefficient, as well as the heat flux to the surface of the plate, is described in detail (see Procedure II). The charts needed to use this procedure have been prepared for the cases where the temperature measurement is made at the $x/L = 0.55$ position for flat or curved plates, and, additionally, for the cases where the temperature is measured at either surface of a flat plate. Values of the thermal properties of the wall material are needed to perform these calculations; values for copper, nickel, and mild steel are given in Appendix B.

The surface heat flux is calculated by using the measured rate of temperature rise in conjunction with the analytically derived value of the heat flux ratio (see Eq. (11) and Figs. 14–21 or Fig. 30), where it is to be noted that this ratio turns out to be essentially invariant with Fo and Bi and to depend only on the curvature ratio, when the temperature is measured at the $x/L = 0.55$ position within the plate.

The method of determining the hot-gas temperature and gas heat transfer coefficient is based on Eq. (12). It was shown previously in the formulation of Eq. (12) that the temperature rise to rate of temperature rise ratio is independent of T_g and depends only on the Fourier Number and on the Biot Number, which is directly related to the gas heat transfer coefficient. Experimental values of the temperature rise to rate of temperature rise ratio and the Fourier Number can be calculated from the known constants and the measured values of the temperature rise and rate of temperature rise at a particular

[5]A method of fabricating and inserting a "thermocouple plug" for measuring the transient temperature within a wall is described in Appendix A of this report.

[6]The methods described in this report can be used to obtain analytical solutions and corresponding charts for flat or curved plates where the temperature data are obtained at any designated position within the plate.

time. Then the Biot Number corresponding to these two experimentally measured parameters can be determined by referring to a set of curves representing analytical solutions of Eq. (12) (see Figs. 22–28 or the equivalent Figs. 41–45).

Once the Biot Number has been determined in this manner, the gas heat transfer coefficient is computed from Eq. (4), and the gas temperature and the temperature of the heated surface of the plate are found by reference to plotted solutions of Eq. (8) for the temperature ratio (see Figs. 3–13 or the equivalent figure in Figs. 31–40). Finally, these results can be used to compute a surface heat flux, using Eq. (6), which should compare closely with the previously obtained heat-flux-ratio value of the heat flux.

The detailed steps to be followed in making the calculations above are summarized for the reader's convenience in Procedure II (Section VII).

VI. Procedure I: Prediction of Wall Temperature and Heat Flux, Given the Gas Temperature and Heat Transfer Coefficient

This procedure enables the prediction of wall temperature and surface heat flux as a function of time for suddenly initiated convective heat transfer, when the initial wall temperature, the thickness and curvature of the wall, the physical properties of the wall material, the hot gas temperature, and the gas heat transfer coefficient are known. The procedure is as follows:

(1) Calculate $Bi = hL/k$.

(2) Calculate corresponding values of time and $Fo = \alpha t/L^2$. When the problem involves a curved plate, it will generally be desirable to use the integer values of Fo ($Fo = 0.60, 0.80, 1.00, 1.20, 1.40$), for which the L/R_i crossplot curves have been prepared (see Figs. 30–45), and to calculate the corresponding times.

(3) Enter Figs. 9–13, or Figs. 36–40, for $x/L = 1.00$, with L/R_i, Fo, and Bi to read the hot-wall temperature ratio at several values of Fo, where

$$\left[\frac{(T_w - T_0)}{(T_g - T_0)}\right] \equiv \left[\frac{(T_x - T_0)}{(T_g - T_0)}\right]_{(x/L)=1.00}$$

(4) Calculate

$$T_w = \left\{(T_g - T_0)\left[\frac{(T_w - T_0)}{(T_g - T_0)}\right]_{\substack{\text{chart} \\ (x/L)=1.00}} + T_0\right\}$$

(5) Calculate the heat flux:

$$q = h\,(T_g - T_w)$$

VII. Procedure II: Direct Method of Analyzing Transient Wall Temperature Data to Determine Gas Temperature, Gas Heat Transfer Coefficient, and Surface Heat Flux for Convective Heat Transfer

This procedure can be used to determine gas temperature, gas heat transfer coefficient, and surface heat flux for convective heat transfer. The procedure requires that the temperature be measured within the heated plate at a position for which the requisite charts have been prepared; in this case at $x/L = 0.55$ for a curved plate and at $x/L = 0.00$, 0.55, or 1.00 for a flat plate.[7] The procedure is as follows:

(1) Prepare the data.

(a) Plot the measured T_x at $(x/L)_{\text{test}} \simeq 0.55$ as a function of time.

(b) Plot vs time some parameter which will serve as an indication of the state of development of the convective heat transfer process. In the case of a rocket motor, this could be the chamber pressure.

(c) Select an appropriate effective starting time for the fully developed convective heat transfer process, and a corresponding initial wall temperature.

(d) Select a time–space mean wall temperature and tabulate the corresponding properties (ρ, c_p, and k), which will be assumed constant for the data analysis.

(2) Select a time near the end of the test. Measure T_x and dT_x/dt from a curve faired through the plotted data. Compute $Fo = \alpha t/L^2$, where $\alpha = k/\rho c_p$ and t is measured from the effective starting time. The selected time must be such that $Fo \geq 0.60$.

[7]The calculation steps described here are specifically for temperature measurement at the $x/L = 0.55$ position within the wall. The special cases of a flat plate with temperature measurement at the hot wall, $x/L = 1.00$, or at the cold wall, $x/L = 0$, can be handled in a manner analogous to that shown.

(3) Calculate the heat flux directly from the measured rate of temperature rise and the heat flux ratio (read from Fig. 30 for the curvature ratio corresponding to the test conditions when T_x is measured at $x/L = 0.55$; Bi is a minor variable on Fig. 30). Thus

$$q = \rho c_p L \left(\frac{dT_x}{dt}\right)_{\text{test}} \left[\frac{q}{\rho c_p L \left(\frac{dT_x}{dt}\right)}\right]_{\substack{\text{chart,} \\ (x/L)=0.55,(L/R_i)}} \tag{13}$$

(4) Compute the dimensionless ratio

$$\left[\frac{2\alpha}{L^2}\frac{(T_x - T_0)}{\left(\frac{dT_x}{dt}\right)}\right]_{\text{test}} \tag{14}$$

Note: For a curved plate it is best to select the time to correspond to the highest integer value of Fo for which the analytical curves are crossplotted vs the curvature ratio and which falls within the test data.

(5) Enter the temperature rise to rate of temperature rise ratio curves for $x/L = 0.55$ (Figs. 23–27, or the equivalent Figs. 41–45), with L/R_i, Fo, and the value of

$$\left[\frac{2\alpha}{L^2}\frac{(T_x - T_0)}{\left(\frac{dT_x}{dt}\right)}\right]_{\text{test}}$$

and interpolate to find the value of Bi which corresponds to these input parameters.

(6) Enter the temperature ratio curves (Figs. 4–13, or the equivalent Figs. 31–40) with L/R_i, Fo, and the value of Bi determined above and read the temperature ratio corresponding to $x/L = 0.55$ and to $x/L = 1.00$ (the heated surface). Then calculate T_g and T_w from the following equations:

$$(T_g - T_0) = \frac{(T_x - T_0)_{\text{test, } (x/L)=0.55}}{\left[\frac{(T_x - T_0)}{(T_g - T_0)}\right]_{\text{chart, } (x/L)=0.55}} \tag{15}$$

$$T_g = [(T_g - T_0) + T_0] \tag{16}$$

$$(T_w - T_0) = (T_x - T_0)_{\substack{\text{test} \\ (x/L)=0.55}} \left\{\frac{\left[\frac{(T_x - T_0)}{(T_g - T_0)}\right]_{(x/L)=1.00}}{\left[\frac{(T_x - T_0)}{(T_g - T_0)}\right]_{(x/L)=0.55}}\right\}_{\text{chart}} \tag{17}$$

$$T_w = [(T_w - T_0) + T_0] \tag{18}$$

(7) Compute the heat transfer coefficient from the equation

$$h = \frac{Bi\, k}{L} \tag{19}$$

using the value of Bi obtained in Step 3.

(8) Compute the surface heat flux from Eq. (20), where the quantity in the curved brackets is a moderately weak inverse function of Bi. This value of heat flux should be reasonably close to the more accurate value obtained in Step 3:

$$q = h(T_g - T_w) = \frac{k}{L}(T_x - T_0)_{\substack{\text{test} \\ (x/L)=0.55}} \left\{Bi\left[\frac{1 - \left[\frac{(T_x - T_0)}{(T_g - T_0)}\right]_{(x/L)=1.00}}{\left[\frac{(T_x - T_0)}{(T_g - T_0)}\right]_{(x/L)=0.55}}\right]_{\text{chart}}\right\} \tag{20}$$

Uncertainties involved in the determination of heat flux, gas temperature, and gas heat transfer coefficient by the methods of Procedure II are discussed below.

Heat flux, as computed from Step 3 of Procedure II (Eq. 13), has the lowest uncertainty of any of the quantities determined. Equation (13) involves only the physical properties and dimensions of the plate material, the measured rate of temperature rise, and the analytically determined heat flux ratio as read from a prepared chart. Each of these quantities can be looked up or measured with an uncertainty of a few percent or less. (The heat flux ratio is invariant with Fo and is almost invariant with Bi.)

A potential source of indirect error arises if the wall thermocouple is not located at exactly the $x/L = 0.55$ position for which the heat flux ratio chart (Fig. 30) is prepared. However, examination of Tables 20–22 in the text shows that the percentage correction to the measured rate of temperature rise for a deviation from the desired $x/L = 0.55$ temperature measurement position is of the order of the dimensionless deviation from the $x/L = 0.55$ position and thus should be no more than 1 or 2% at most, and in a known direction: i.e., if $(x/L)_{test} < 0.55$, the measured rate of temperature rise should be increased, and vice versa.

Heat flux is also computed in Step 8 (Eq. 20) of Procedure II. Here the evaluation depends on the measured temperature rise and on a function of the Biot Number. The uncertainty in determining Bi will be discussed below, but for purposes of calculating heat flux, it is sufficient to note that the function of Bi involved changes value only in the order of $\mp 10\%$ for wide variations of Bi around a nominal value. Thus a reasonable estimate of Bi applied to Eq. (20) will yield a good approximation to the true heat flux, though the uncertainty of this value will exceed that of the heat flux calculated from Eq. (13).

The evaluation of heat flux is qualitatively equivalent to the evaluation of the product of the gas temperature and the gas heat transfer coefficient. It is the separation and individual evaluation of these two quantities which pose the greatest problem and involve the highest uncertainties in the data analysis procedure described here.

Determination of individual values of gas temperature and of the gas heat transfer coefficient starts with the determination of the Biot Number in Step 5 of Procedure II. Inspection of Tables 23–27 and Figs. 23–27, as well as of the crossplots of Figs. 41–45, shows that the inverse determination of Biot Number from the Fourier Number and the ratio of temperature rise to rate of temperature rise is highly sensitive to small changes in either of these latter two quantities. Some calculations of the percentage change in Bi corresponding to a percentage change in Fo at a fixed value of the ratio of temperature rise to rate of temperature rise, and of the percentage change in Bi corresponding to a percentage change in the ratio of temperature rise to rate of temperature rise at a fixed value of Fo, were made for the flat plate case over a range of values of Fo and Bi. The Biot Number uncertainty ratios so obtained are plotted on Figs. 46 and 47. Additional calculations, not shown on Figs. 46 and 47, indicate that for a curved plate with a curvature ratio of $L/R_i = 1.3$, the Biot Number uncertainty ratios are 50 to 60% higher than for a flat plate.

Examination of Figs. 46 and 47 indicates that, for best determination of the Biot Number, test conditions should be designed so that data are obtained in the region of $Fo \geq 1.0$ to as high as 2.0 or more if possible and with $Bi \geq 0.50$. Even in the region of $Fo = 2.0$ and $Bi = 1.0$, the percentage uncertainty in Bi will be several times the uncertainty of the experimental data.

The uncertainty of the Biot Number determination by the methodology described herein is in sharp contrast to the uncertainty of the heat flux determination. For values of Fourier Number above $Fo = 0.60$, the heat transfer ratio is invariant with Fo and nearly invariant with Bi (for the $x/L = 0.55$ temperature measurement position) and depends only on the plate curvature ratio. Thus the heat flux uncertainty is only the uncertainty in the measured rate of temperature rise and in the average values of the physical properties of the material.

As shown in Step 7 of Procedure II, the gas heat transfer coefficient is directly related to the Biot Number, and any uncertainty in Bi will be directly carried over as an uncertainty in the gas heat transfer coefficient. The uncertainty in the determination of the hot-gas temperature will be of approximately the same magnitude as that in the heat transfer coefficient and in the Biot Number.

Thus, while in principle the methodology developed here and summarized in Procedure II enables analysis of transient heat flux test data to obtain separate values for heat flux, gas temperature, and gas heat transfer coefficient, in practice the methodology leads principally to a unique means of accurately determining the heat flux, while the calculated separate values of gas temperature and gas heat transfer coefficient remain subject to an appreciable degree of uncertainty.

VIII. Conclusions

The methodology and charts presented here enable prediction of heat flux and surface temperature for convective heat transfer to a flat or curved plate, if the hot gas temperature and heat transfer coefficient are known.

The methodology and charts also enable experimental determination of the heat flux, the hot-gas temperature,

and the gas heat transfer coefficient, providing that the temperature at a position midway in the thickness of the plate can be measured as a function of time.

Because of the nature of the analytical solution to the convective heat transfer problem, the hot-gas temperature and the gas heat transfer coefficient determined from the midwall temperature measurement have an uncertainty several times that of the experimental data involved in their determination. However, the heat flux is determined with the same uncertainty as the experimental data.

Despite its limitations, the methodology is useful in that it provides a new technique for experimentally measuring convective heat flux and for obtaining a reasonable estimate of the corresponding hot gas temperature and heat transfer coefficient.

Definition of Symbols

Bi Biot Number $= hL/k$

c_p specific heat of plate material

Fo Fourier Number $= \alpha t/L^2$

h gas heat transfer coefficient

L thickness of flat or curved plate

q heat flux at heated surface of plate

R_i radius of curvature of inside surface of cylinder

T_0 uniform initial temperature of plate

T_g hot-gas recovery temperature

T_w temperature of heated surface of plate

T_x temperature at interior position x within the plate

x location of position within plate, measured inward from the outside (insulated) surface of plate (see Fig. 1)

α thermal diffusivity of plate material $= k/\rho c_p$

δ_n root of transcendental equation (see Table 1)

ρ density of plate material

$$\text{Temperature ratio} = \left[\frac{(T_x - T_0)}{(T_g - T_0)}\right]$$

$$\text{Heat flux ratio} = \left[\frac{q}{\rho c_p L\left(\frac{dT_x}{dt}\right)}\right]$$

Ratio of temperature rise to rate of temperature rise

$$= \left[\frac{\frac{2\alpha}{L^2}(T_x - T_0)}{\left(\frac{dT_x}{dt}\right)}\right]$$

References

1. Kreith, F., *Principles of Heat Transfer*, International Textbook Co., Scranton, Pennsylvania, Sept., 1959.
2. Thorne, C. J., and Morrin, H. C., *Temperature Tables—Part 2, One-Layer Cylindrical Shell, Internal Heating, One-Space Variable, Linear*, NOTS TP2511, NAVORD Report 5562, Part 2, U.S. Naval Weapons Center, China Lake, Calif., Mar. 15, 1960.
3. Dodge, C. H., Riebling, R. W., and Nunz, G. J., "Experimental Evolution of an Earth-Storable Bimodal Rocket Engine," Paper 72-1128, presented at the AIAA/SAE 8th Joint Propulsion Specialist Conference, New Orleans, Louisiana, Nov. 29, 1972, American Institute of Aeronautics and Astronautics, New York.

Table 1. Roots of transcendental equation cot $\delta_n = \delta_n/Bi$ for flat plate solution

Bi	δ_1	δ_2	δ_3	δ_4	δ_5	δ_6	δ_7	δ_8
.05	.22176	3.1574	6.2911	9.4301	12.5703	15.7111	18.8522	21.9934
.10	.31105	3.1731	6.2991	9.4354	12.5743	15.7143	18.8549	21.9957
.15	.37788	3.1886	6.3070	9.4407	12.5783	15.7175	18.8575	21.9980
.20	.43284	3.2039	6.3148	9.4459	12.5823	15.7207	18.8602	22.0002
.25	.48009	3.2191	6.3227	9.4512	12.5862	15.7239	18.8628	22.0025
.30	.52179	3.2341	6.3305	9.4565	12.5902	15.7270	18.8655	22.0048
.35	.55922	3.2989	6.3383	9.4618	12.5942	15.7302	18.8681	22.0071
.40	.59324	3.2636	6.3461	9.4670	12.5981	15.7334	18.8707	22.0093
.45	.62444	3.2780	6.3539	9.4722	12.6021	15.7366	18.8734	22.0116
.50	.65327	3.2923	6.3616	9.4775	12.6060	15.7397	18.8760	22.0139
.55	.68006	3.3064	6.3693	9.4827	12.6100	15.7429	18.8787	22.0161
.60	.70507	3.3204	6.3770	9.4879	12.6139	15.7460	18.8813	22.0184
.65	.72851	3.3341	6.3846	9.4931	12.6178	15.7492	18.8840	22.0207
.70	.75056	3.3477	6.3923	9.4983	12.6218	15.7524	18.8866	22.0229
.75	.77136	3.3611	6.3998	9.5035	12.6257	15.7555	18.8892	22.0252
.80	.79103	3.3744	6.4074	9.5087	12.6296	15.7587	18.8919	22.0275
.85	.80968	3.3874	6.4149	9.5139	12.6336	15.7618	18.8945	22.0297
.90	.82740	3.4003	6.4224	9.5190	12.6375	15.7650	18.8971	22.0320
.95	.84426	3.4131	6.4299	9.5242	12.6414	15.7681	18.8998	22.0342
1.00	.86033	3.4256	6.4373	9.5293	12.6453	15.7713	18.9024	22.0365
2.00	1.07687	3.6436	6.5783	9.6296	12.7223	15.8336	18.9547	22.0815
4.00	1.26459	3.9352	6.8140	9.8119	12.8678	15.9536	19.0565	22.1697
5.00	1.31384	4.03354	6.9096	9.8928	12.9352	16.0107	19.1055	22.2126

Table 2. Temperature ratio $(T_x - T_0)/(T_g - T_0)$ vs Fourier and Biot Numbers; $L/R_i = 0$; $x/L = 0$

Fo	Ratio for indicated Biot Number								
	$Bi =$ 0.05	$Bi =$ 0.1	$Bi =$ 0.2	$Bi =$ 0.3	$Bi =$ 0.5	$Bi =$ 0.7	$Bi =$ 1.0	$Bi =$ 2.0	$Bi =$ 5.0
.1	.00039	.00078	.00153	.00227	.00368	.00501	.00689	.01222	.02269
.2	.00303	.00600	.01172	.01719	.02740	.03674	.04936	.08211	.13512
.3	.00708	.01393	.02702	.03933	.06185	.08192	.10820	.17222	.26367
.6	.02115	.04126	.07862	.11256	.17175	.22144	.28232	.41241	.55976
.8	.03071	.05959	.11244	.15951	.23940	.30429	.38097	.53398	.68827
1.0	.04019	.07761	.14507	.20404	.30162	.37841	.46614	.63044	.77928
1.2	.04959	.09529	.17651	.24622	.35875	.44464	.53960	.70694	.84372
1.4	.05889	.11262	.20680	.28617	.41121	.50381	.60295	.76760	.88934
1.6	.06810	.12963	.23597	.32400	.45938	.55668	.65758	.81571	.92165
1.8	.07722	.14631	.26407	.35983	.50361	.60392	.70470	.85386	.94452
2.0	.08625	.16267	.29113	.39375	.54422	.64612	.74533	.88411	.96072

Table 3. Temperature ratio $(T_x - T_0)/(T_g - T_0)$ vs Fourier and Biot Numbers; $L/R_i = 0$; $x/L = 0.55$

Fo	Ratio for indicated Biot Number								
	Bi = 0.05	*Bi* = 0.1	*Bi* = 0.2	*Bi* = 0.3	*Bi* = 0.5	*Bi* = 0.7	*Bi* = 1.0	*Bi* = 2.0	*Bi* = 5.0
.1	.00365	.00722	.01417	.02084	.03344	.04513	.06113	.10398	.17745
.2	.00887	.01747	.03392	.04940	.07780	.10317	.13644	.21769	.33329
.3	.01387	.02722	.05242	.07581	.11779	.15432	.20081	.30770	.44416
.6	.02839	.05520	.10451	.14873	.22448	.28668	.36102	.51239	.66976
.8	.03790	.07331	.13746	.19387	.28795	.36271	.44897	.61335	.76618
1.0	.04732	.09107	.16918	.23659	.34621	.43062	.52480	.69339	.83444
1.2	.05665	.10849	.19974	.27705	.39970	.49129	.59018	.75686	.88278
1.4	.06588	.12558	.22917	.31536	.44881	.54550	.64657	.80719	.91700
1.6	.07502	.14234	.25752	.35165	.49390	.59392	.69520	.84710	.94123
1.8	.08407	.15877	.28482	.38601	.53531	.63719	.73714	.87875	.95839
2.0	.09304	.17490	.31113	.41855	.57332	.67585	.77331	.90385	.97054

Table 4. Temperature ratio $(T_x - T_0)/(T_g - T_0)$ vs Fourier and Biot Numbers; $L/R_i = 0.214$; $x/L = 0.55$

Fo	Ratio for indicated Biot Number								
	Bi = 0.05	*Bi* = 0.1	*Bi* = 0.2	*Bi* = 0.3	*Bi* = 0.5	*Bi* = 0.7	*Bi* = 1.0	*Bi* = 2.0	*Bi* = 5.0
.6	.026	.051	.095	.139	.209	.268	.338	.485	.643
.8	.034	.067	.125	.180	.267	.337	.420	.582	.739
1.0	.042	.084	.155	.218	.322	.401	.493	.662	.812
1.2	.051	.099	.192	.256	.373	.461	.558	.727	.862
1.4	.060	.115	.210	.291	.420	.513	.614	.779	.900
1.6	.070	.131	.237	.326	.463	.559	.662	.821	.927
1.8	.079	.148	.263	.358	.502	.604	.706	.857	.948
2.0	.087	.161	.290	.383	.539	.641	.745	.886	.962

Table 5. Temperature ratio $(T_x - T_0)/(T_g - T_0)$ vs Fourier and Biot Numbers; $L/R_i = 0.540$; $x/L = 0.55$

Fo	Ratio for indicated Biot Number								
	Bi = 0.05	*Bi* = 0.1	*Bi* = 0.2	*Bi* = 0.3	*Bi* = 0.5	*Bi* = 0.7	*Bi* = 1.0	*Bi* = 2.0	*Bi* = 5.0
.6	.023	.046	.086	.120	.185	.239	.303	.442	.598
.8	.030	.060	.112	.160	.239	.304	.380	.536	.695
1.0	.038	.073	.137	.194	.288	.362	.450	.615	.768
1.2	.045	.087	.162	.228	.336	.417	.510	.679	.825
1.4	.053	.100	.188	.260	.379	.466	.565	.734	.869
1.6	.060	.115	.210	.292	.419	.512	.613	.780	.901
1.8	.069	.129	.234	.321	.457	.555	.655	.817	.927
2.0	.076	.142	.256	.350	.494	.594	.694	.851	.945

Table 6. Temperature ratio $(T_x - T_0)/(T_g - T_0)$ vs Fourier and Biot Numbers; $L/R_i = 0.893$; $x/L = 0.55$

Fo	Ratio for indicated Biot Number								
	Bi = 0.05	Bi = 0.1	Bi = 0.2	Bi = 0.3	Bi = 0.5	Bi = 0.7	Bi = 1.0	Bi = 2.0	Bi = 5.0
.6	.021	.030	.077	.108	.169	.217	.276	.408	.563
.8	.028	.052	.100	.141	.217	.277	.348	.499	.662
1.0	.034	.066	.123	.175	.261	.332	.412	.575	.736
1.2	.040	.078	.146	.205	.304	.383	.471	.640	.794
1.4	.047	.090	.168	.235	.343	.428	.522	.696	.840
1.6	.053	.101	.190	.262	.382	.470	.570	.742	.876
1.8	.060	.114	.210	.290	.417	.512	.612	.782	.905
2.0	.066	.127	.231	.316	.452	.550	.652	.817	.925

Table 7. Temperature ratio $(T_x - T_0)/(T_g - T_0)$ vs Fourier and Biot Numbers; $L/R_i = 1.303$; $x/L = 0.55$

Fo	Ratio for indicated Biot Number								
	Bi = 0.05	Bi = 0.1	Bi = 0.2	Bi = 0.3	Bi = 0.5	Bi = 0.7	Bi = 1.0	Bi = 2.0	Bi = 5.0
.6	.019	.034	.068	.098	.148	.193	.250	.374	.527
.8	.023	.045	.089	.128	.190	.248	.313	.459	.6
1.0	.030	.057	.110	.157	.232	.297	.372	.533	.703
1.2	.035	.068	.130	.182	.272	.343	.429	.598	.762
1.4	.041	.078	.150	.210	.319	.387	.480	.653	.810
1.6	.047	.089	.169	.237	.344	.430	.526	.702	.848
1.8	.052	.100	.188	.261	.379	.468	.570	.742	.880
2.0	.060	.111	.206	.285	.411	.504	.608	.777	.907

Table 8. Temperature ratio $(T_x - T_0)/(T_g - T_0)$ vs Fourier and Biot Numbers; $L/R_i = 0$; $x/L = 1.00$

Fo	Ratio for indicated Biot Number								
	Bi = 0.05	Bi = 0.1	Bi = 0.2	Bi = 0.3	Bi = 0.5	Bi = 0.7	Bi = 1.0	Bi = 2.0	Bi = 5.0
.1	.01760	.03470	.06755	.09865	.15610	.20788	.27642	.44639	.69121
.2	.02477	.04858	.09354	.13520	.20985	.27459	.35661	.54236	.76847
.3	.03040	.05938	.11341	.16268	.24899	.32177	.41115	.60160	.81057
.6	.04507	.08718	.16344	.23046	.34205	.43040	.53173	.72132	.88810
.8	.05444	.10471	.19427	.27133	.39598	.49120	.59626	.77906	.92078
1.0	.06370	.12187	.22391	.30996	.44541	.54542	.65182	.82480	.94391
1.2	.07286	.13870	.25246	.34653	.49078	.59386	.69973	.86106	.96028
1.4	.08193	.15521	.27995	.38116	.53244	.63714	.74105	.88982	.97188
1.6	.09092	.17140	.30643	.41396	.57069	.67580	.77668	.91263	.98009
1.8	.09982	.18728	.33194	.44502	.60582	.71034	.80741	.93072	.98590
2.0	.10863	.20285	.35651	.47443	.63806	.74121	.83391	.94506	.99002

Table 9. Temperature ratio $(T_x - T_0)/(T_g - T_0)$ vs Fourier and Biot Numbers; $L/R_i = 0.214$; $x/L = 1.00$

Fo	Ratio for indicated Biot Number								
	Bi = 0.05	*Bi* = 0.1	*Bi* = 0.2	*Bi* = 0.3	*Bi* = 0.5	*Bi* = 0.7	*Bi* = 1.0	*Bi* = 2.0	*Bi* = 5.0
.6	.042	.081	.154	.214	.323	.410	.510	.705	.876
.8	.050	.098	.181	.255	.374	.466	.572	.757	.910
1.0	.059	.113	.210	.291	.421	.517	.627	.803	.933
1.2	.068	.130	.237	.325	.467	.565	.672	.842	.950
1.4	.075	.144	.262	.358	.505	.608	.714	.872	.964
1.6	.083	.159	.285	.389	.541	.647	.750	.897	.974
1.8	.091	.174	.308	.417	.575	.682	.781	.927	.981
2.0	.100	.189	.332	.440	.607	.711	.809	.934	.988

Table 10. Temperature ratio $(T_x - T_0)/(T_g - T_0)$ vs Fourier and Biot Numbers; $L/R_i = 0.540$; $x/L = 1.00$

Fo	Ratio for indicated Biot Number								
	Bi = 0.05	*Bi* = 0.1	*Bi* = 0.2	*Bi* = 0.3	*Bi* = 0.5	*Bi* = 0.7	*Bi* = 1.0	*Bi* = 2.0	*Bi* = 5.0
.6	.040	.075	.143	.202	.303	.387	.482	.673	.858
.8	.047	.089	.169	.236	.350	.439	.540	.728	.891
1.0	.053	.103	.192	.268	.392	.485	.590	.774	.918
1.2	.061	.117	.214	.300	.432	.529	.637	.813	.938
1.4	.068	.130	.238	.329	.467	.569	.677	.844	.954
1.6	.075	.143	.260	.358	.503	.605	.712	.870	.965
1.8	.082	.157	.282	.385	.535	.640	.744	.891	.973
2.0	.090	.170	.303	.412	.567	.673	.773	.911	.980

Table 11. Temperature ratio $(T_x - T_0)/(T_g - T_0)$ vs Fourier and Biot Numbers; $L/R_i = 0.893$; $x/L = 1.00$

Fo	Ratio for indicated Biot Number								
	Bi = 0.05	*Bi* = 0.1	*Bi* = 0.2	*Bi* = 0.3	*Bi* = 0.5	*Bi* = 0.7	*Bi* = 1.0	*Bi* = 2.0	*Bi* = 5.0
.6	.037	.070	.131	.187	.282	.361	.455	.644	.838
.8	.044	.082	.154	.217	.324	.410	.508	.700	.874
1.0	.050	.094	.177	.246	.362	.454	.556	.745	.902
1.2	.056	.106	.197	.273	.400	.495	.600	.783	.924
1.4	.061	.118	.218	.300	.434	.532	.640	.817	.941
1.6	.069	.130	.238	.327	.467	.569	.674	.845	.954
1.8	.075	.142	.258	.353	.498	.603	.706	.869	.965
2.0	.082	.154	.277	.377	.528	.634	.737	.890	.973

Table 12. Temperature ratio $(T_x - T_0)/(T_g - T_0)$ vs Fourier and Biot Numbers; $L/R_i = 1.303$; $x/L = 1.00$

Fo	Ratio for indicated Biot Number								
	Bi = 0.05	*Bi* = 0.1	*Bi* = 0.2	*Bi* = 0.3	*Bi* = 0.5	*Bi* = 0.7	*Bi* = 1.0	*Bi* = 2.0	*Bi* = 5.0
.6	.032	.064	.119	.172	.262	.335	.427	.617	.818
.8	.038	.074	.139	.199	.299	.380	.477	.668	.856
1.0	.043	.085	.160	.225	.334	.421	.524	.714	.885
1.2	.050	.095	.180	.250	.368	.459	.566	.752	.909
1.4	.056	.107	.199	.275	.400	.494	.604	.785	.928
1.6	.061	.117	.217	.299	.430	.527	.639	.814	.942
1.8	.068	.128	.233	.323	.460	.561	.670	.839	.953
2.0	.074	.139	.250	.345	.490	.592	.700	.864	.964

Table 13. Heat flux ratio $q/[\rho c_p L(dT_x/dt)]$ vs Fourier and Biot Numbers; $L/R_i = 0$; $x/L = 0$

Fo	Ratio for indicated Biot Number								
	Bi = 0.05	*Bi* = 0.1	*Bi* = 0.2	*Bi* = 0.3	*Bi* = 0.5	*Bi* = 0.7	*Bi* = 1.0	*Bi* = 2.0	*Bi* = 5.0
.1	3.37053	3.35259	3.29027	3.23913	3.13227	3.03505	2.90450	2.56361	2.01977
.2	1.13694	1.35776	1.33332	1.31081	1.26874	1.23104	1.18144	1.06000	.89044
.3	1.10522	1.09572	1.07712	1.05983	1.02821	1.00027	.96415	.87897	.76817
.6	.99704	.98902	.97383	.95971	.93430	.91217	.88396	.81915	.73653
.8	.99254	.98464	.96970	.95582	.93086	.90913	.88144	.81776	.73616
1.0	.99192	.98405	.96915	.95531	.93044	.90877	.88116	.81764	.73614
1.2	.99184	.98396	.96908	.95525	.93038	.90872	.88113	.81763	.73614
1.4	.99183	.98395	.96907	.95524	.93038	.90872	.88112	.81763	.73614
1.6	.99182	.98395	.96907	.95524	.93038	.90872	.88112	.81763	.73614
1.8	.99182	.98395	.96907	.95524	.93038	.90872	.88112	.81763	.73614
2.0	.99182	.98395	.96907	.95524	.93038	.90872	.88112	.81763	.73614

Table 14. Heat flux ratio $q/[\rho c_p L(dT_s/dt)]$ vs Fourier and Biot Numbers; $L/R_i = 0$; $x/L = 0.55$

Fo	Ratio for indicated Biot Number								
	Bi = 0.05	Bi = 0.1	Bi = 0.2	Bi = 0.3	Bi = 0.5	Bi = 0.7	Bi = 1.0	Bi = 2.0	Bi = 5.0
.1	.92317	.92026	.91450	.90896	.89864	.88906	.87593	.84125	.78600
.2	.95746	.95585	.95292	.95014	.94516	.94081	.93529	.92333	.91364
.3	.98308	.98208	.98027	.97860	.97572	.97333	.97052	.96551	.96414
.6	.99841	.99769	.99635	.99514	.99302	.99127	.98916	.98494	.98119
.8	.99913	.99842	.99708	.99586	.99374	.99196	.98981	.98544	.98140
1.0	.99923	.99851	.99718	.99596	.99383	.99204	.98988	.98548	.98141
1.2	.99924	.99853	.99719	.99597	.99384	.99205	.98989	.98548	.98141
1.4	.99925	.99853	.99719	.99597	.99384	.99205	.98989	.98548	.98141
1.6	.99925	.99853	.99719	.99597	.99384	.99205	.98989	.98548	.98141
1.8	.99925	.99853	.99719	.99597	.99384	.99205	.98989	.98548	.98141
2.0	.99925	.99853	.99719	.99597	.99384	.99205	.98989	.98548	.98141

Table 15. Heat flux ratio $q/[\rho c_p L(dT_s/dt)]$ vs Fourier and Biot Numbers; $L/R_i = 0.214$; $x/L = 0.55$

Fo	Ratio for indicated Biot Number								
	Bi = 0.05	Bi = 0.1	Bi = 0.2	Bi = 0.3	Bi = 0.5	Bi = 0.7	Bi = 1.0	Bi = 2.0	Bi = 5.0
.6	1.100	1.100	1.099	1.098	1.097	1.096	1.096	1.095	1.096
.8	1.101	1.100	1.100	1.099	1.098	1.097	1.096	1.095	1.096
1.0	1.101	1.100	1.100	1.099	1.098	1.097	1.096	1.095	1.096
1.2	1.101	1.100	1.100	1.099	1.098	1.097	1.096	1.095	1.096
1.4	1.101	1.100	1.100	1.099	1.098	1.097	1.096	1.095	1.096
1.6	1.101	1.100	1.100	1.099	1.098	1.097	1.096	1.095	1.096
1.8	1.101	1.100	1.100	1.099	1.098	1.097	1.096	1.095	1.096
2.0	1.101	1.100	1.100	1.099	1.098	1.097	1.096	1.095	1.096

Table 16. Heat flux ratio $q/[\rho c_p L(dT_s/dt)]$ vs Fourier and Biot Numbers; $L/R_i = 0.540$; $x/L = 0.55$

Fo	Ratio for indicated Biot Number								
	Bi = 0.05	Bi = 0.1	Bi = 0.2	Bi = 0.3	Bi = 0.5	Bi = 0.7	Bi = 1.0	Bi = 2.0	Bi = 5.0
.6	1.266	1.266	1.265	1.265	1.265	1.265	1.264	1.265	1.269
1.0	1.267	1.267	1.266	1.266	1.266	1.265	1.265	1.266	1.269
1.2	1.267	1.267	1.266	1.266	1.266	1.265	1.265	1.266	1.269
1.4	1.267	1.267	1.266	1.266	1.266	1.265	1.265	1.266	1.269
1.6	1.267	1.267	1.266	1.266	1.266	1.265	1.265	1.266	1.269
1.8	1.267	1.267	1.266	1.266	1.266	1.265	1.265	1.266	1.269
2.0	1.267	1.267	1.266	1.266	1.266	1.266	1.265	1.266	1.269

Table 17. Heat flux ratio $q/[\rho c_p L(dT_s/dt)]$ vs Fourier and Biot Numbers; $L/R_i = 0.893$; $x/L = 0.55$

Fo	Ratio for indicated Biot Number								
	Bi = 0.05	Bi = 0.1	Bi = 0.2	Bi = 0.3	Bi = 0.5	Bi = 0.7	Bi = 1.0	Bi = 2.0	Bi = 5.0
.6	1.444	1.444	1.445	1.446	1.447	1.448	1.450	1.455	1.467
.8	1.446	1.446	1.447	1.447	1.448	1.449	1.451	1.456	1.467
1.0	1.446	1.446	1.447	1.447	1.448	1.449	1.451	1.456	1.467
1.2	1.446	1.446	1.447	1.447	1.448	1.449	1.451	1.456	1.467
1.4	1.446	1.446	1.447	1.447	1.448	1.449	1.451	1.456	1.467
1.6	1.446	1.446	1.447	1.447	1.448	1.449	1.451	1.456	1.467
1.8	1.446	1.446	1.447	1.447	1.448	1.449	1.451	1.456	1.467
2.0	1.446	1.446	1.447	1.447	1.448	1.449	1.451	1.456	1.467

Table 18. Heat flux ratio $q/[\rho c_p L(dT_s/dt)]$ vs Fourier and Biot Numbers; $L/R_i = 1.303$; $x/L = 0.55$

Fo	Ratio for indicated Biot Number								
	Bi = 0.05	Bi = 0.1	Bi = 0.2	Bi = 0.3	Bi = 0.5	Bi = 0.7	Bi = 1.0	Bi = 2.0	Bi = 5.0
.6	1.652	1.652	1.653	1.655	1.656	1.657	1.659	1.666	1.679
.8	1.654	1.654	1.655	1.655	1.657	1.658	1.661	1.667	1.679
1.2	1.654	1.654	1.655	1.655	1.657	1.659	1.661	1.667	1.679
1.4	1.654	1.654	1.655	1.655	1.657	1.659	1.661	1.667	1.679
1.6	1.654	1.654	1.655	1.655	1.657	1.659	1.661	1.667	1.679
1.8	1.654	1.654	1.655	1.655	1.657	1.659	1.661	1.667	1.679
2.0	1.654	1.654	1.655	1.655	1.657	1.659	1.661	1.667	1.679

Table 19. Heat flux ratio $q/[\rho c_p L(dT_s/dt)]$ vs Fourier and Biot Numbers; $L/R_i = 0$; $x/L = 1.00$

Fo	Ratio for indicated Biot Number								
	Bi = 0.05	Bi = 0.1	Bi = 0.2	Bi = 0.3	Bi = 0.5	Bi = 0.7	Bi = 1.0	Bi = 2.0	Bi = 5.0
.1	.56662	.57188	.58374	.59538	.61947	.64413	.68219	.81770	1.28538
.2	.79349	.80435	.82711	.85004	.89728	.94595	1.02152	1.29272	2.21993
.3	.92082	.93531	.96504	.99516	1.05692	1.12041	1.21858	1.56582	2.69960
.6	1.01135	1.02812	1.06202	1.09632	1.16602	1.23703	1.34559	1.71999	2.89390
.8	1.01598	1.03281	1.06678	1.10114	1.17091	1.24193	1.35042	1.72422	2.89646
1.0	1.01662	1.03345	1.06742	1.10177	1.17152	1.24252	1.35096	1.72460	2.89660
1.2	1.01671	1.03354	1.06750	1.10185	1.17160	1.24259	1.35102	1.72463	2.89661
1.4	1.01672	1.03355	1.06751	1.10186	1.17161	1.24260	1.35103	1.72464	2.89661
1.6	1.01672	1.03355	1.06751	1.10186	1.17161	1.24260	1.35103	1.72464	2.89661
1.8	1.01672	1.03355	1.06751	1.10186	1.17161	1.24260	1.35103	1.72464	2.89661
2.0	1.01672	1.03355	1.06751	1.10186	1.17161	1.24260	1.35103	1.72464	2.89661

Table 20. Rate of temperature rise $(dT_x/dt)/[(2\alpha/L^2)(T_g - T_0)]$ vs Fourier and Biot Numbers; $L/R_i = 0$; $x/L = 0$

Fo	Ratio for indicated Biot Number								
	Bi = 0.05	*Bi* = 0.1	*Bi* = 0.2	*Bi* = 0.3	*Bi* = 0.5	*Bi* = 0.7	*Bi* = 1.0	*Bi* = 2.0	*Bi* = 5.0
.1	.00729	.01440	.02834	.04174	.06735	.09135	.12456	.21595	.38221
.2	.01780	.03504	.06798	.09896	.15570	.20624	.27229	.43173	.65005
.3	.02193	.04292	.08231	.11851	.18260	.23732	.30537	.45325	.61652
.6	.02394	.04615	.08590	.12028	.17605	.21856	.26487	.34020	.37982
.8	.02382	.04546	.08309	.11435	.16222	.19588	.22902	.27018	.26904
1.0	.02360	.04462	.08008	.10835	.14901	.17508	.19757	.21428	.19050
1.2	.02337	.04376	.07714	.10261	.13683	.15643	.17039	.16992	.13488
1.4	.02314	.04293	.07430	.09718	.12564	.13976	.14694	.13475	.09551
1.6	.02291	.04210	.07157	.09202	.11536	.12487	.12672	.10686	.06762
1.8	.02269	.04130	.06894	.08715	.10592	.11156	.10929	.08474	.04788
2.0	.02247	.04051	.06640	.08253	.09725	.09968	.09425	.06720	.03390

Table 21. Rate of temperature rise $(dT_x/dt)/[(2\alpha/L^2)(T_g - T_0)]$ vs Fourier and Biot Numbers; $L/R_i = 0$; $x/L = 0.55$

Fo	Ratio for indicated Biot Number								
	Bi = 0.05	*Bi* = 0.1	*Bi* = 0.2	*Bi* = 0.3	*Bi* = 0.5	*Bi* = 0.7	*Bi* = 1.0	*Bi* = 2.0	*Bi* = 5.0
.1	.02660	.05245	.10196	.14874	.23477	.31184	.41303	.65807	.98215
.2	.02546	.04977	.09512	.13653	.20900	.26987	.34395	.49564	.63354
.3	.02466	.04789	.09044	.12834	.19242	.24389	.30337	.41262	.49120
.6	.02391	.04575	.08396	.11600	.16564	.20112	.23670	.28294	.28512
.8	.02366	.04483	.08081	.10976	.15196	.17953	.20395	.22420	.20181
1.0	.02343	.04397	.07783	.10393	.13951	.16038	.17587	.17778	.14289
1.2	.02320	.04313	.07496	.09842	.12809	.14329	.15167	.14098	.10117
1.4	.02297	.04230	.07221	.09320	.11761	.12802	.13080	.11180	.07164
1.6	.02274	.04149	.06955	.08826	.10799	.11438	.11280	.08866	.05072
1.8	.02252	.04070	.06699	.08358	.09916	.10219	.09728	.07034	.03591
2.0	.02230	.03992	.06453	.07915	.09104	.09130	.08389	.05575	.02543

Table 22. Rate of temperature rise $(dT_x/dt/[2\alpha/L^2)(T_g - T_0)]$ vs Fourier and Biot Numbers; $L/R_i = 0$; $x/L = 1.00$

Fo	Ratio for indicated Biot Number								
	Bi = 0.05	Bi = 0.1	Bi = 0.2	Bi = 0.3	Bi = 0.5	Bi = 0.7	Bi = 1.0	Bi = 2.0	Bi = 5.0
.1	.04334	.08439	.15974	.22709	.34057	.43041	.53033	.67703	.60058
.2	.03073	.05914	.10959	.15260	.22015	.26840	.31492	.35401	.26074
.3	.02632	.05028	.09187	.12621	.17764	.21187	.24161	.25443	.17543
.6	.02360	.04439	.07877	.10529	.14107	.16116	.17400	.16202	.09670
.8	.02327	.04334	.07553	.09926	.12896	.14339	.14949	.12814	.06838
1.0	.02302	.04248	.07271	.09394	.11835	.12805	.12886	.10159	.04841
1.2	.02280	.04167	.07003	.08896	.10866	.11440	.11113	.08056	.03428
1.4	.02257	.04087	.06745	.08424	.09977	.10221	.09583	.06388	.02427
1.6	.02235	.04008	.06497	.07978	.09161	.09132	.08265	.05066	.01719
1.8	.02213	.03932	.06258	.07555	.08411	.08159	.07128	.04017	.01217
2.0	.02192	.03856	.06028	.07155	.07723	.07290	.06147	.03186	.00862

Table 23. Ratio of temperature rise to rate of temperature rise $(2\alpha/L^2)[(T_x - T_0)/(dT_x/dt)]$ vs Fourier and Biot Numbers; $L/R_i = 0$; $x/L = 0.55$

Fo	Ratio for indicated Biot Number								
	Bi = 0.05	Bi = 0.1	Bi = 0.2	Bi = 0.3	Bi = 0.5	Bi = 0.7	Bi = 1.0	Bi = 2.0	Bi = 5.0
.1	.1372	.1377	.1390	.1401	.1424	.1447	.1480	.1580	.1807
.2	.3484	.3511	.3565	.3618	.3722	.3823	.3967	.4392	.5261
.3	.5627	.5684	.5796	.5907	.6121	.6327	.6620	.7457	.9042
.6	1.1874	1.2067	1.2448	1.2822	1.3552	1.4254	1.5252	1.8110	2.3491
.8	1.6021	1.6352	1.7010	1.7664	1.8950	2.0204	2.2014	2.7357	3.7965
1.0	2.0201	2.0712	2.1738	2.2765	2.4816	2.6850	2.9840	3.9002	5.8397
1.2	2.4421	2.5156	2.6644	2.8150	3.1204	3.4287	3.8913	5.3685	8.7253
1.4	2.8682	2.9867	3.1737	3.3837	3.8160	4.2610	4.9433	7.2200	12.801
1.6	3.2985	3.4306	3.7025	3.9841	4.5736	5.1926	6.1632	9.5549	18.556
1.8	3.7331	3.9015	4.2514	4.6182	5.3986	6.2352	7.5776	12.499	26.685
2.0	4.1720	4.3816	4.8214	5.2877	6.2972	7.4022	9.2178	16.212	38.166

Table 24. Ratio of temperature rise to rate of temperature rise $(2\alpha/L^2)[(T_x - T_0)/(dT_x/dt)]$ vs Fourier and Biot Numbers; $L/R_i = 0.214$; $x/L = 0.55$

Fo	Ratio for indicated Biot Number								
	Bi = 0.05	Bi = 0.1	Bi = 0.2	Bi = 0.3	Bi = 0.5	Bi = 0.7	Bi = 1.0	Bi = 2.0	Bi = 5.0
.6	1.21	1.24	1.26	1.28	1.36	1.42	1.52	1.78	2.27
.8	1.61	1.64	1.71	1.77	1.88	2.00	2.16	2.64	3.57
1.0	2.02	2.08	2.17	2.26	2.46	2.63	2.92	3.72	5.38
1.2	2.43	2.51	2.66	2.80	3.17	3.35	3.76	5.04	7.93
1.4	2.87	2.96	3.15	3.36	3.72	4.12	4.72	6.67	11.30
1.6	3.29	3.43	3.68	3.94	4.44	4.98	5.81	8.67	
1.8	3.72	3.88	4.21	4.55	5.23	5.93	7.08	11.17	
2.0	4.17	4.37	4.76	5.18	6.07	7.00	8.56	14.27	

Table 25. Ratio of temperature rise to rate of temperature rise $(2\alpha/L^2)[(T_x - T_0)/(dT_x/dt)]$ vs Fourier and Biot Numbers; $L/R_i = 0.540$; $x/L = 0.55$

Fo	Ratio for indicated Biot Number								
	Bi = 0.05	*Bi* = 0.1	*Bi* = 0.2	*Bi* = 0.3	*Bi* = 0.5	*Bi* = 0.7	*Bi* = 1.0	*Bi* = 2.0	*Bi* = 5.0
.6	1.21	1.22	1.26	1.28	1.34	1.41	1.48	1.70	2.12
.8	1.62	1.64	1.70	1.75	1.86	1.95	2.09	2.50	3.27
1.0	2.02	2.07	2.15	2.24	2.40	2.56	2.78	3.44	4.82
1.2	2.45	2.52	2.62	2.75	2.98	3.19	3.55	4.58	6.83
1.4	2.87	2.96	3.13	3.28	3.60	3.93	4.40	5.97	9.54
1.6	3.29	3.41	3.62	3.84	4.26	4.73	5.38	7.66	13.04
1.8	3.72	3.86	4.14	4.42	4.98	5.60	6.52	9.64	
2.0	4.15	4.31	4.67	5.02	5.74	6.52	7.74	12.07	

Table 26. Ratio of temperature rise to rate of temperature rise $(2\alpha/L^2)[(T_x - T_0)/(dT_x/dt)]$ vs Fourier and Biot Numbers; $L/R_i = 0.893$; $x/L = 0.55$

Fo	Ratio for indicated Biot Number								
	Bi = 0.05	*Bi* = 0.1	*Bi* = 0.2	*Bi* = 0.3	*Bi* = 0.5	*Bi* = 0.7	*Bi* = 1.0	*Bi* = 2.0	*Bi* = 5.0
.6	1.22	1.24	1.26	1.29	1.35	1.40	1.48	1.68	2.04
.8	1.63	1.66	1.70	1.75	1.84	1.93	2.06	2.42	3.10
1.0	2.05	2.09	2.15	2.23	2.38	2.50	2.70	3.29	4.45
1.2	2.47	2.52	2.61	2.71	2.94	3.12	3.43	4.32	6.19
1.4	2.90	2.97	3.10	3.22	3.52	3.79	4.23	5.54	8.38
1.6	3.31	3.42	3.58	3.76	4.15	4.54	5.12	6.96	11.32
1.8	3.74	3.87	4.10	4.32	4.81	5.31	6.10	8.65	
2.0	4.15	4.32	4.60	4.90	5.53	6.16	7.19	10.66	

Table 27. Ratio of temperature rise to rate of temperature rise $(2\alpha/L^2)[(T_x - T_0)/(dT_x/dt)]$ vs Fourier and Biot Numbers; $L/R_i = 1.303$; $x/L = 0.55$

Fo	Ratio for indicated Biot Number								
	Bi = 0.05	*Bi* = 0.1	*Bi* = 0.2	*Bi* = 0.3	*Bi* = 0.5	*Bi* = 0.7	*Bi* = 1.0	*Bi* = 2.0	*Bi* = 5.0
.6	1.22	1.24	1.27	1.29	1.31	1.38	1.45	1.62	1.96
.8	1.63	1.66	1.70	1.74	1.77	1.90	2.02	2.32	2.90
1.0	2.05	2.10	2.13	2.20	2.32	2.45	2.62	3.10	4.09
1.2	2.45	2.50	2.60	2.68	2.87	3.04	3.30	4.05	5.58
1.4	2.87	2.92	3.05	3.18	3.43	3.67	4.03	5.12	4.74
1.6	3.28	3.37	3.54	3.70	4.03	4.35	4.84	6.36	9.86
1.8	3.72	3.82	4.04	4.23	4.65	5.08	5.73	7.82	12.87
2.0	4.16	4.28	4.54	4.78	5.34	5.87	6.73	9.50	

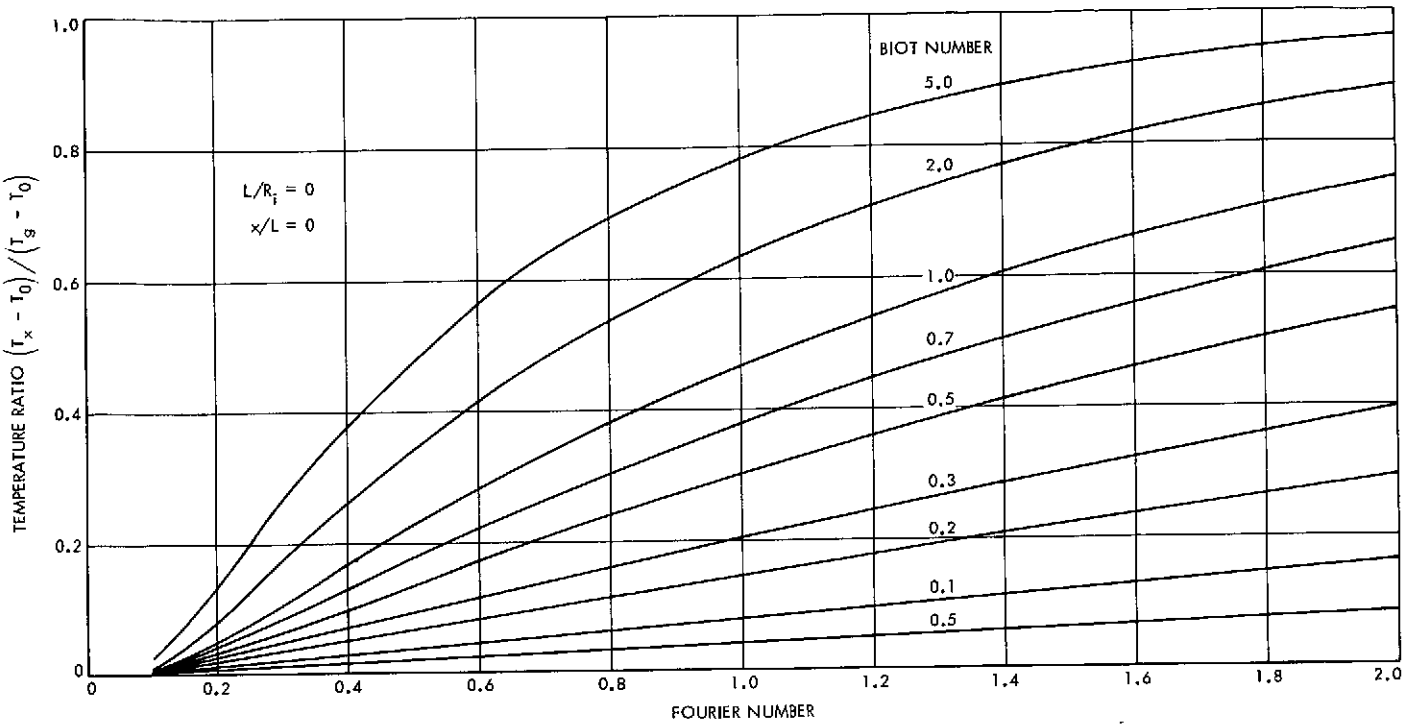

Fig. 3. Temperature ratio vs Fourier and Biot Numbers; $L/R_i = 0$; $x/L = 0$

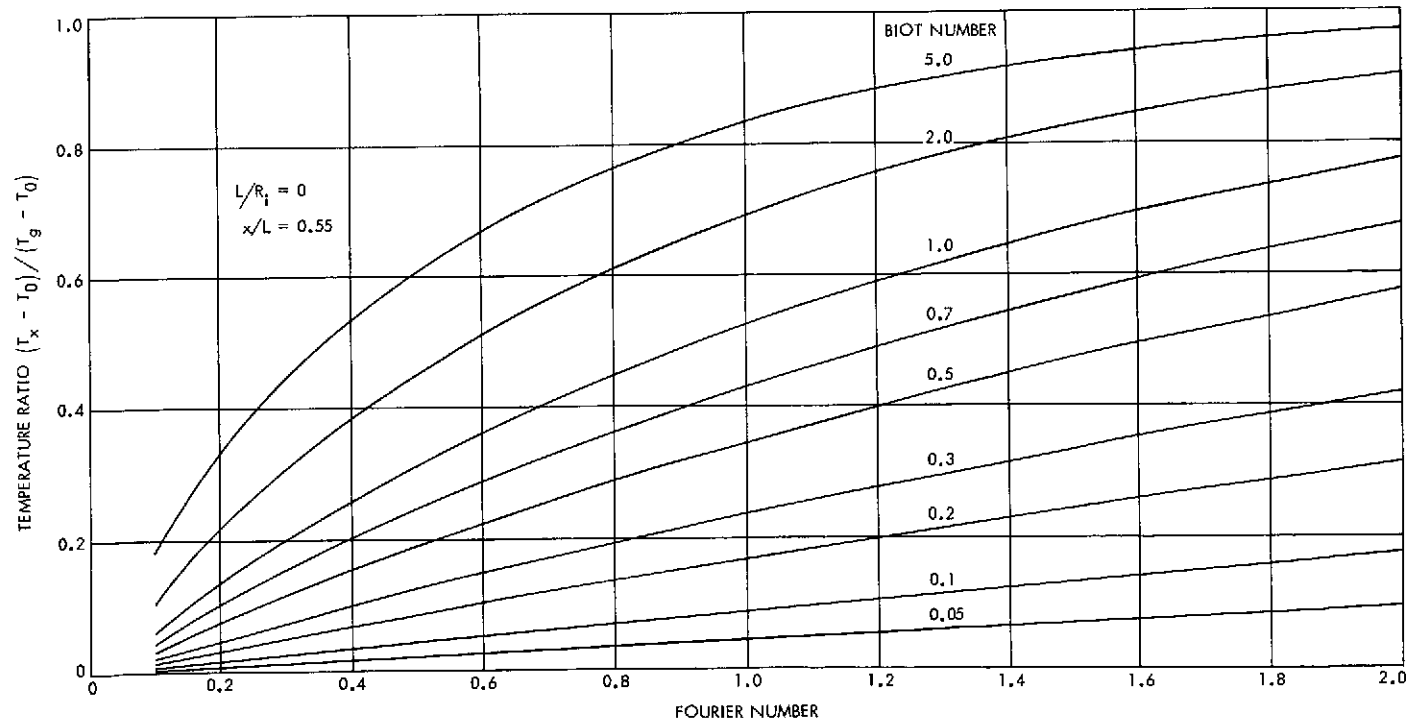

Fig. 4. Temperature ratio vs Fourier and Biot Numbers; $L/R_i = 0$; $x/L = 0.55$

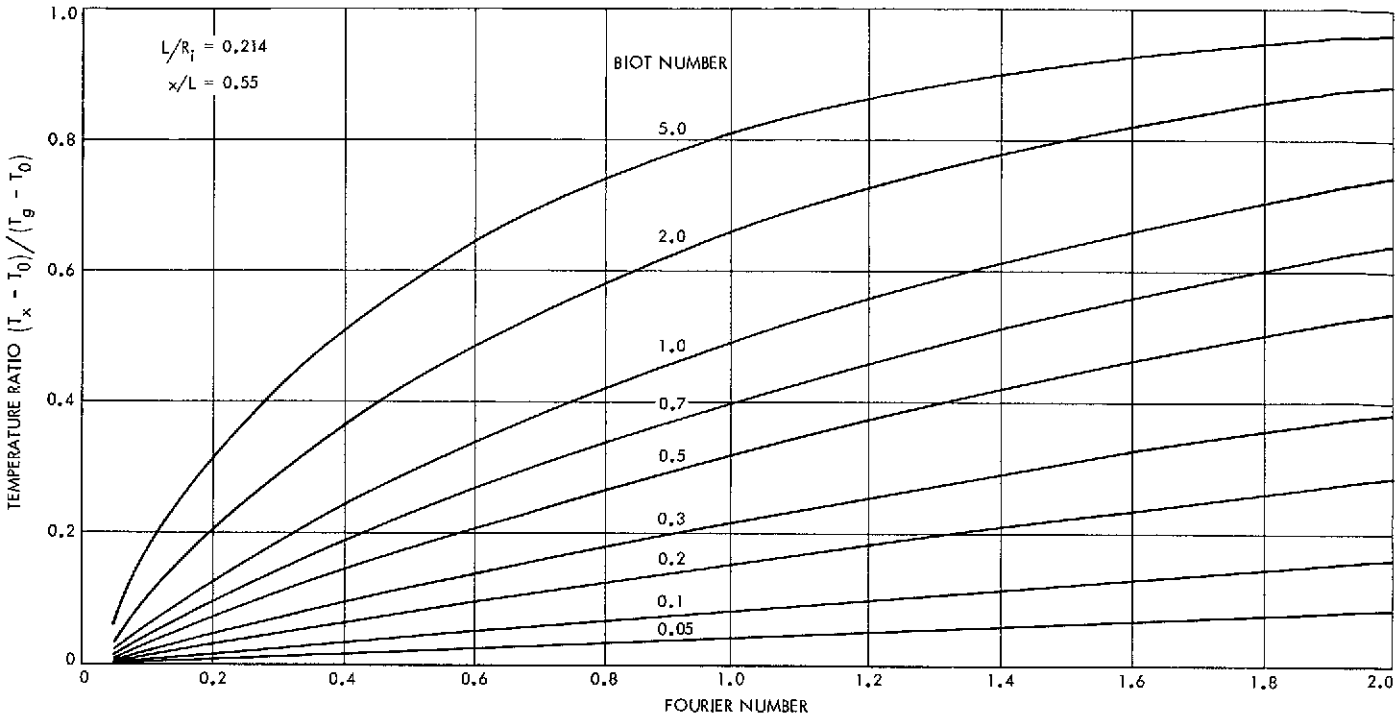

Fig. 5. Temperature ratio vs Fourier and Biot Numbers; $L/R_i = 0.214$; $x/L = 0.55$

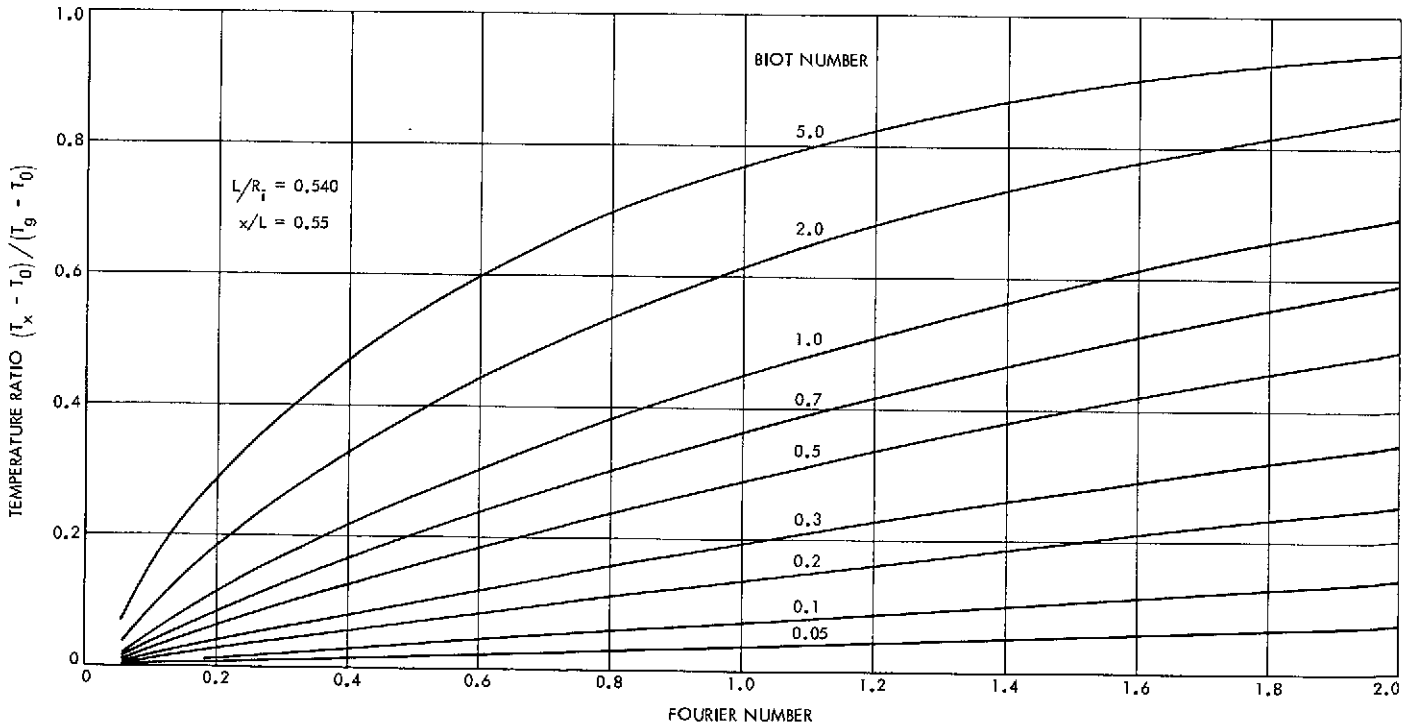

Fig. 6. Temperature ratio vs Fourier and Biot Numbers; $L/R_i = 0.540$; $x/L = 0.55$

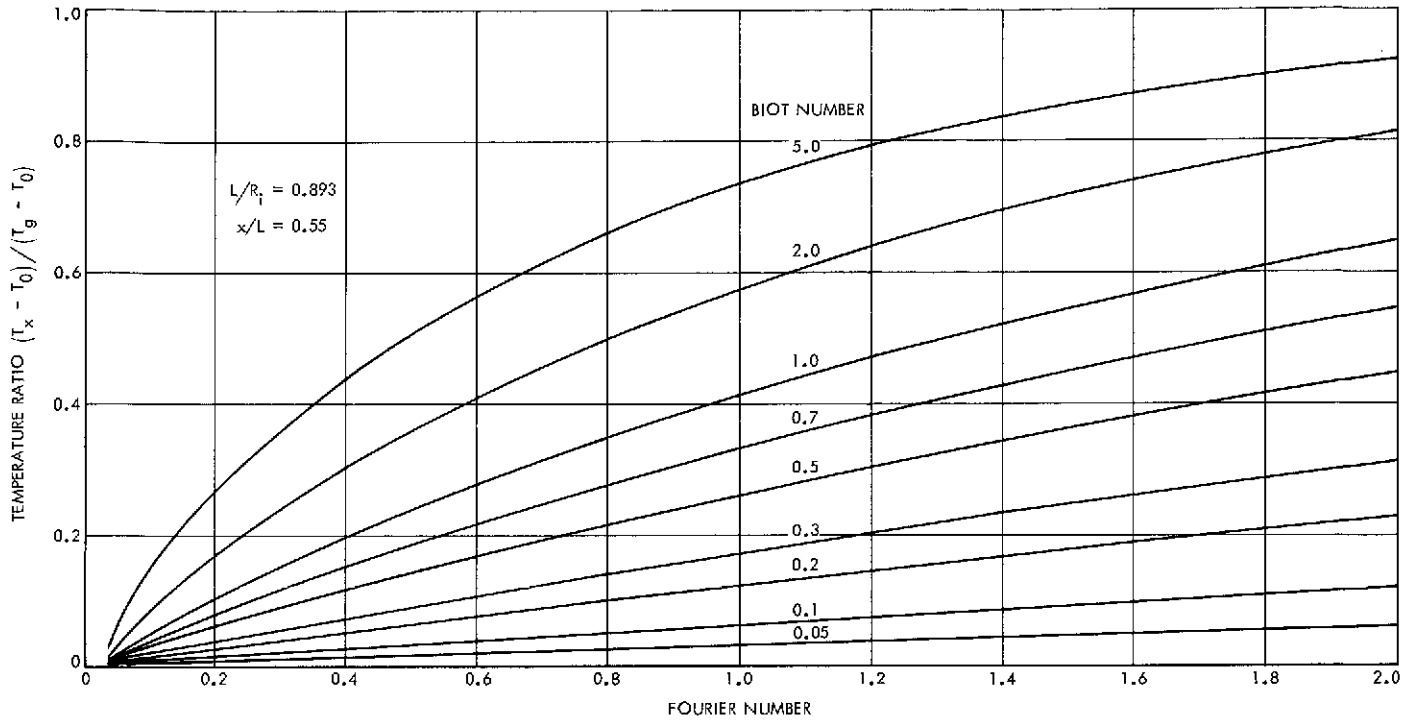

Fig. 7. Temperature ratio vs Fourier and Biot Numbers; L/R_i = 0.893; x/L = 0.55

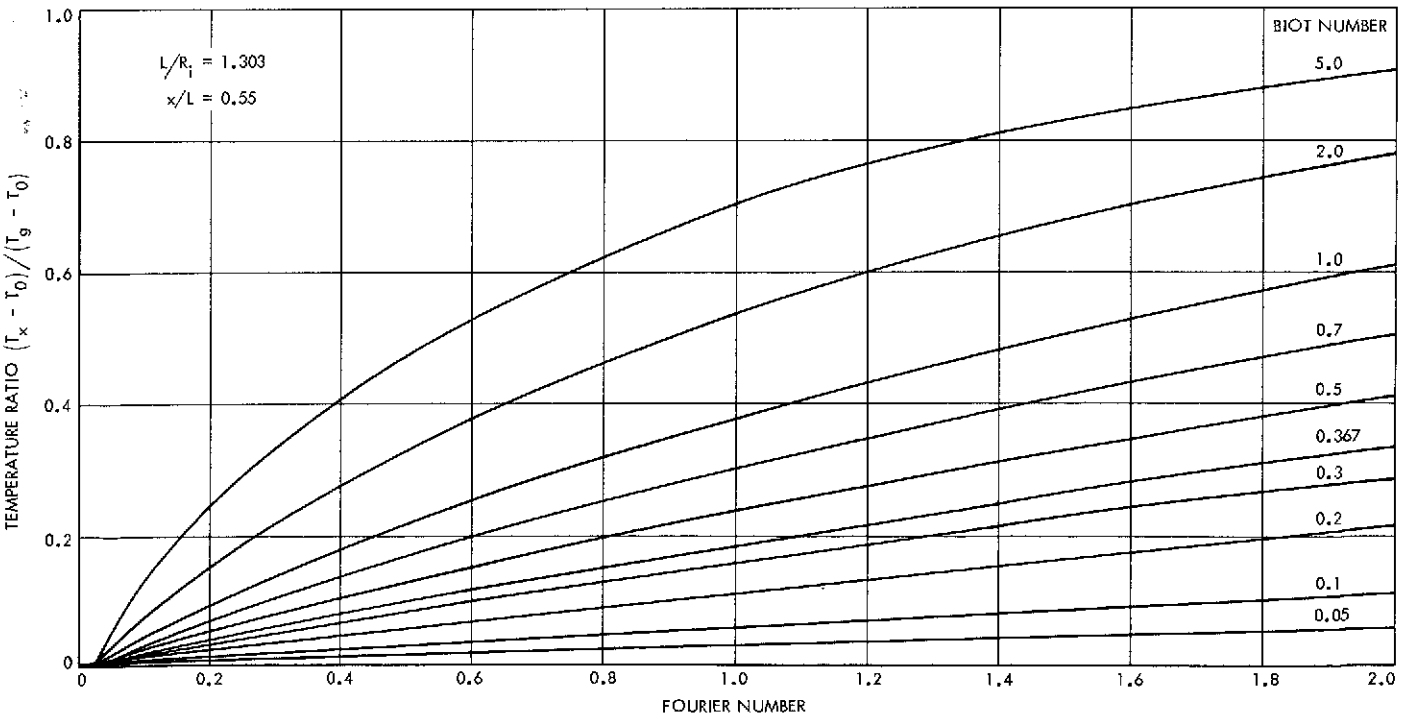

Fig. 8. Temperature ratio vs Fourier and Biot Numbers; L/R_i = 1.303; x/L = 0.55

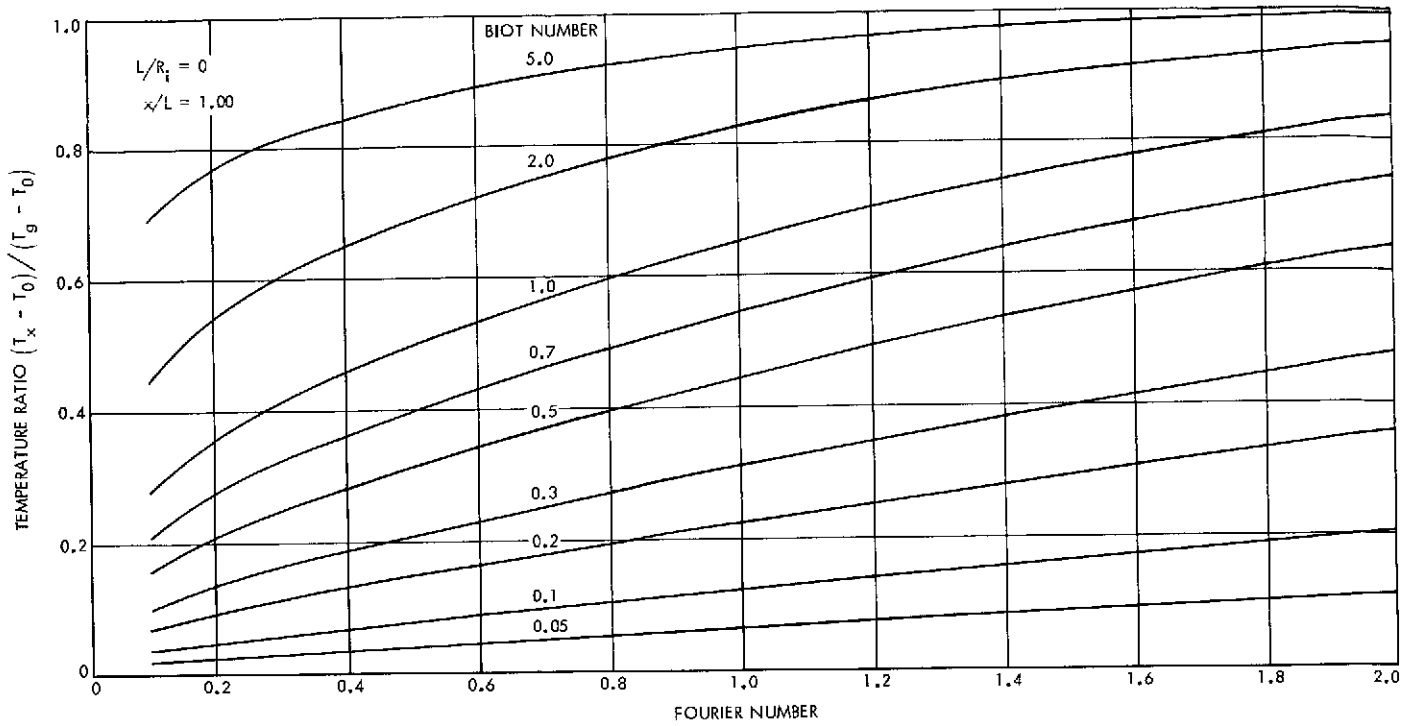

Fig. 9. Temperature ratio vs Fourier and Biot Numbers; $L/R_i = 0$; $x/L = 1.00$

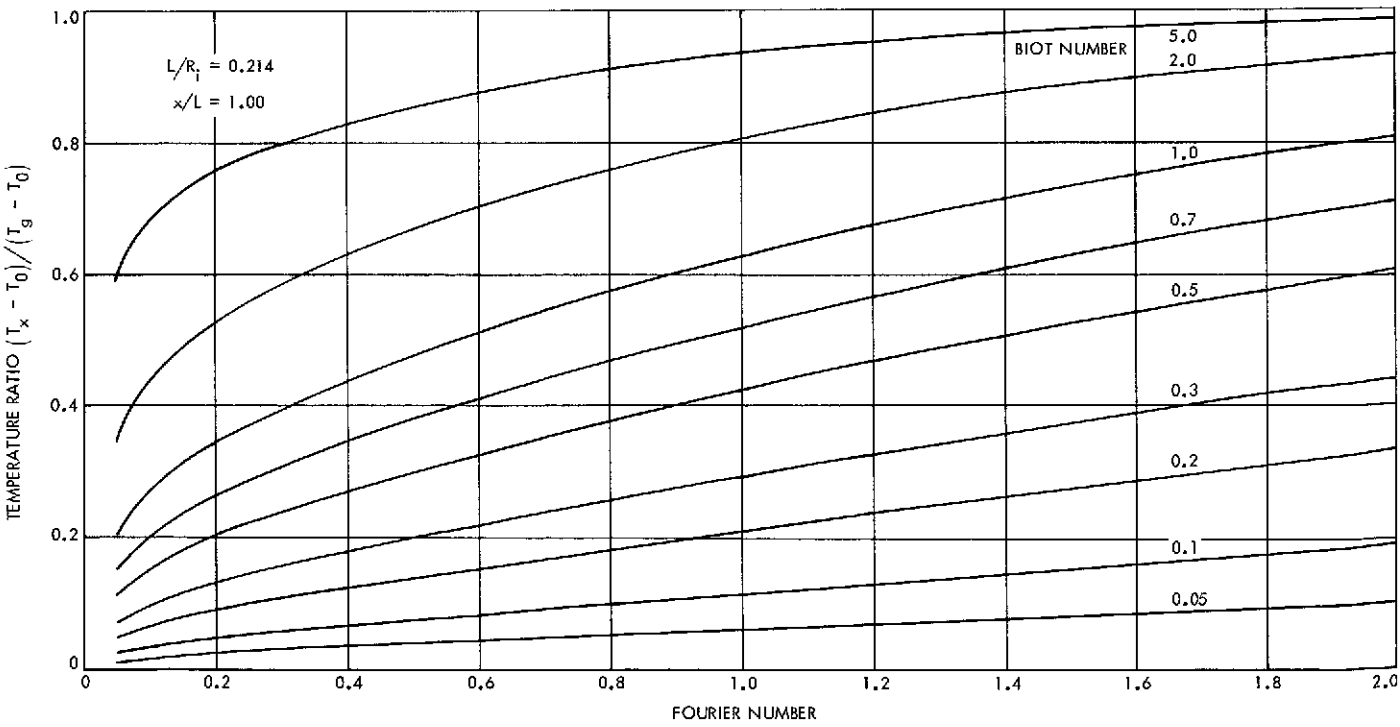

Fig. 10. Temperature ratio vs Fourier and Biot Numbers; $L/R_i = 0.214$; $x/L = 1.00$

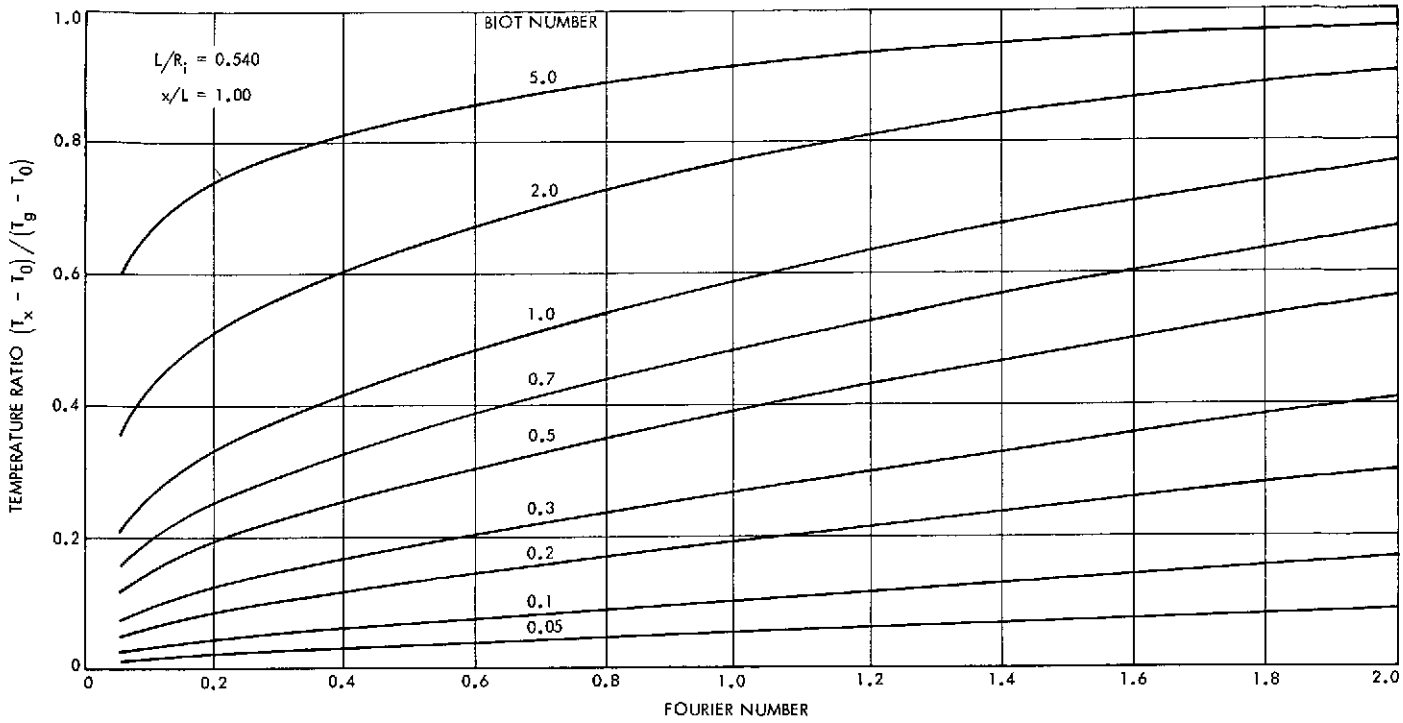

Fig. 11. Temperature ratio vs Fourier and Biot Numbers; L/R_i = 0.540; x/L = 1.00

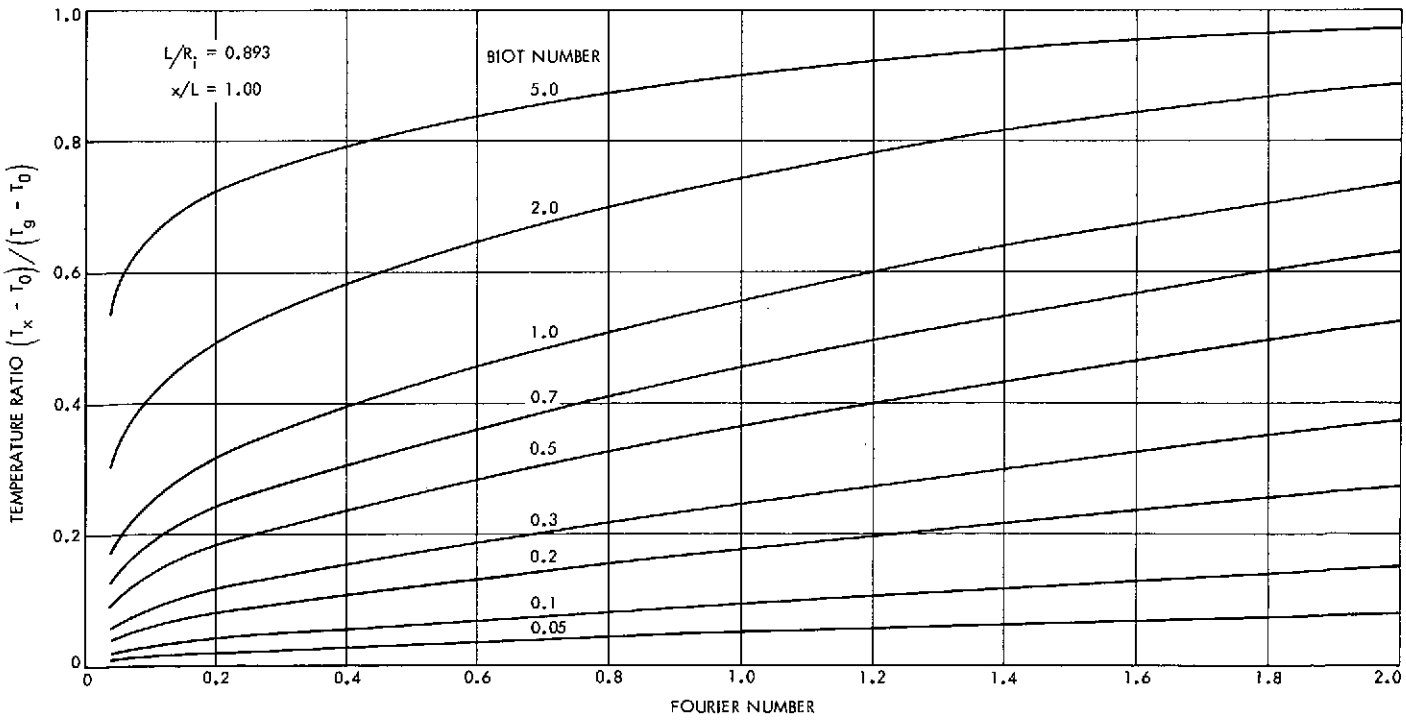

Fig. 12. Temperature ratio vs Fourier and Biot Numbers; L/R_i = 0.893; x/L = 1.00

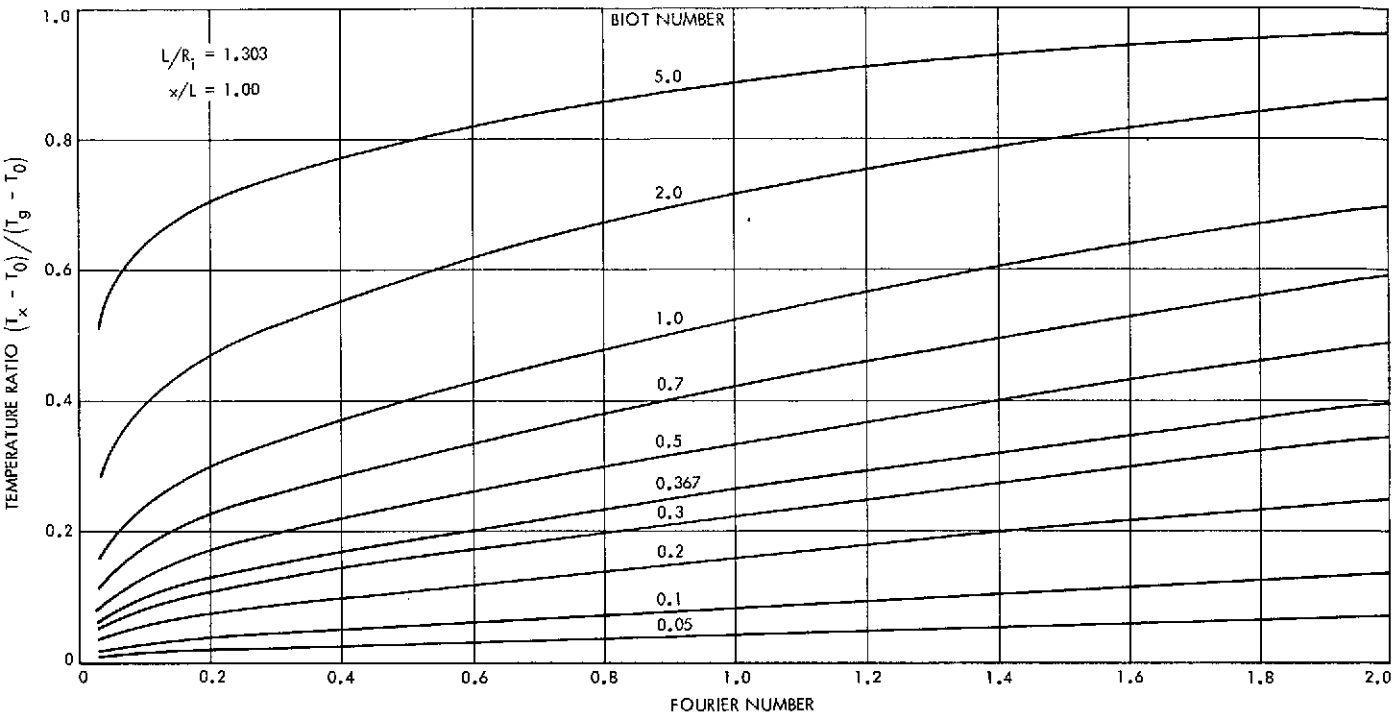

Fig. 13. Temperature ratio vs Fourier and Biot Numbers; $L/R_i = 1.303$; $x/L = 1.00$

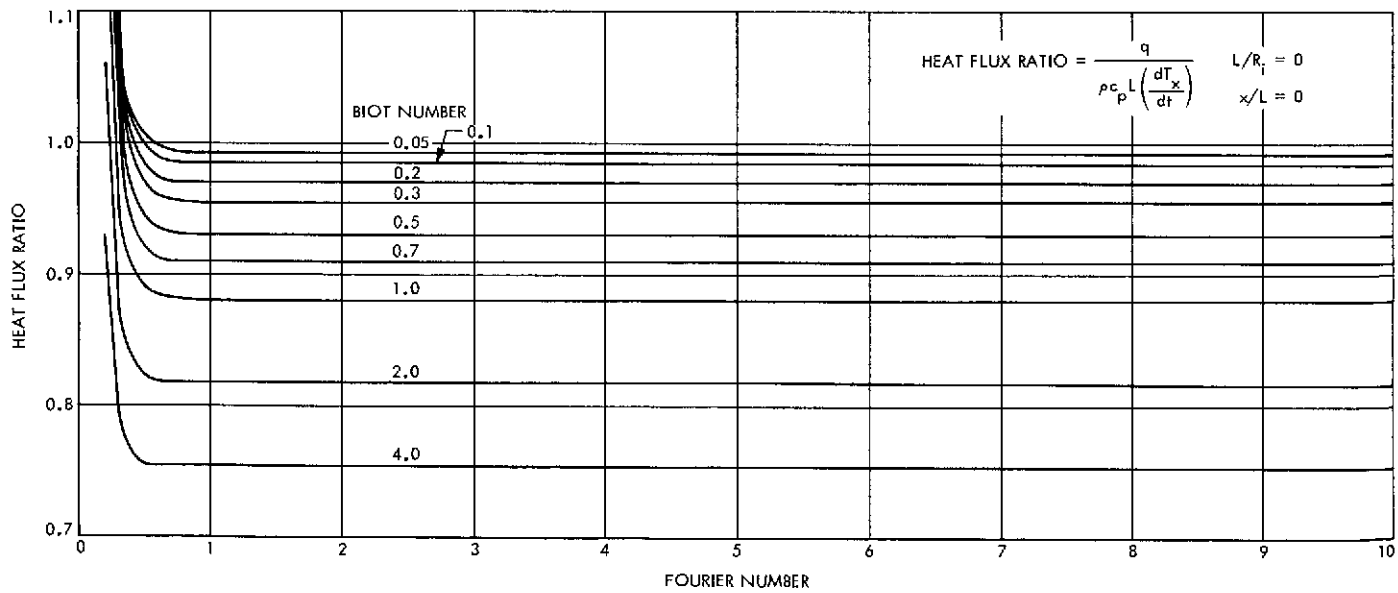

Fig. 14. Heat flux ratio vs Fourier and Biot Numbers; $L/R_i = 0$; $x/L = 0$

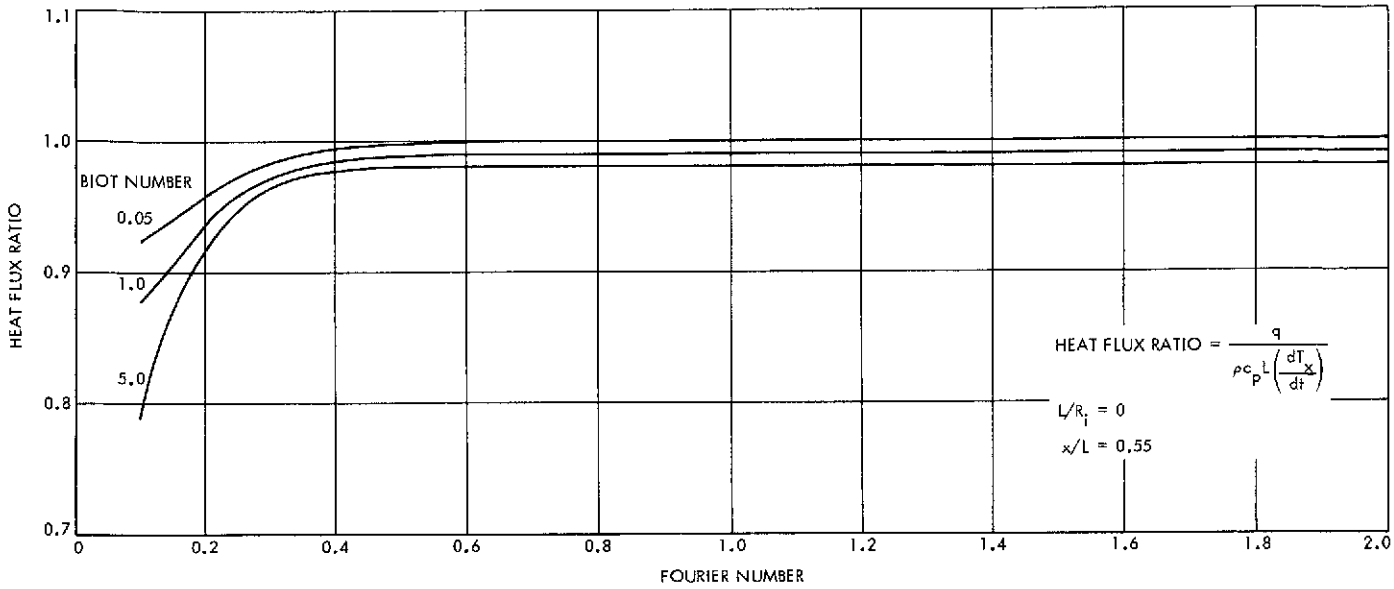

Fig. 15. Heat flux ratio vs Fourier and Biot Numbers; $L/R_i = 0$; $x/L = 0.55$

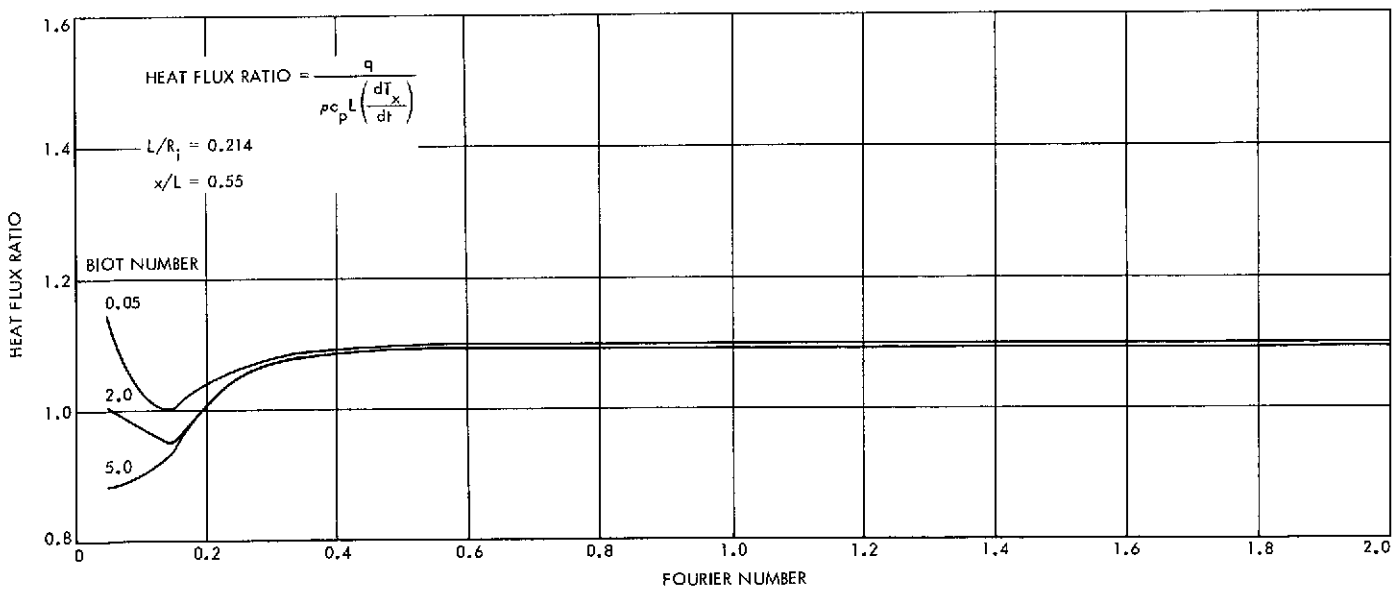

Fig. 16. Heat flux ratio vs Fourier and Biot Numbers; $L/R_i = 0.214$; $x/L = 0.55$

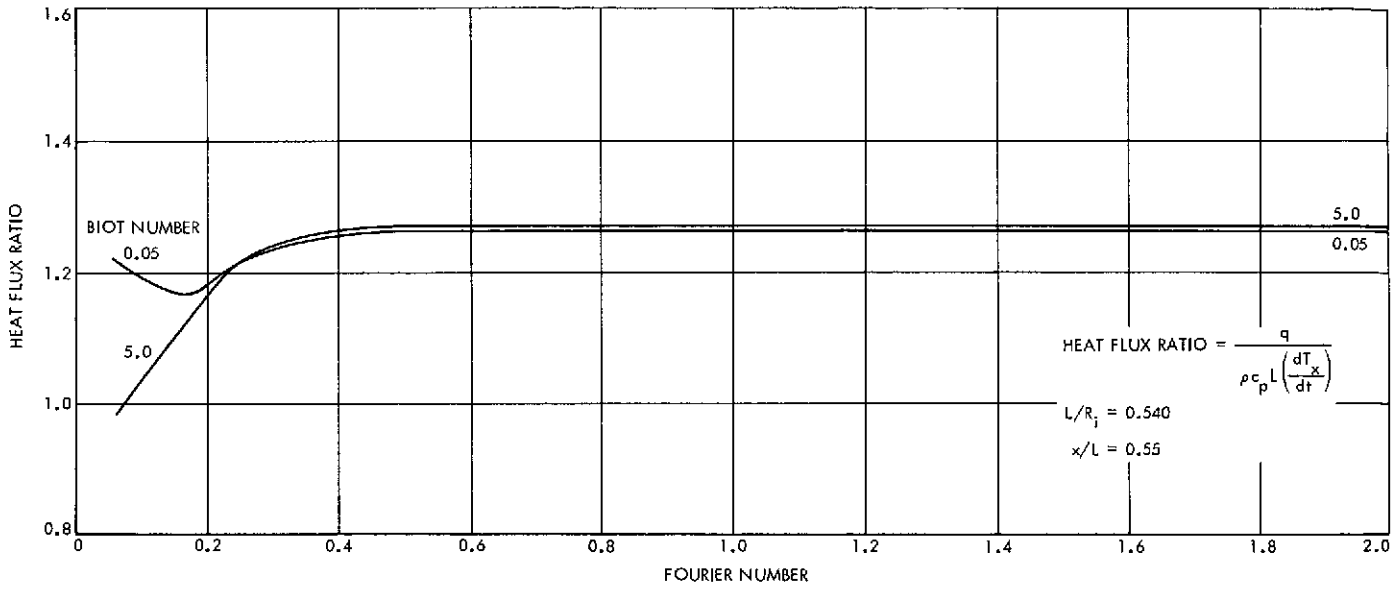

Fig. 17. Heat flux ratio vs Fourier and Biot Numbers; L/R_i = 0.540; x/L = 0.55

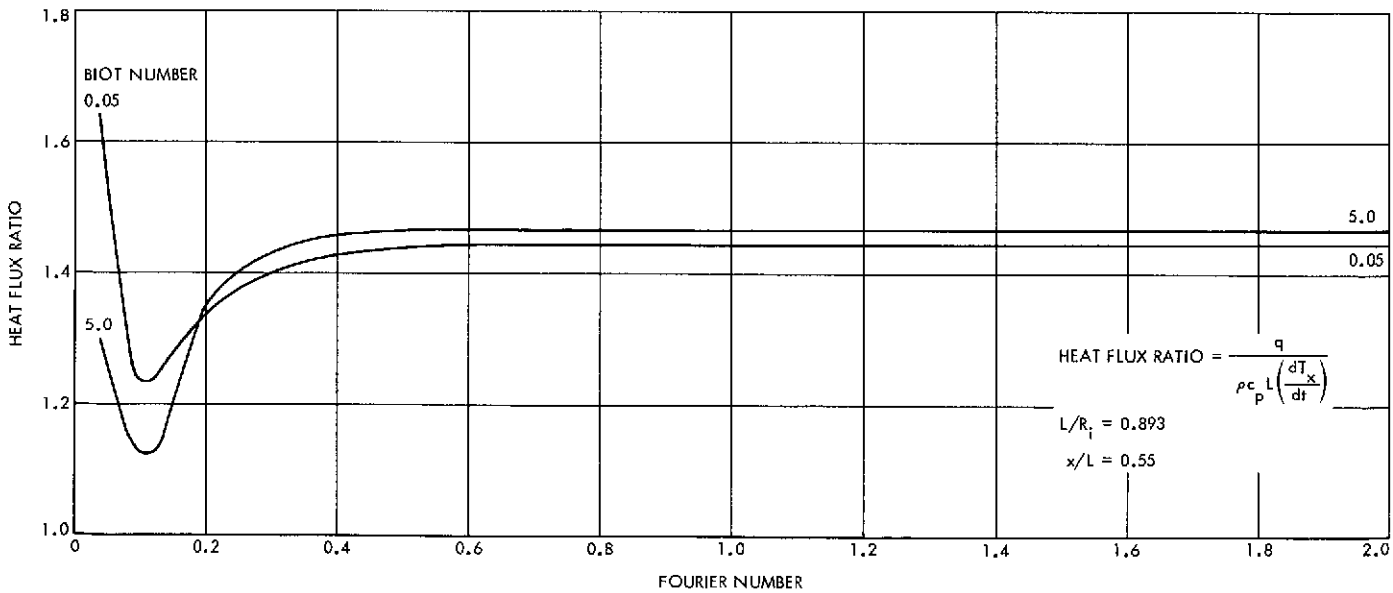

Fig. 18. Heat flux ratio vs Fourier and Biot Numbers; L/R_i = 0.893; x/L = 0.55

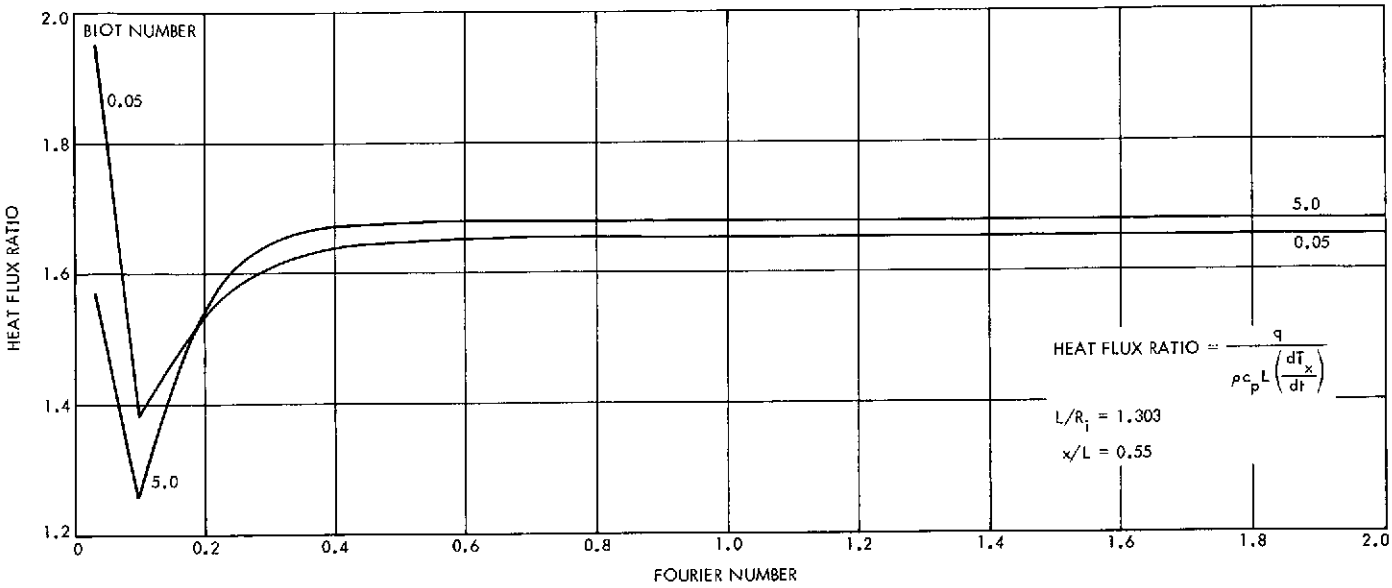

Fig. 19. Heat flux ratio vs Fourier and Biot Numbers; L/R_i = 1.303; x/L = 0.55

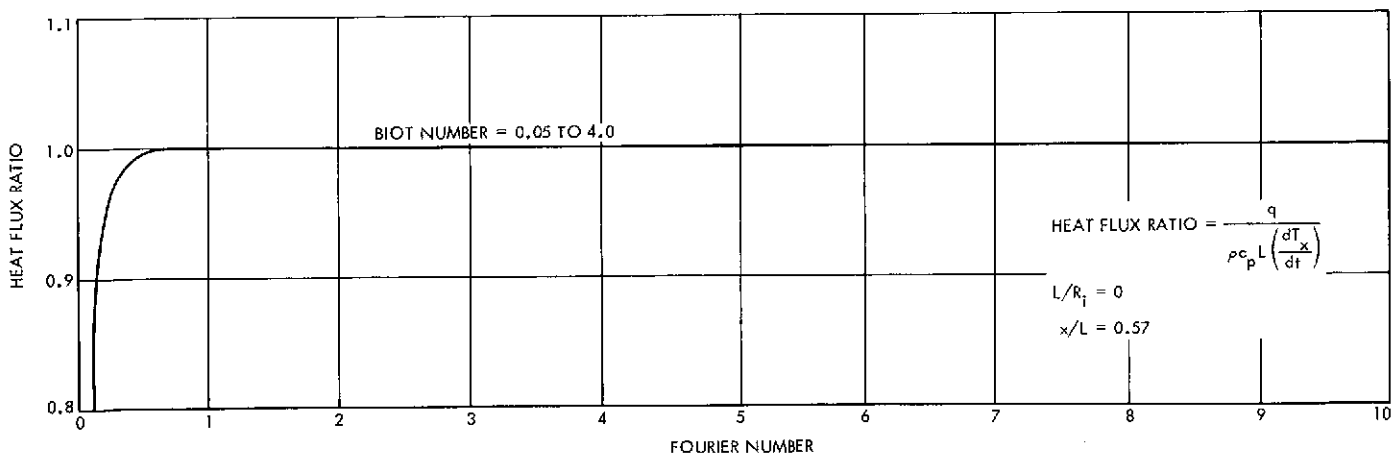

Fig. 20. Heat flux ratio vs Fourier and Biot Numbers; L/R_i = 0; x/L = 0.57

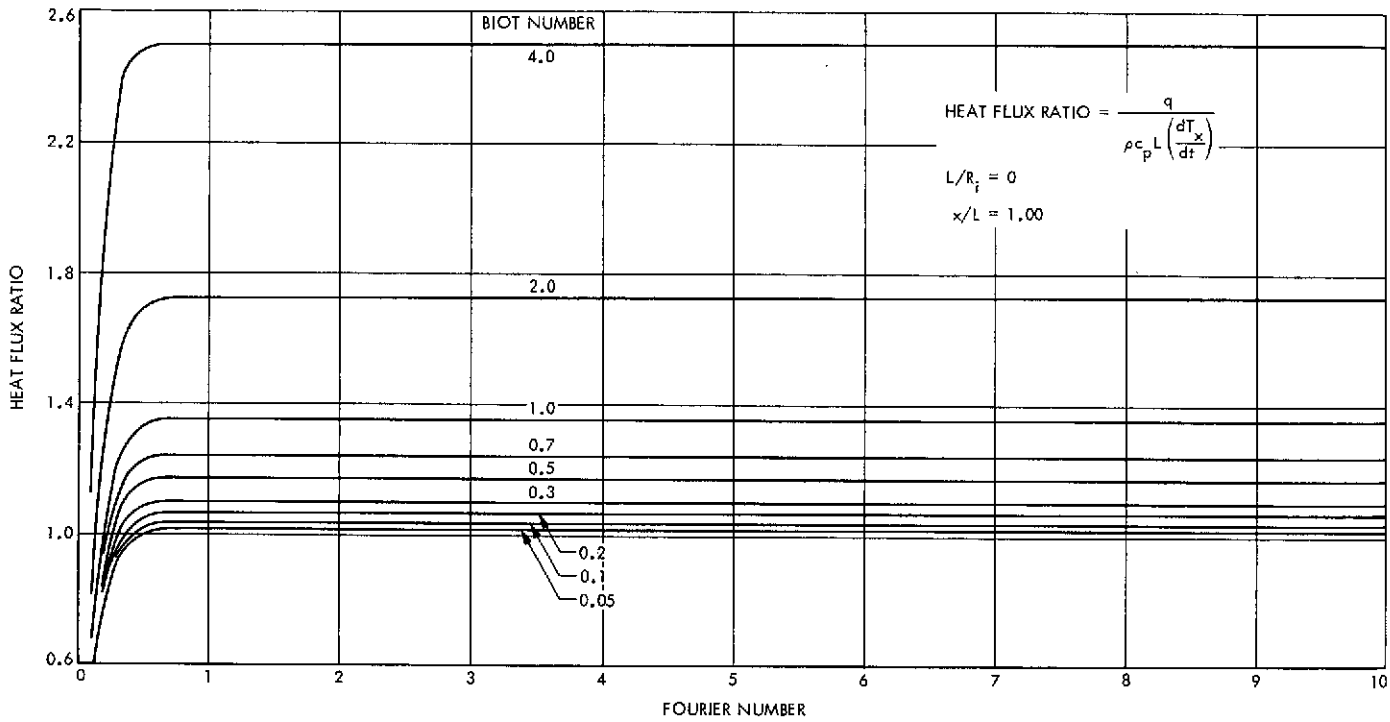

Fig. 21. Heat flux ratio vs Fourier and Biot Numbers; $L/R_i = 0$; $x/L = 1.00$

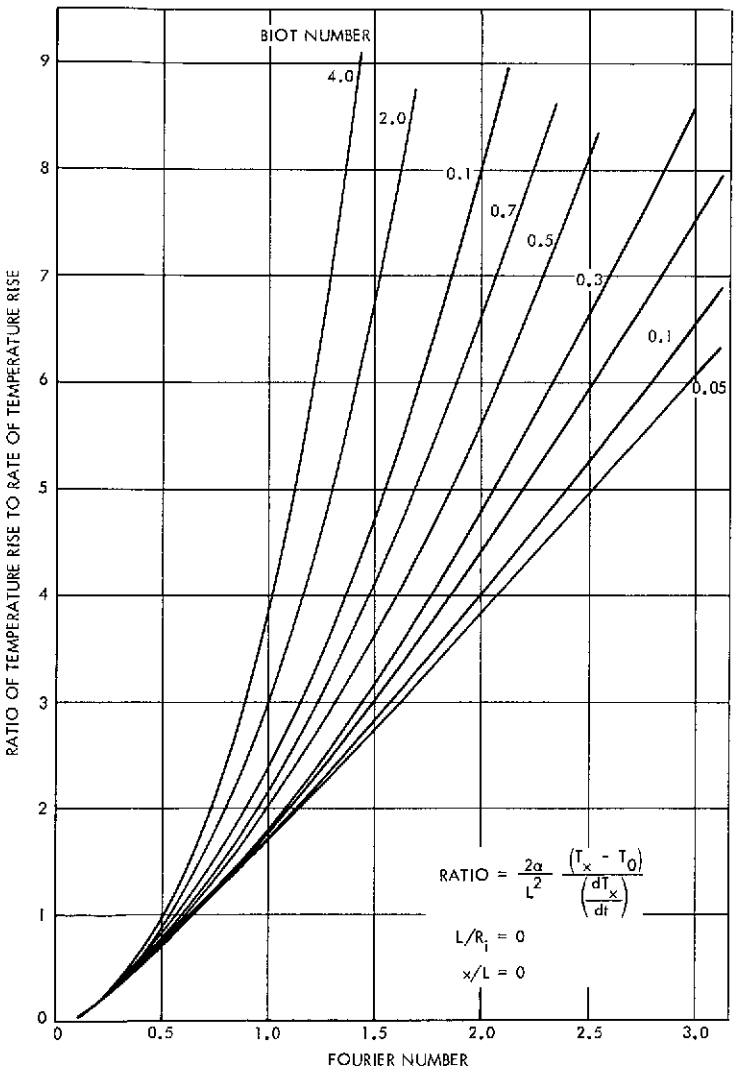

Fig. 22. Ratio of temperature rise to rate of temperature rise vs Fourier and Biot Numbers; $L/R_i = 0$; $x/L = 0$

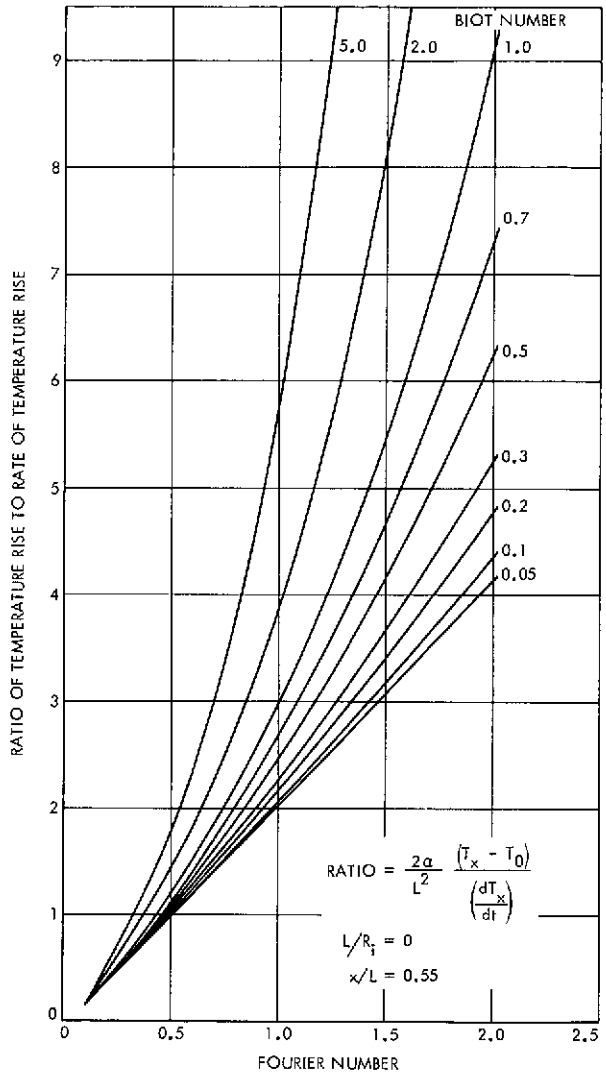

Fig. 23. Ratio of temperature rise to rate of temperature rise vs Fourier and Biot Numbers; $L/R_i = 0$; $x/L = 0.55$

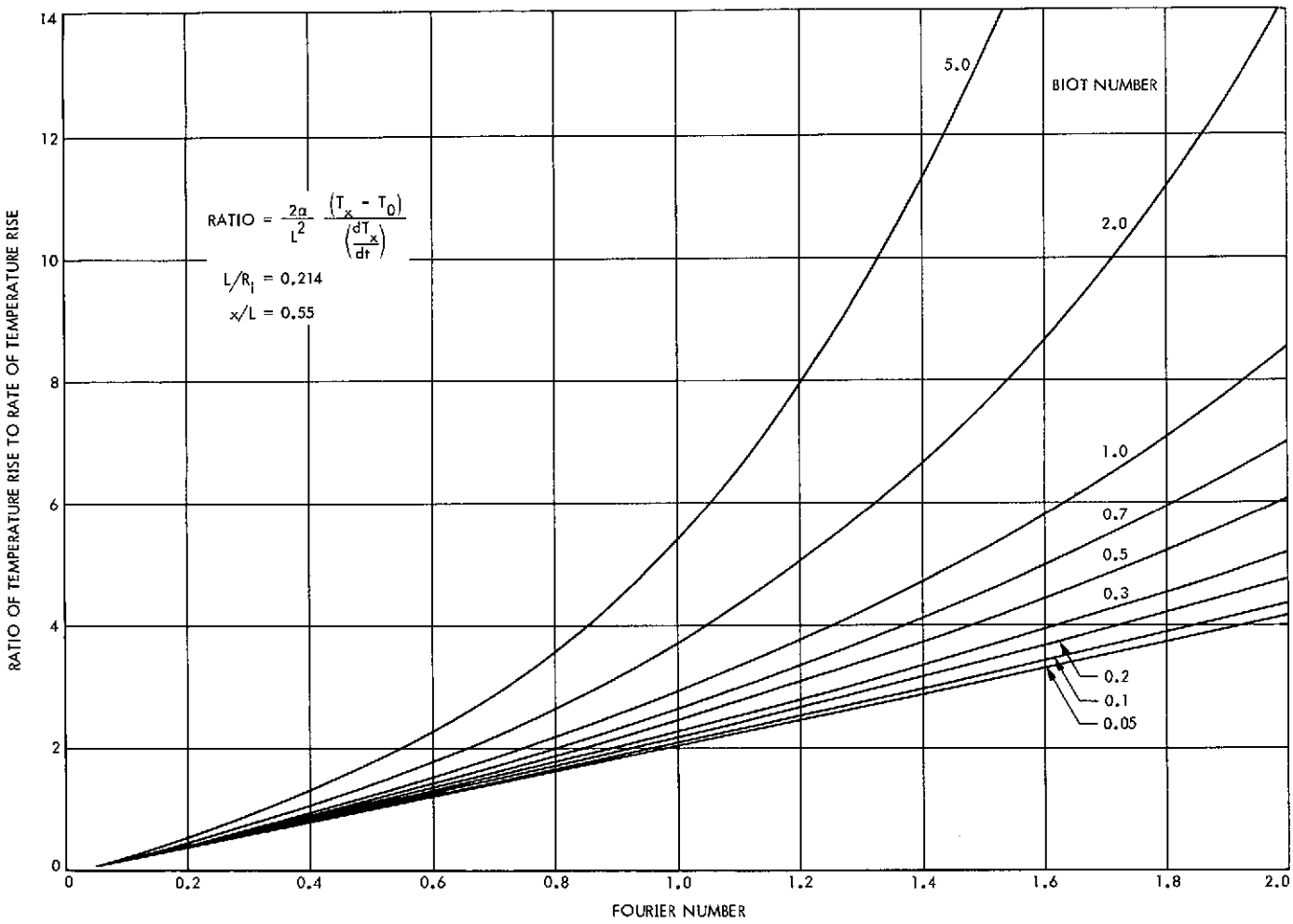

Fig. 24. Ratio of temperature rise to rate of temperature rise vs Fourier and Biot Numbers; L/R_i = 0.214; x/L = 0.55

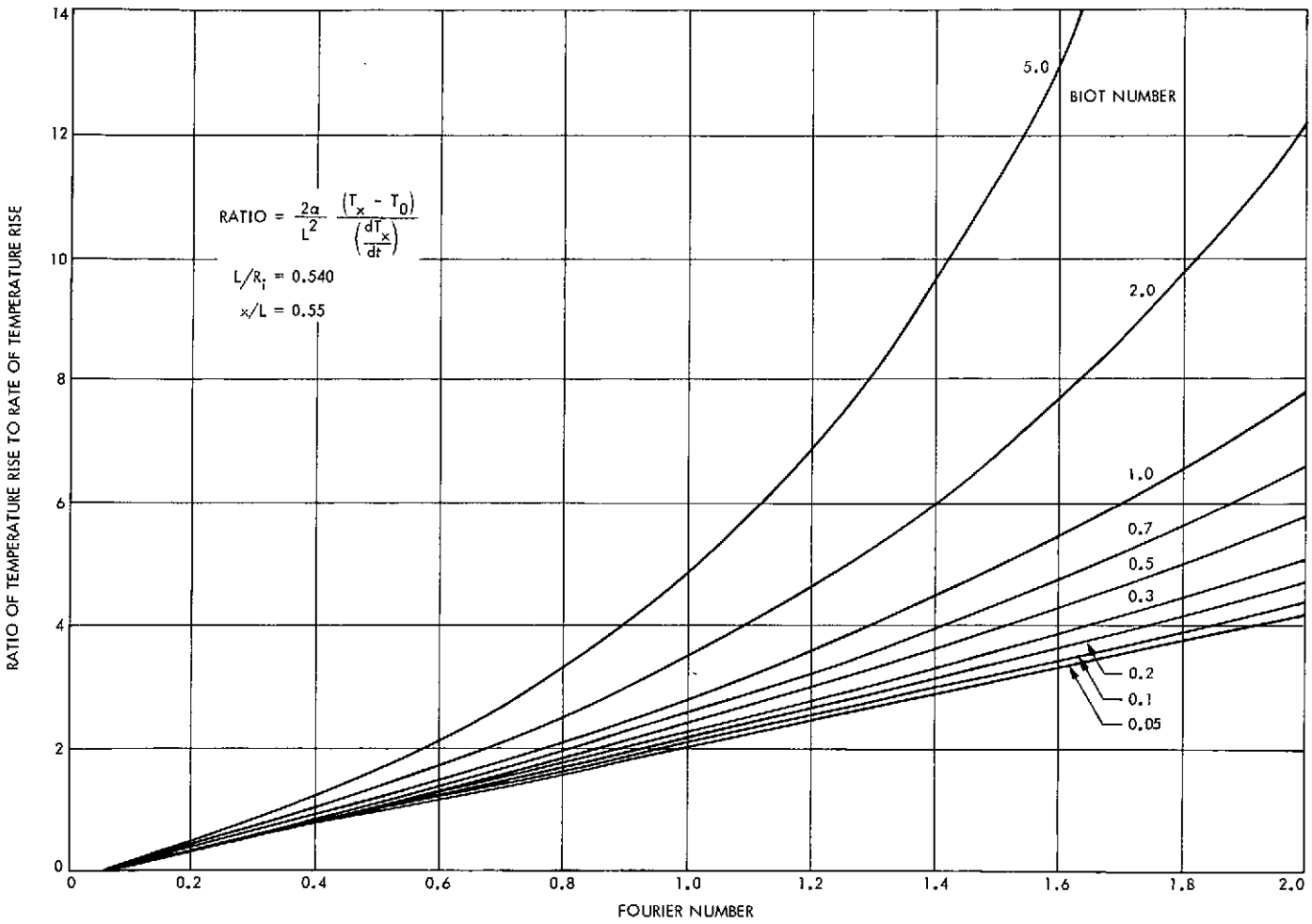

Fig. 25. Ratio of temperature rise to rate of temperature rise vs Fourier and Biot Numbers; L/R_i = 0.540; x/L = 0.55

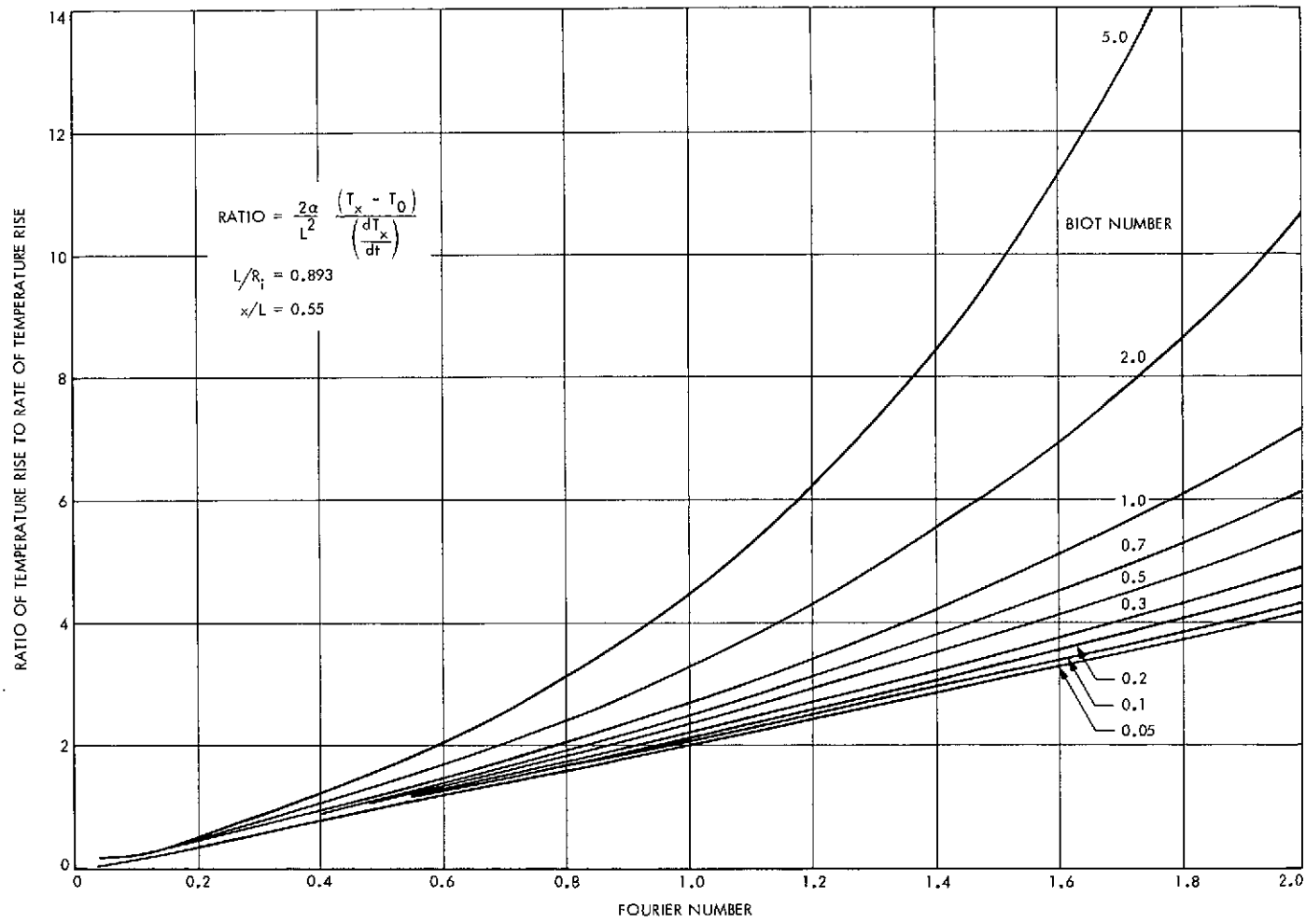

Fig. 26. Ratio of temperature rise to rate of temperature rise vs Fourier and Biot Numbers; L/R_i = 0.893; x/L = 0.55

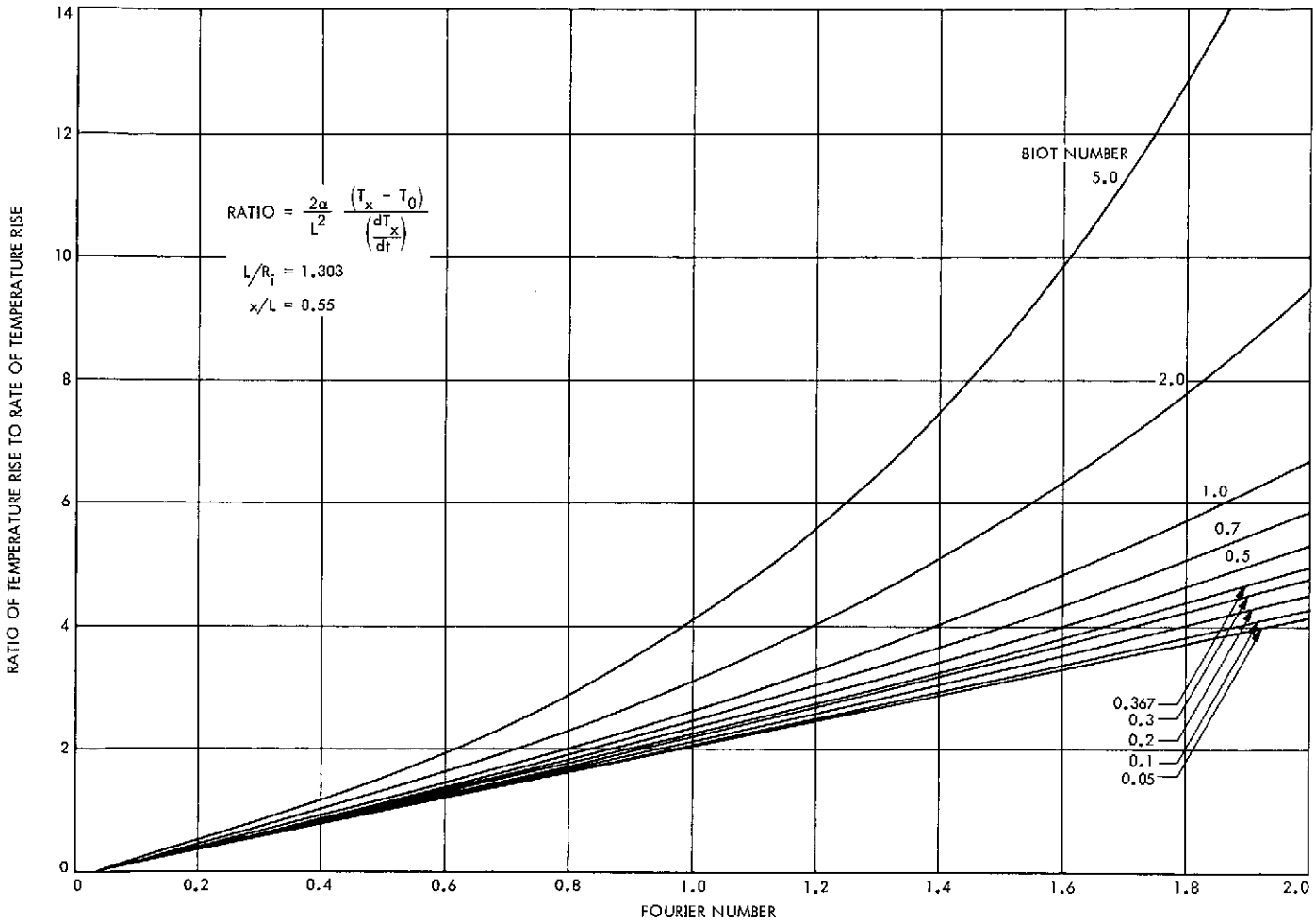

Fig. 27. Ratio of temperature rise to rate of temperature rise vs Fourier and Biot Numbers; L/R_i = 1.303; x/L = 0.55

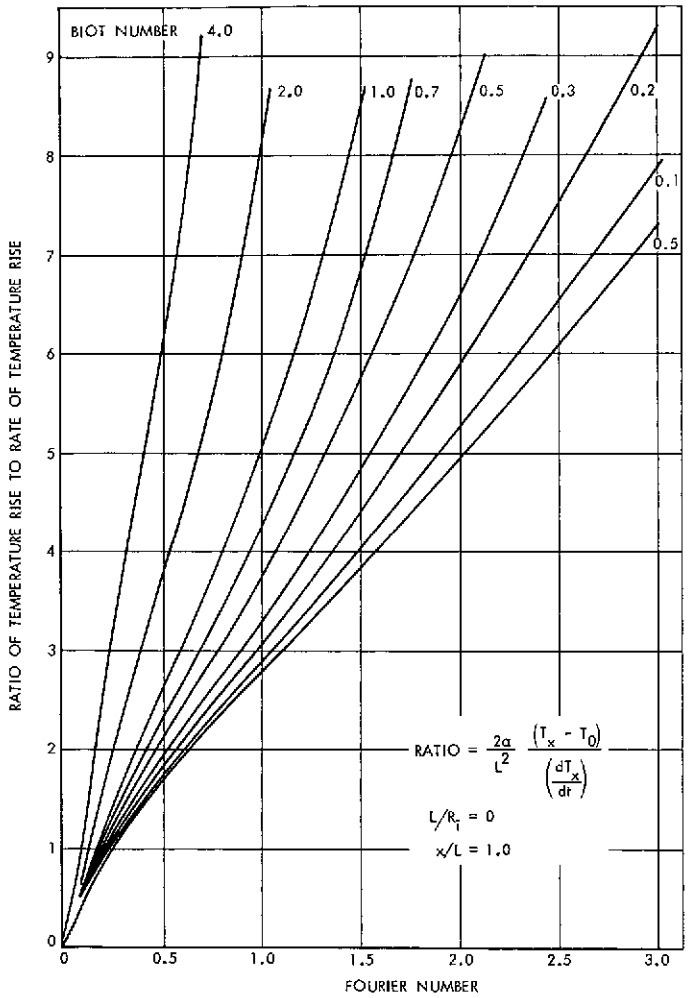

Fig. 28. Ratio of temperature rise to rate of temperature rise vs Fourier and Biot Numbers; $L/R_i = 0$; $x/L = 1.00$

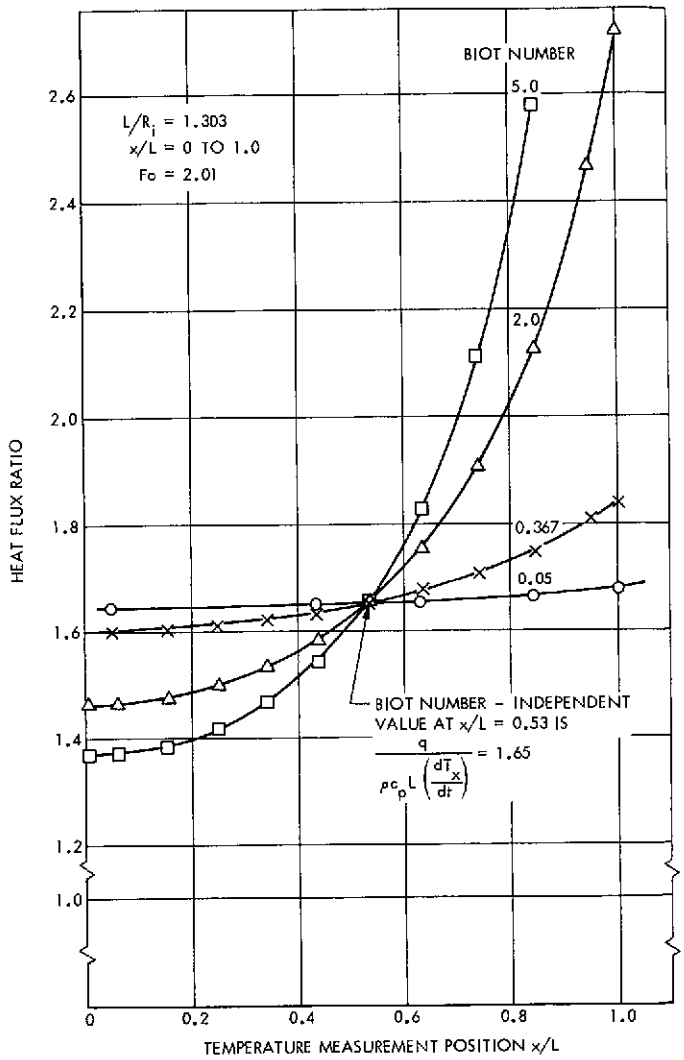

Fig. 29. Variation of heat flux ratio with Biot Number and x/L value for $L/R_i = 1.303$

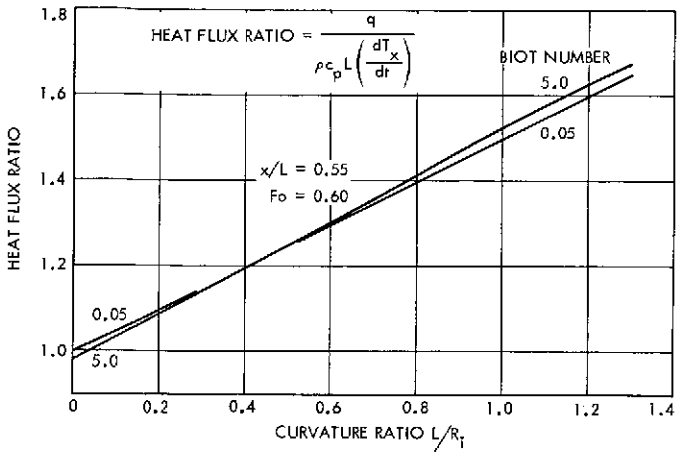

Fig. 30. Variation of heat flux ratio with L/R_i and Biot Number for $x/L = 0.55$ and for a Fourier Number ≥ 0.60

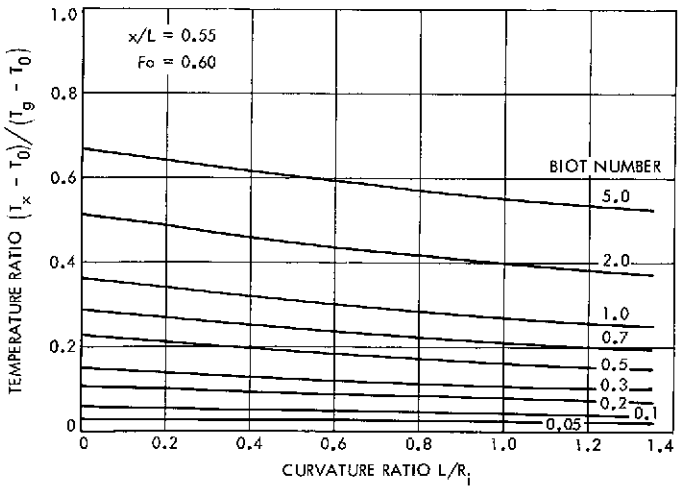

Fig. 31. Crossplot of temperature ratio vs curvature ratio and Biot Number; Fourier Number = 0.60; $x/L = 0.55$

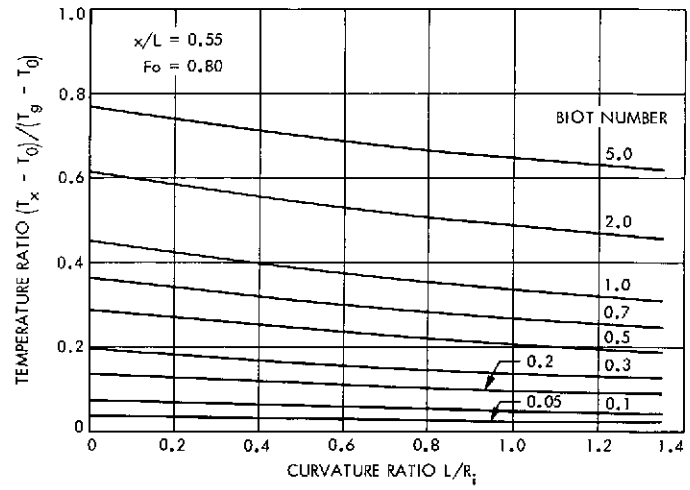

Fig. 32. Crossplot of temperature ratio vs curvature ratio and Biot Number; Fourier Number = 0.80; $x/L = 0.55$

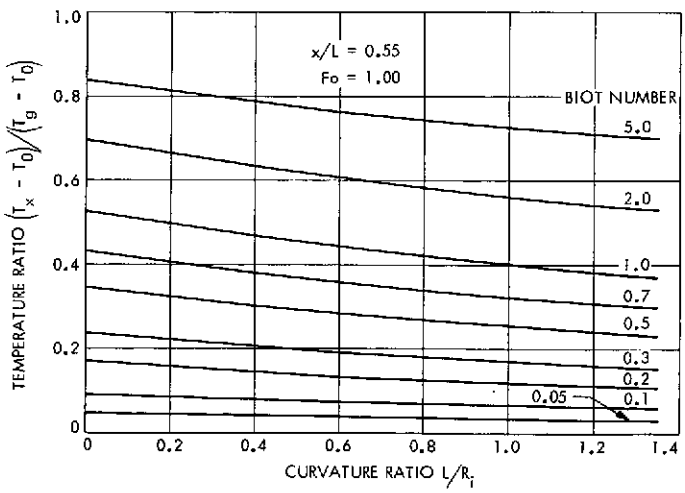

Fig. 33. Crossplot of temperature ratio vs curvature ratio and Biot Number; Fourier Number = 1.00; $x/L = 0.55$

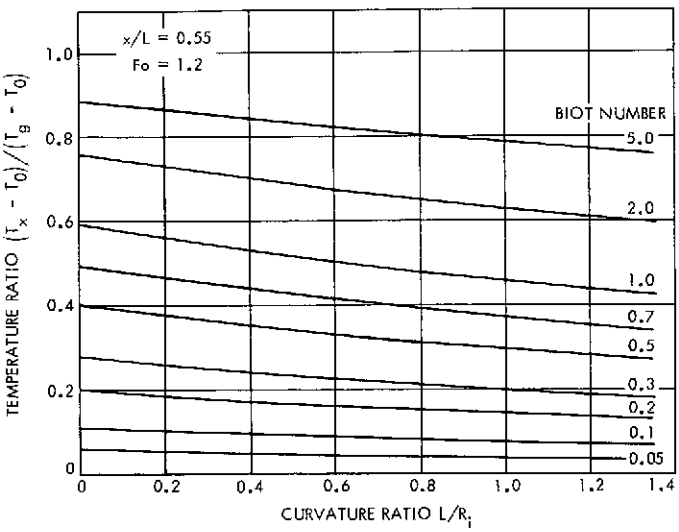

Fig. 34. Crossplot of temperature ratio vs curvature ratio and Biot Number; Fourier Number = 1.20; x/L = 0.55

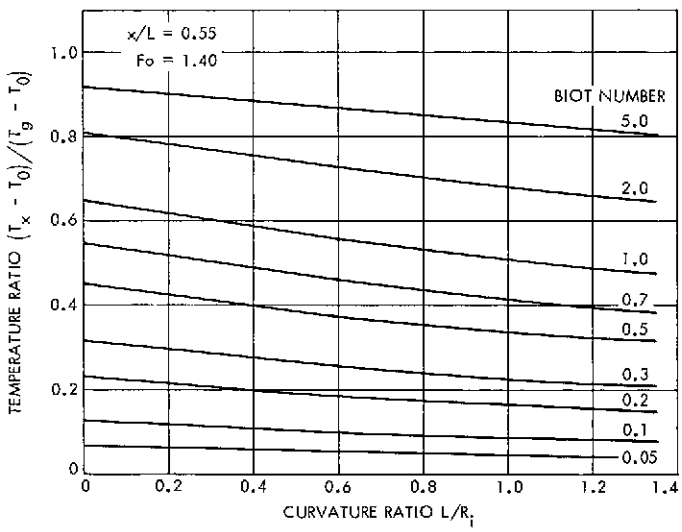

Fig. 35. Crossplot of temperature ratio vs curvature ratio and Biot Number; Fourier Number = 1.40; x/L = 0.55

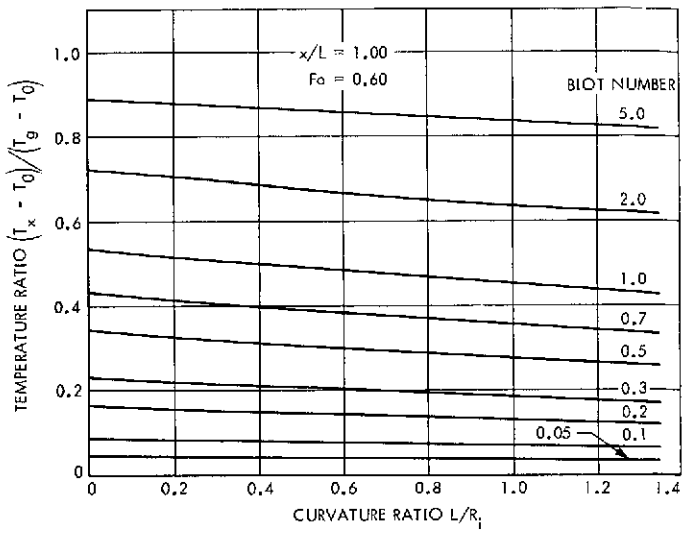

Fig. 36. Crossplot of temperature ratio vs curvature ratio and Biot Number; Fourier Number = 0.60; x/L = 1.00

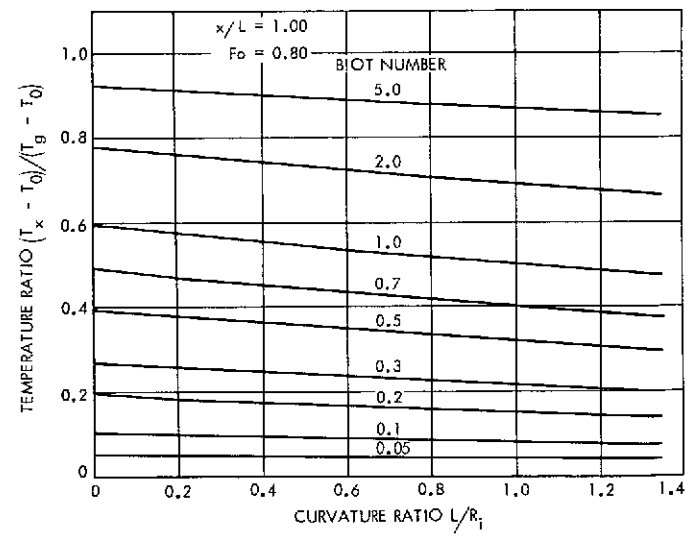

Fig. 37. Crossplot if temperature ratio vs curvature ratio and Biot Number; Fourier Number = 0.80; x/L = 1.00

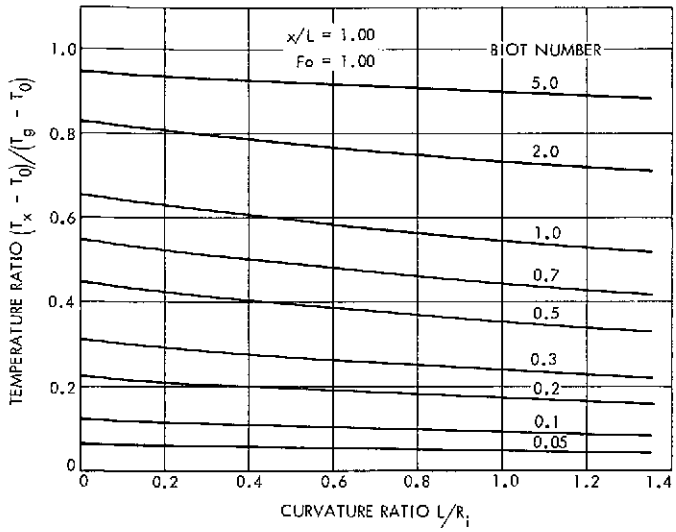

Fig. 38. Crossplot of temperature ratio vs curvature ratio and Biot Number; Fourier Number = 1.00; x/L = 1.00

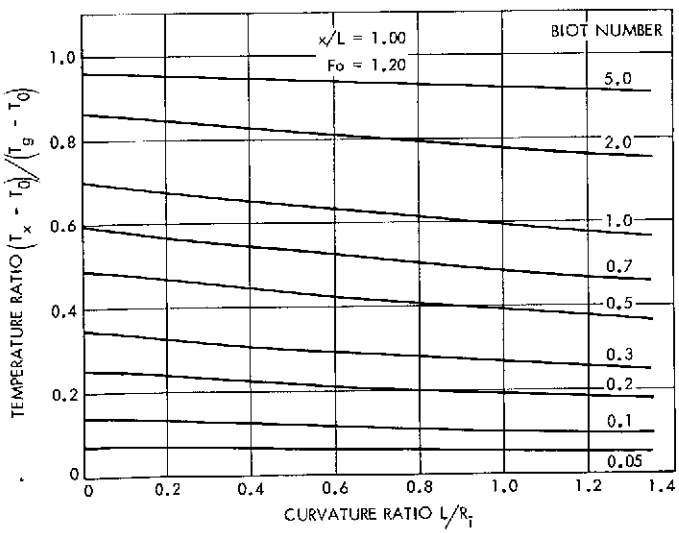

Fig. 39. Crossplot of temperature ratio vs curvature ratio and Biot Number; Fourier Number = 1.20; x/L = 1.00

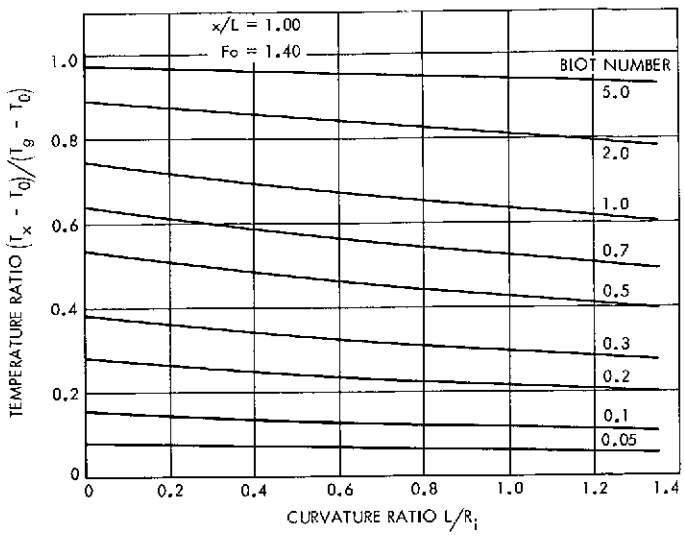

Fig. 40. Crossplot of temperature ratio vs curvature ratio and Biot Number; Fourier Number = 1.40; x/L = 1.00

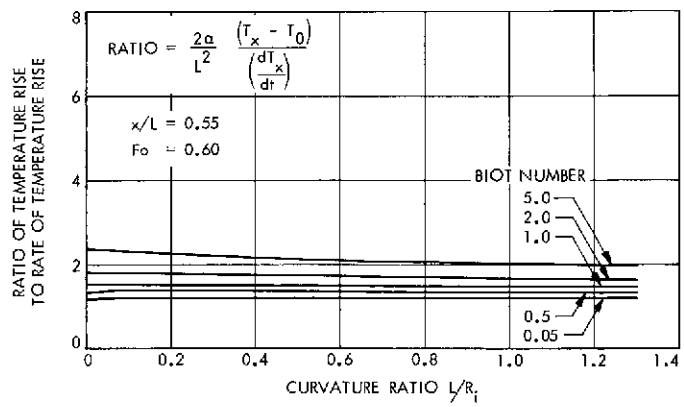

Fig. 41. Crossplot of ratio of temperature rise to rate of temperature rise vs curvature ratio and Biot Number; Fourier Number = 0.60; x/L = 0.55

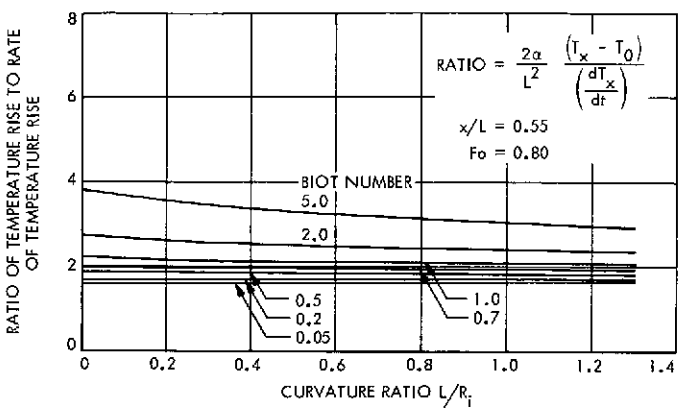

Fig. 42. Crossplot of ratio of temperature rise to rate of temperature rise vs curvature ratio and Biot Number; Fourier Number = 0.80; x/L = 0.55

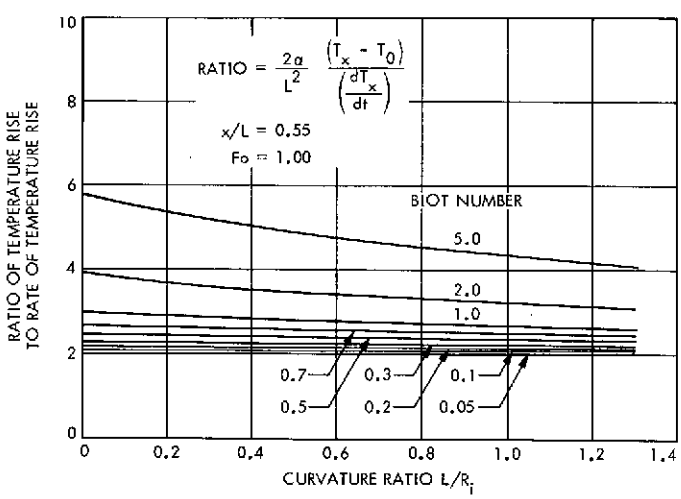

Fig. 43. Crossplot of ratio of temperature rise to rate of temperature rise vs curvature ratio and Biot Number; Fourier Number = 1.00; x/L = 0.55

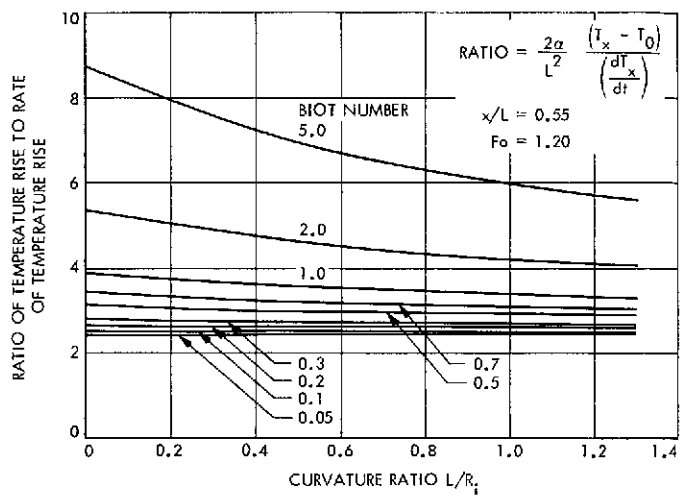

Fig. 44. Crossplot of ratio of temperature rise to rate of temperature rise vs curvature ratio and Biot Number; Fourier Number = 1.20; x/L = 0.55

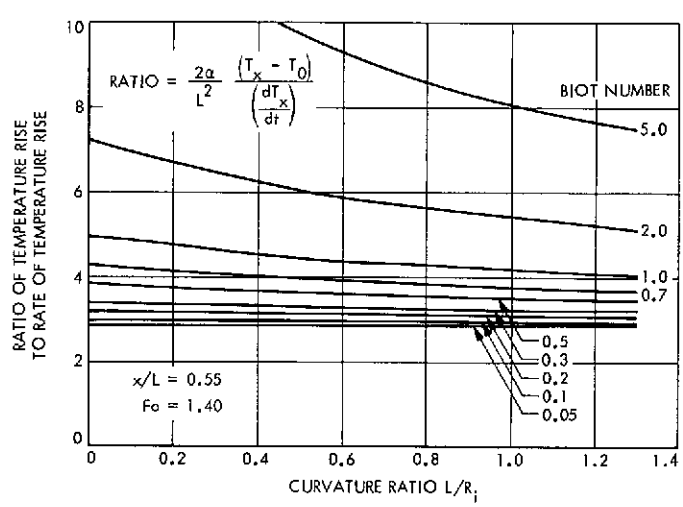

Fig. 45. Crossplot of ratio of temperature rise to rate of temperature rise vs curvature ratio and Biot Number; Fourier Number = 1.40; x/L = 0.55

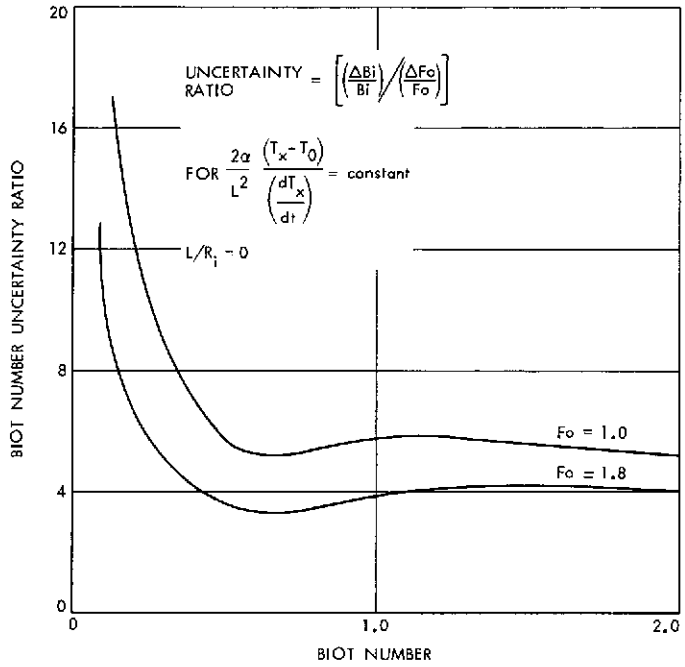

Fig. 46. Biot Number uncertainty ratio for uncertainty in Fourier Number only

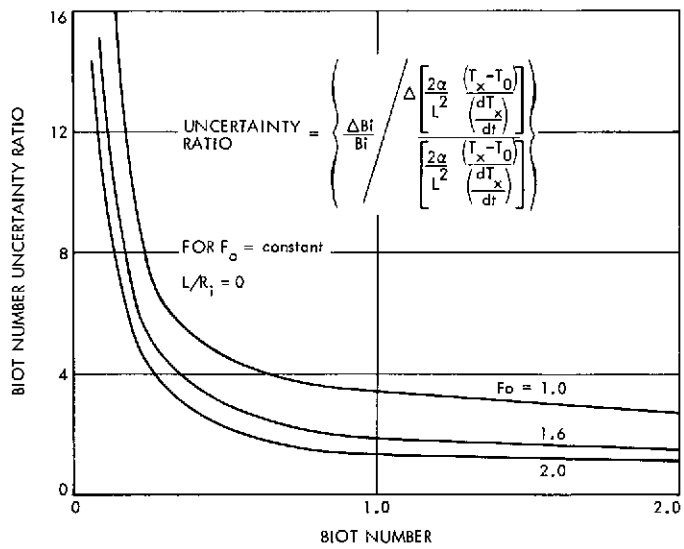

Fig. 47. Biot Number uncertainty ratio for uncertainty in ratio of temperature rise to rate of temperature rise only

Appendix A

Thermocouple Plug Design, Fabrication, and Installation

I. Introduction

This report describes the development and application of a methodology for analyzing transient temperature data obtained during convective heating of a flat or curved plate, so as to determine the temperature and the heat transfer coefficient of the hot gas. The methodology is in its simplest and most effective form when the temperature measurement is made near the center of the thickness of the plate. In order to make use of the methodology, then, it was necessary to develop a means of measuring the temperature within a metal plate, with a negligible local perturbation of the temperature field.

The technique developed was to fabricate a "thermocouple plug" of the same material as the plate and then to braze the plug into a precisely machined and closely fitting hole in the plate. Separate fabrication of the thermocouple plug enabled special care to be taken in installing the fine thermocouple wires and in forming the thermocouple junction, using a laser welding process, and also enabled inspection of each completed thermocouple plug before it was brazed into the plate.

Brazing of the completed thermocouple plugs into machined holes in the plate, with a thin but complete metallic bond between the plug and the plate, minimized the thermal disturbance due to the introduction of the plug into the plates. Additionally, the depth of the finite-sized machined hole in the plate could be accurately measured before brazing to establish the exact position at which the thermocouple junction would be located after the brazing was completed.

The critical steps in the fabrication and installation of the thermocouple plugs are described below.

II. Thermocouple Plugs

The thermocouple plug was made of the same material as the plate; all of the present work was done with copper.[8] An outside diameter of 0.635 cm (1/4 in.) was chosen for ease in fabrication and handling. The inside of the plug was bored with holes of gradually decreasing diameter to leave a thin closure at the thermocouple end of the plugs as shown on Fig. A-1. The critical part of the thermocouple plug was at the closed end, where a diaphragm only 0.0127 cm (0.005 in.) thick remained at the bottom of the final 0.0914-cm (0.036-in.) diameter bored hole. The final step in machining the body of the plug was to drill two 0.0153-cm (0.006-in.) diameter holes, spaced 0.254 cm (0.010 in.) apart, located symmetrically about the center line of this thin diaphragm.

The preparation of the thermocouple wires used in the plug was also very critical. (Most thermocouples were made with Chromel–Alumel wires, but higher-temperature-capability Platinel–Platinel thermocouple wire was used for some samples.) Thermocouple wires 0.0127 cm (0.005 in.) in diameter (36 gage) were used. The first step was to cut the wires into 15.2-cm (6-in.) lengths and to form a perfectly spherical ball 0.02033 to 0.0254 cm (0.008 to 0.010 in.) in diameter on one end of each wire; this was done with a controlled pulse of a laser beam that was focused on the end of the wire (the axis of the wire was aligned with the axis of the laser beam).[9] The end of the wire was protected from oxidation with an argon purge.

The next step was to thread a pair of thermocouple wires through the holes in the diaphragm at the closed end of the thermocouple plug and through the similarly spaced holes in a piece of 0.0794-cm (1/32-in.) diameter double-bore ceramic insulating tube, as shown in Fig. A-2. The thermocouple plug was then mounted vertically, with its closed end up, under the laser. The ceramic tube was restrained so that its upper end was about 0.158 cm (1/16 in.) below the bottom surface of the diaphragm, and lightweight clamps were attached to the bottom of each wire to provide a slight tension to keep the spherical ball at the top end of each wire in firm contact with the top surface of the diaphragm. Then the laser beam was focused to cover both spherical wire ends, and a controlled pulse fused both thermocouple wires into the diaphragm to form an integral thermocouple junction. The fused end was then flattened by lightly stroking it on a sheet of No. 400 wet-or-dry abrasive grit, with the plug suitably supported to keep the end square.

[8]Tellurium copper was used for the plugs to improve machinability, while OFHC copper was used for the plate. The difference in thermal properties is assumed to be negligible.

[9]The laser used was a CORAD 150-mA machine.

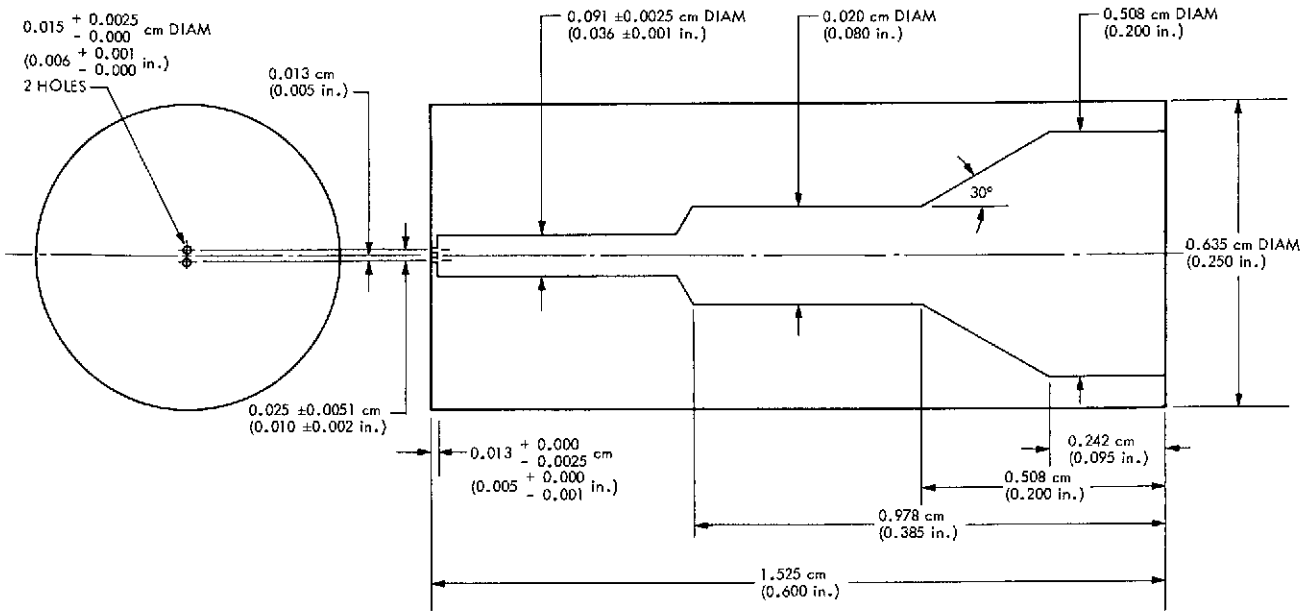

Fig. A-1. Machined thermocouple plug body (tellurium copper)

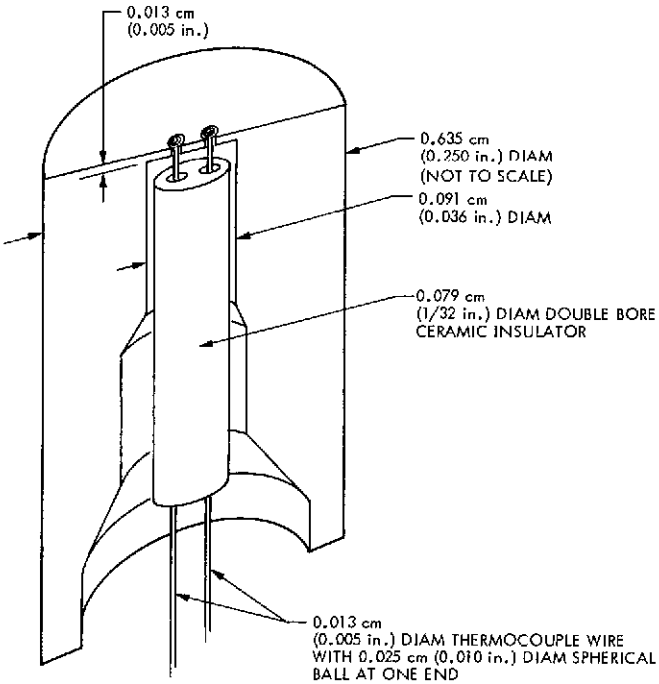

Fig. A-2. Assembly of parts for fusing thermocouple junction in thermocouple plug

After the completion of the laser welding and cleanup operation described above, the thermocouple plug was turned open-end-up, and a high-temperature ceramic insulating cement was used to cement in the double-bore ceramic tubing and part of the space above it; care was taken in this last step to keep the thermocouple wire leads adequately separated.[10] When the cement had dried and set, it was cured at the recommended temperature. The remainder of the cavity in the top of the thermocouple plug was filled with a lower-temperature cement after the plug had been brazed into the plate. At this time, too, woven fiber glass sleeving was slipped over the thermocouple lead wires, to be bonded in place by the cement.[11] The final configuration of the assembled plug was shown in Fig. A-3.

III. Assembly by Brazing

A considerable number of copper test specimens were used in developing a satisfactory brazing procedure. The objective of the brazing operation was to bond the thermocouple plug to the walls of the hole machined into the plate so that there would be an absolute minimum of thermal disturbance; i.e., the bond would be continuous and thin and would be formed from a high-conductivity brazing alloy. These objectives were achieved by adhering to the following step-by-step procedure:

(1) The hole in the plate was machined to receive the thermocouple plug, and a brazing feed-tube hole

[10]The cement used was Ecoceram 21, made by Emmerson and Cumming, which will withstand temperatures of up to 1368 K (2000°F).

[11]The cement was Englehard Industries CA9R cement, for 812 K (1000°F) service.

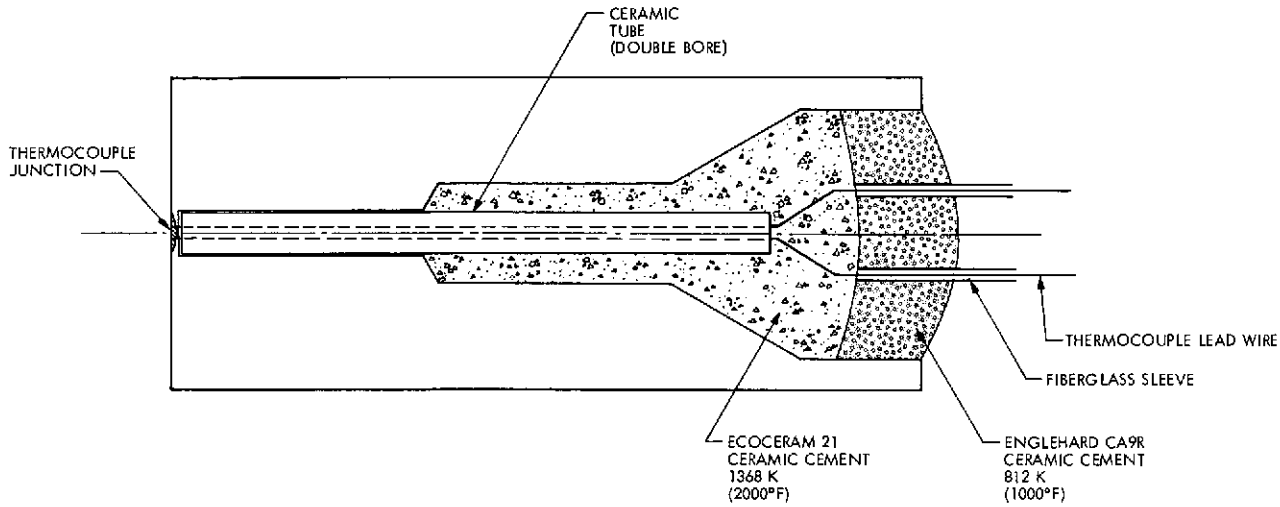

Fig. A-3. Completed thermocouple plug

was also machined, as shown on Fig. A-4. The feed-tube hole was positioned so that there was gravity feed of the brazing alloy when the assembly was loaded into the brazing furnace. The plug-hole was precisely machined with a flat, square bottom and a diameter only 0.00127 to 0.00508 cm (0.0005 to 0.0020 in.) more than that of the plug, depending on the brazing alloy used.

The depth of the hole was such that after assembly the effective thermocouple junction was at the desired position (usually 0.55 of the plate thickness in from the unheated surface). Somewhat arbitrarily, the effective thermocouple junction was assumed to be at the midthickness of the copper diaphragm at the tip of the thermocouple plug, and it was assumed that there was a 0.00254 cm (0.001 in.) thick layer of brazing alloy between the bottom of the plug and the bottom of the hole in the plate; thus, the effective thermocouple junction was 0.00889 cm (0.0035 in.) from the bottom of the machined hole.

(2) The bottom of the machined thermocouple plug hole was coined with a square-ended punch made of hardened steel. This assured that the thermocouple plug could seat firmly on the bottom of the hole and would not ride on the corner radius or any irregularity on the bottom surface of the hole.

(3) The thermocouple plug, the hole in the plate, the copper feed-tube, and the brazing alloy were thoroughly cleaned. (The cleaning process found to be satisfactory was Metal Surfaces, Inc., Specification

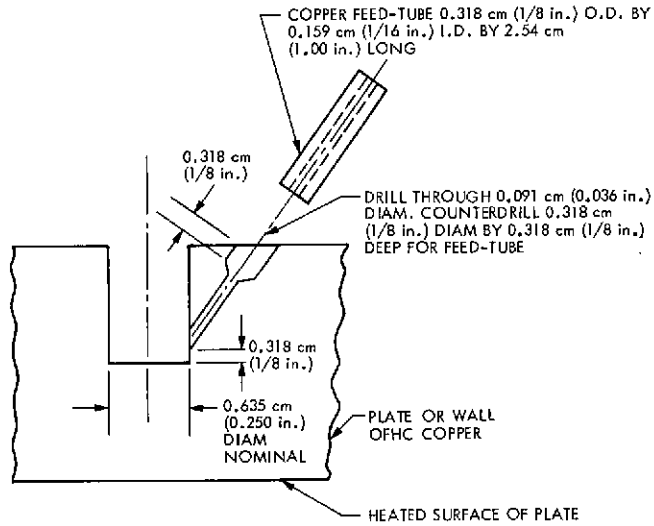

Fig. A-4. Preparation of plate for receiving thermocouple plug

SP 101.)[12] After this step, all parts were handled with clean white gloves.

(4) The parts were assembled for brazing. The thermocouple plug was held down firmly against the bottom of the hole in the plate and locked in position by making a series of punch indentations in the plate around the edge of the hole. A finishing tap on the top of the plug with a light hammer, using a fixture to protect the wires, assured that the plug was firmly seated.

The cleaned copper feed-tube was inserted in its socket (see Fig. A-4), and the brazing wire or slurry

[12]Metal Surfaces, Inc., Bell Gardens, Calif.

was placed in the tube.[13] (When slurry is used, it should be needle-injected so as to fill from the bottom to the top of the feed-hole and tube, thus eliminating the possibility of bubbles in this passage.)

(5) The assembled parts were placed in a hydrogen-atmosphere furnace for brazing. During this operation, the 0.127-cm (0.005-in.) thermocouple lead wires extending from the back of the thermocouple plug were protected from damage.

(6) After the brazing operation was completed, the woven fiber glass sleeve insulation was placed over the thermocouple lead wires and the final increment of insulating ceramic cement was placed in the top of the thermocouple plug, as previously described. (At this time the protruding brazing-alloy feed-tube can be snipped off.) When the thermocouple lead wires have been connected to the appropriate terminals and/or cold junction and instrumentation lead wires and covered to protect them from damage, the thermocouple plug installation can be considered complete.

A few comments on the final design of the thermocouple plug should be added here, lest the reader be tempted to take shortcuts and be forced to retrace ground that was covered in the present investigation.

The laser-fused closed tip is a most important feature of the thermocouple plug developed here. Numerous earlier attempts to incorporate prewelded thermocouple junctions into a plug configuration failed because outgassing from ceramic insulating material destroyed the integrity of the brazed joints, or were impractical because of the several temperature levels of brazing operations which were required. The laser-fuzing of the thermocouple junction and the tip of the thermocouple plug provides a high-temperature closure that is made under conditions where any possible outgassing from the single piece of double-bore ceramic tubing is harmlessly vented away from the weld area. The final brazing of the thermocouple plug into the recess in the plate is then not limited by the melting point of any previous brazing operation; the brazing alloy can be chosen freely to obtain the desired melting temperature and bonding characteristics. Further, any outgassing from the ceramic cement within the plug at the time of the brazing operation is sealed off from the braze and must vent to the back through the bore in the center of the plug.

During the evolution of the brazing procedures, a number of types of fixtures for holding the plug firmly against the bottom of the hole in the plate were considered and tried. None of the external fixtures was satisfactory, both because of bulk and mechanical complexity, and because loading derived from elastic deflection could not be depended upon at brazing temperatures. The assembly technique finally adopted was to mechanically wedge the plug in place by center-punching around the top edge of the hole in the plate; this was simple and reliable.

Several methods of supplying brazing alloy to the joint area were tried before the external feed-tube was adopted: no other method provided the versatility of using wire or slurry brazing alloy, provided complete coverage of the plug–plate interface surfaces, and kept the reservoir cavity and thermal disturbance region as far from the thermocouple junction area. Test-specimen braze joints obtained using the procedures described here are shown in Figs. A-5–A-7. In these figures, the light-colored band at the interface between the plug and the body indicates a change in metallographic structure where the brazing alloy has diffused into the copper parts; the band width is many times the initial clearance between the parts.

Satisfactory brazing assembly joints were demonstrated with two brazing alloys and over a range of diametral clearances (brazing alloy joint thickness). As a practical matter, it is desirable to strive for the minimum workable joint thickness, if only to assure that possible cocking of the plug in the hole is minimized. Some control over cocking can also be exercised during the punch-wedging operation by punching lightly first on one side and then on the other side of the plug.

Absolute cleanliness of the brazing surfaces and alloy is essential if a complete bond is to be obtained. A cleaning process at least as good as the one referenced must be used. Copper must be used for the brazing alloy feed tube; it was found that stainless steel contaminated the braze alloy and caused an imperfect bond.

[13]Two different brazing alloys, having different melting temperatures, were characterized during the brazing procedure development tests. The choice of alloy depends on the anticipated temperature to which the brazed joint will be exposed during test: BT alloy (72% Ag, 28% Cu) is supplied in wire form and flows at 1052 K (1435°F). Optimum diametral clearance for this alloy appears to be 0.00127 to 0.00254 cm (0.0005 to 0.0010 in.). Premabraze 130 alloy (82% Au, 18% Ni) is used as a slurry and flows at 1222 K (1740°F). Optimum diametral clearance for this alloy appears to be 0.00254 to 0.00508 cm (0.001 to 0.002 in.).

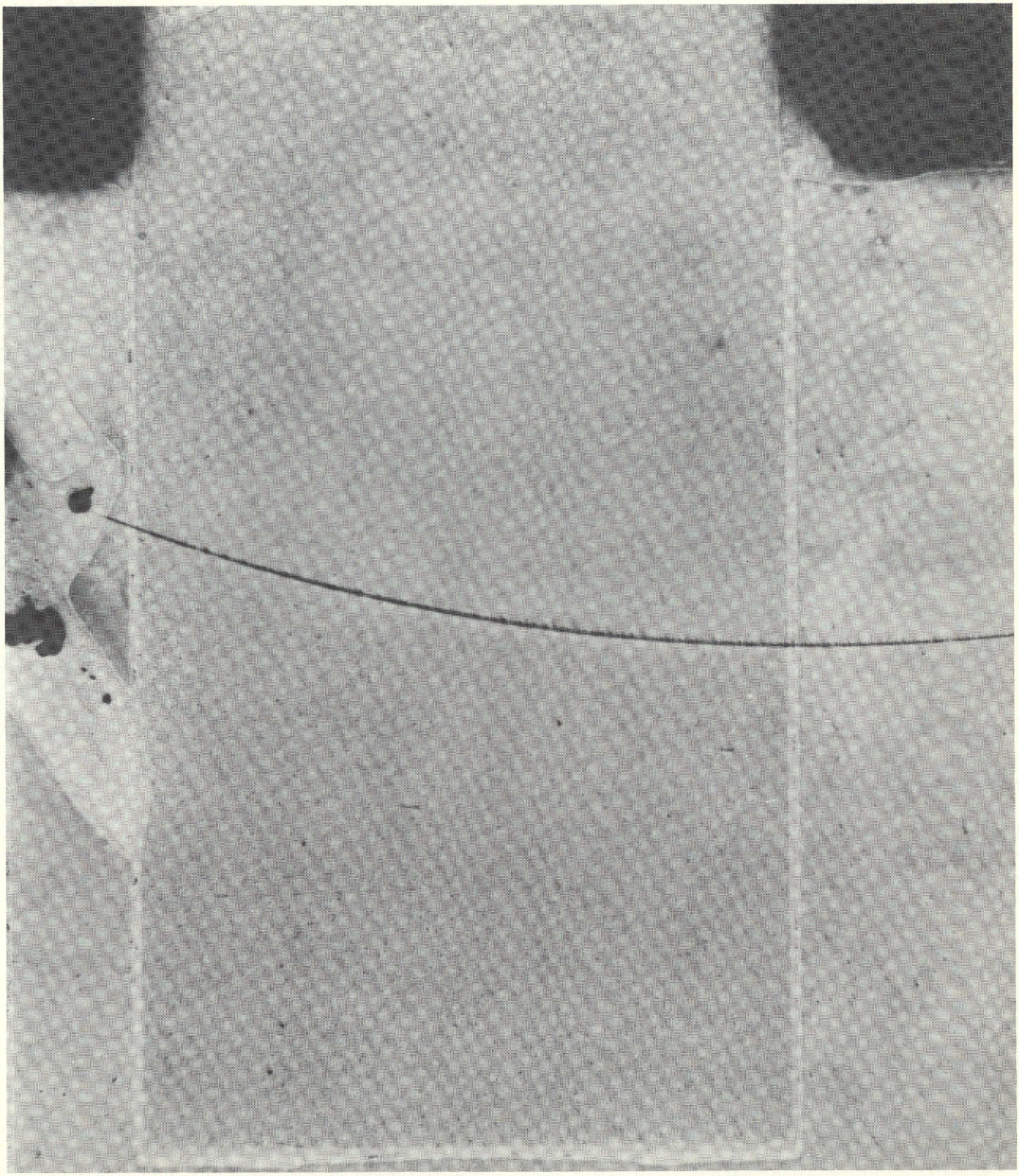

Fig. A-5. Bond obtained with 0.635-cm (0.250-in.) diameter tellurium–copper plug brazed into hole in OFHC copper block; 0.0025-cm (0.001-in.) diametral clearance, BT braze alloy (72% silver–28% copper)

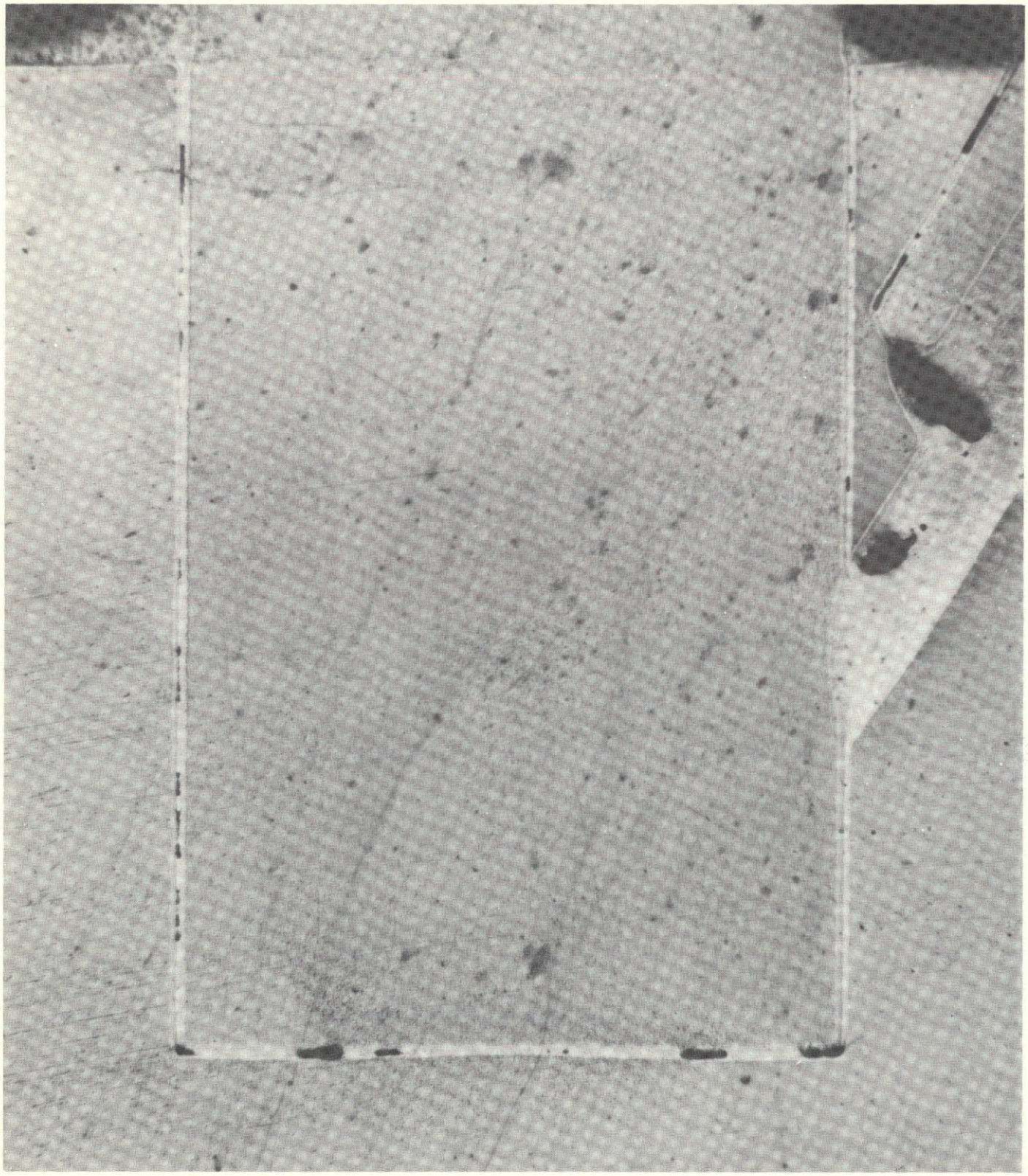

Fig. A-6. Bond obtained with 0.635-cm (0.250-in.) diameter tellurium–copper plug brazed into hole in OFHC copper block; 0.0051-cm (0.002-in.) diametral clearance, BT braze alloy (72% silver–28% copper)

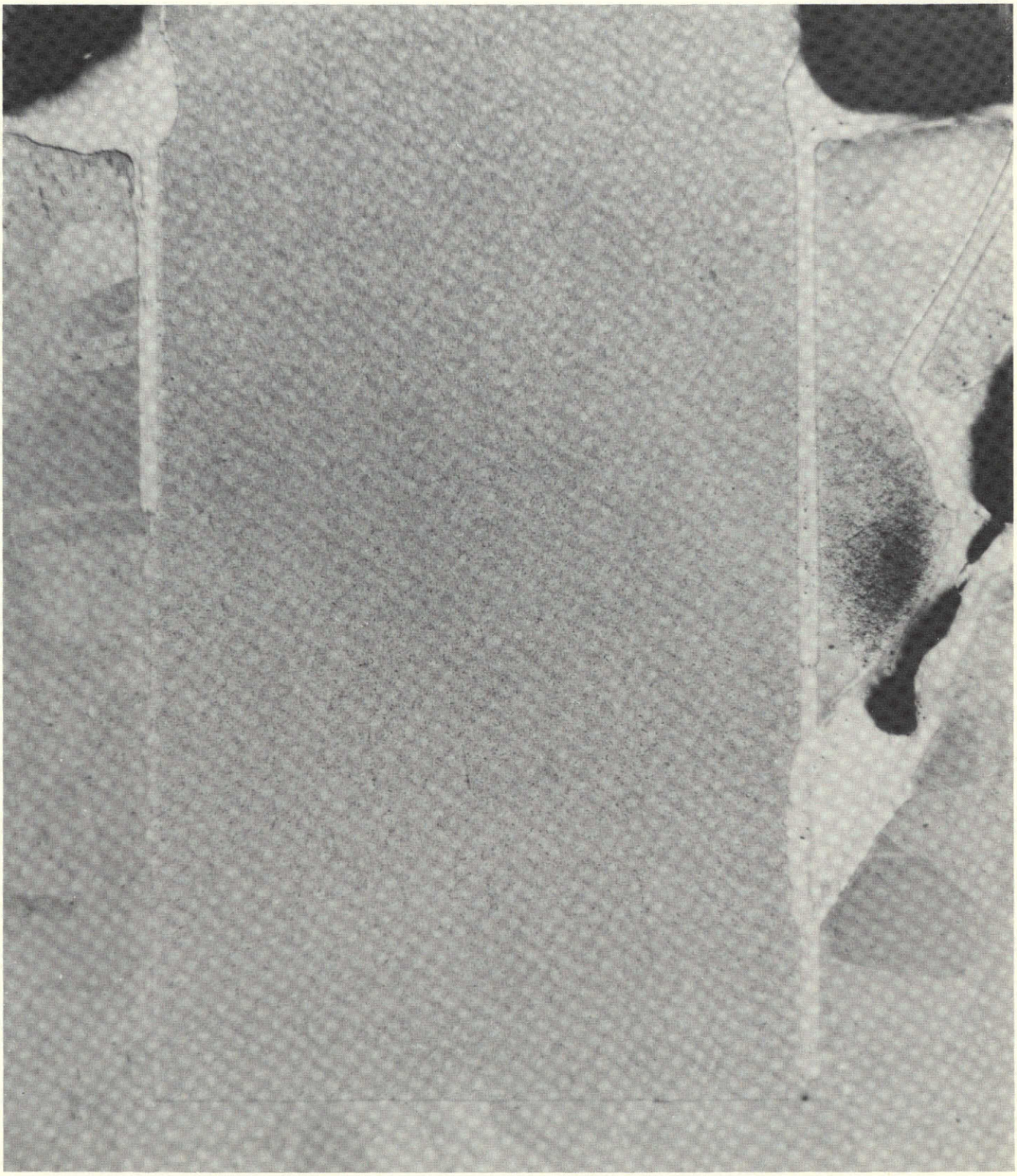

Fig. A-7. Bond obtained with 0.635-cm (0.250-in.) diameter tellurium–copper plug brazed into hole in OFHC copper block; 0.0051-cm (0.002-in.) diametral clearance, Premabraze 130 alloy (82% gold–18% nickel)

Appendix B

Thermal Properties of Useful Metals

A fundamental assumption in the transient heat transfer analysis and in the resultant curves presented in the body of this report is that the thermal properties of the plate material are constant. A further constraint on the plate materials which can be used in practice is that the level of the thermal conductivity and the thermal diffusivity must be high; this ensures that the thermal response is felt throughout the plate before the temperature of the heated surface exceeds its limiting value.

The number of materials of construction which can be used to fabricate transient heat transfer devices and which will withstand fairly high temperatures, have high thermal conductivity, and have nearly constant thermal properties over a wide temperature range is relatively small. The thermal properties of three materials which have been used for rocket motor combustion chambers and nozzles are tabulated here for reference.

Copper appears to be the most satisfactory material for the applications discussed herein. The thermal conductivity is higher than that of any other commonly available material, and the thermal diffusivity decreases by only 20% over a temperature range from ambient to about 1258 K (1800°F). The principal limitation of copper is in its low strength and its low "softening" temperature. The yield strength of OFHC copper starts to decline rapidly when the temperature exceeds about 811 K (1000°F). For this reason, the surface temperature of a copper heat transfer apparatus should not be allowed to exceed a temperature of 811 K, except for a very short time.

Mild steel is a readily available material, but in use has two limitations: the thermal conductivity and diffusivity are an order of magnitude lower than that of copper, and there is a phase change which causes a discontinuity in thermal properties at a temperature of 998 K (1337°F), which effectively limits the maximum temperature of operation. Over the operating temperature range, the thermal diffusivity changes by a factor of more than two. For these reasons, mild steel experimental apparatus can only be used when the heat flux level is low (say, up to 196 W/cm^2, or 1.20 Btu/in.^{2}s) and there will always be more uncertainty in the results than when the experimental apparatus is made of copper.

Nickel is another material from which heat transfer apparatus can be fabricated. While the melting point of nickel is considerably higher than that of copper (1717 K, or 2630°F, vs 1358 K, or 1981°F), the strength of nickel drops rapidly at temperatures above about 616 K (650°F), and at 1200 K (1700°F) the tensile strength is only 10% of the strength at room temperature. Nickel has a magnetic transformation point at about 880 K (1125°F), and in this region the thermal properties are perturbed.

The thermal properties of copper, mild steel, and nickel as collected from the literature are given in Table B-1. The data in this table show that the variation in thermal properties is much less for copper than for mild steel or nickel.

A comparison of the transient heat flux capabilities of copper, mild steel, and nickel is given in Table B-2. To achieve a common basis for the comparison, it is assumed that the heated surface of each material reaches its maximum allowable working temperature in 8 s, a time which should be large compared to any initial buildup period of the hot gas temperature and heat transfer coefficient in an experimental apparatus, and a time which is well within the response capability of ordinary data-recording equipment. It is further assumed that the 8-s time corresponds to $Fo = 1.00$, thus assuring that the data are obtained into a region where the methods of analysis described here are applicable. The comparison is made for a flat plate having an initial temperature of $T_0 = 256$ K (0°F), and the effect of a wide range of hot-gas temperatures is considered. The first step in the comparison is to determine the characteristic plate thickness for each material. The definition of the Fourier Number can be rearranged to give the plate thickness as

$$L = \left[\frac{\alpha t}{Fo}\right]^{1/2}$$

The temperature ratio at the heated surface of the plate at $Fo = 1.00$ is evaluated as

$$\left(\frac{T_{w\,(\max)} - T_0}{T_g - T_0}\right)$$

using the allowable maximum temperature for the material and the assumed gas temperature, and the Biot

Table B-1. Thermal properties of useful metals

Material	T		ρ		c_p		k		$\alpha = \frac{k}{\rho c_p}$	
	K	°F	g/cm³	lbm/in.³	joule/g K	Btu/lbm °F	W/cm² K	Btu/in. s °F	cm²/s	in.²/s
Mild steel (1020 alloy)	478	400	7.86	0.284	0.529	0.126	0.192	6.54×10^{-4}	0.118	.01826
	589	600	↓	↓	0.575	0.137	0.179	6.08×10^{-4}	0.101	.01562
	700	800			0.630	0.150	0.164	5.59×10^{-4}	0.0847	.01312
	811	1000			0.714	0.170	0.149	5.08×10^{-4}	0.0679	.01052
	922	1200			0.823	0.196	0.132	4.50×10^{-4}	0.0523	.0081
Copper (OFHC)	389	240	8.93	0.3228	0.397	.0945	1.48	.005042	1.068	.1653
	500	440	8.88	.3212	0.408	.0971	1.46	.004975	1.029	.1595
	611	640	8.83	.3193	0.419	.0998	1.45	.004925	0.997	.1545
	722	840	8.77	.3170	0.430	.1024	1.44	.004883	0.970	.1504
	834	1040	8.70	.3145	0.441	.1050	1.43	.004858	0.949	.1471
	945	1240	8.62	.3117	0.452	.1077	1.42	.004842	0.931	.1443
	1057	1440	8.55	.3089	0.464	.1103	1.42	.004817	0.913	.1415
	1168	1640	8.48	.3061	0.474	.1129	1.41	.004808	0.895	.1389
	1279	1840	8.39	.3033	0.485	.1157	1.41	.004796	0.880	.1365
Nickel	111	−260	8.88	0.321	0.252	.0600	0.453	.001551	0.520	0.0807
	139	−210	↓	↓	0.311	.0740	0.409	.001390	0.378	0.0586
	208	−85			0.395	.0940	0.320	.001088	0.233	0.0361
	278	+40			0.433	0.1030	0.269	.000915	0.179	0.0277
	417	290			0.494	0.1175	0.219	7.46×10^{-4}	0.127	0.01975
	556	540			0.571	0.136	0.188	6.41	0.095	.01469
	625	665			0.609	0.145	0.179	6.10	0.085	.01310
	695	790			0.534	0.127	0.185	6.30	0.100	.01548
	834	1040			0.525	0.1250	0.202	6.86	0.110	.01710
	972	1290			0.546	0.1300	0.218	7.41	0.115	.01776
	1111	1540			0.566	0.1350	0.231	7.87	0.117	.01820
	1250	1790			0.596	0.1420	0.247	8.41	0.119	.01846
	1390	2040			0.650	0.1500	0.264	8.96	0.122	0.01882
	1528	2290			0.664	0.1580	0.278	9.45	0.115	.01865
	1668	2540			0.697	0.1660	0.293	9.96	0.121	.01870
	2222	3540	↓	↓	0.840	0.200	0.357	12.15	0.122	.01894

Number corresponding to this temperature ratio at $Fo = 1.00$ is determined by interpolation on Fig. 9. From the Biot Number and from the thickness and thermal conductivity of the plate, the gas heat transfer coefficient is determined, and then the surface heat transfer rate is calculated.

The comparison shows that the limiting heat transfer rate for copper (approximately 490 W/cm², or 3.0 Btu/in.² s) is twice that which can be absorbed by mild steel or nickel without overheating the inner surface of the material.

For all three metals the maximum surface temperature is limited to 811 to 922 K (1000 to 1200°F), either by structural weakening or by a discontinuity in thermal properties which invalidates one of the assumptions of the analysis.

Since copper can be used to nearly as high a wall temperature as the other metals, has a high heat flux capability, and has much less variation of thermal properties, it is clear that copper is the preferred metal for fabrication of transient heat transfer measurement experimental apparatus.

Table B-2. Comparison of transient heat flux apparatus materials[a]

Material	L		T_g		$\frac{(T_w - T_0)}{(T_g - T_0)}$	Bi	h		$(T_g - T_w)$		q	
	cm	in.	K	°F			W/cm² K	Btu/in.² s °F	K	°F	W/cm²	Btu/in.² s
Mild steel (1020 alloy)	.820	0.323	1368	2000	.60	.86	.439	.001492	445	800	195	1.195
T_w (max) = 922 K (1200°F)			3035	5000	.24	.22	.113	.000382	211	3800	237	1.45
k = 0.165 W/cm² K (0.00056 Btu/in. s °F)												
α = 0.0838 cm²/s (0.013 in.²/s)												
Copper	2.83	1.1135	1368	2000	.50	.61	.790	.002685	556	1000	437	2.68
T_w (max) = 811 K (1000°F)			1923	3000	.33	.33	.427	.001452	1112	2000	475	2.91
k = 1.44 W/cm² K (0.0049 Btu/in. s °F)			2480	4000	.25	.23	.298	.001012	1667	3000	496	3.04
α = 1.00 cm²/s (0.155 in.²/s)			3035	5000	.20	.18	.233	.000792	2224	4000	516	3.16
Nickel	.940	0.370	1368	2000	.60	.86	.505	.001720	445	800	225	1.377
T_w (max) = 922 K (1200°F)			3035	5000	.24	.22	.129	.000440	211	3800	273	1.672
k = 0.218 W/cm² K (0.00074 Btu/in. s °F)												
α = 0.110 cm²/s (0.0171 in.²/s)												

[a]Comparison made on the basis of taking 8 s to attain $Fo = 1.00$ and $T_w = T_{max}$ for the material, assuming $T_0 = 0$°F (flat plate).

Equations used: $L = \left[\frac{\alpha t}{Fo}\right]^{1/2}$ $\quad h = \frac{Bi\,k}{L}$ $\quad q = h\,(T_g - T_w)$

Appendix C

Sample Problem

The analysis and procedures described in this report are applied here to a set of data obtained at the Jet Propulsion Laboratory during a series of tests conducted to determine both performance and heat transfer for a given rocket propellant, in this case Flox (88% F_2, 12% O_2–monomethylhydrazine, in a rocket motor designed to produce about 267 N (600 lbf) thrust.

The thrust chamber and nozzle configuration are shown in Fig. C-1, which also shows the location of the thermocouples. The thrust chamber is made of OFHC copper, with a wall thickness of approximately 2.54 cm (1 in.) (as shown to be optimum in Table B-2). Figure C-2 and Table C-1 show the actual dimensions associated with the thermocouple plug installation. Note that the thermocouple junction location is assumed to be 0.00889 cm (0.0035 in.) above the bottom of the hole. In the conical nozzle section, the equivalent cylindrical-plate radius of curvature is taken as the distance to the axis normal to the surface of the nozzle (shown as R_i in Fig. C-2 and Table C-1).

Data obtained during one firing of the rocket engine are plotted on Figs. C-3 and C-4. Figure C-3 shows the combustion chamber pressure as a function of time; it can be seen that the rise in pressure at the start of the test is quite rapid, which can be taken as an indication that the analytical requirement for sudden application of hot gas and convective heat flux is adequately satisfied. On the time scale on which the data were taken, the effective starting time for fully developed convective heat transfer appears to be approximately $t_0 = 0.55$ s. Figure C-4 shows the temperature response vs time of a thermocouple plug located at the throat plane (Station ③ on Fig. C-2); the initial temperature is seen to be $T_0 = 302°K$ (84°F), and the midwall temperature at the end of the test is 545°K (520°F).

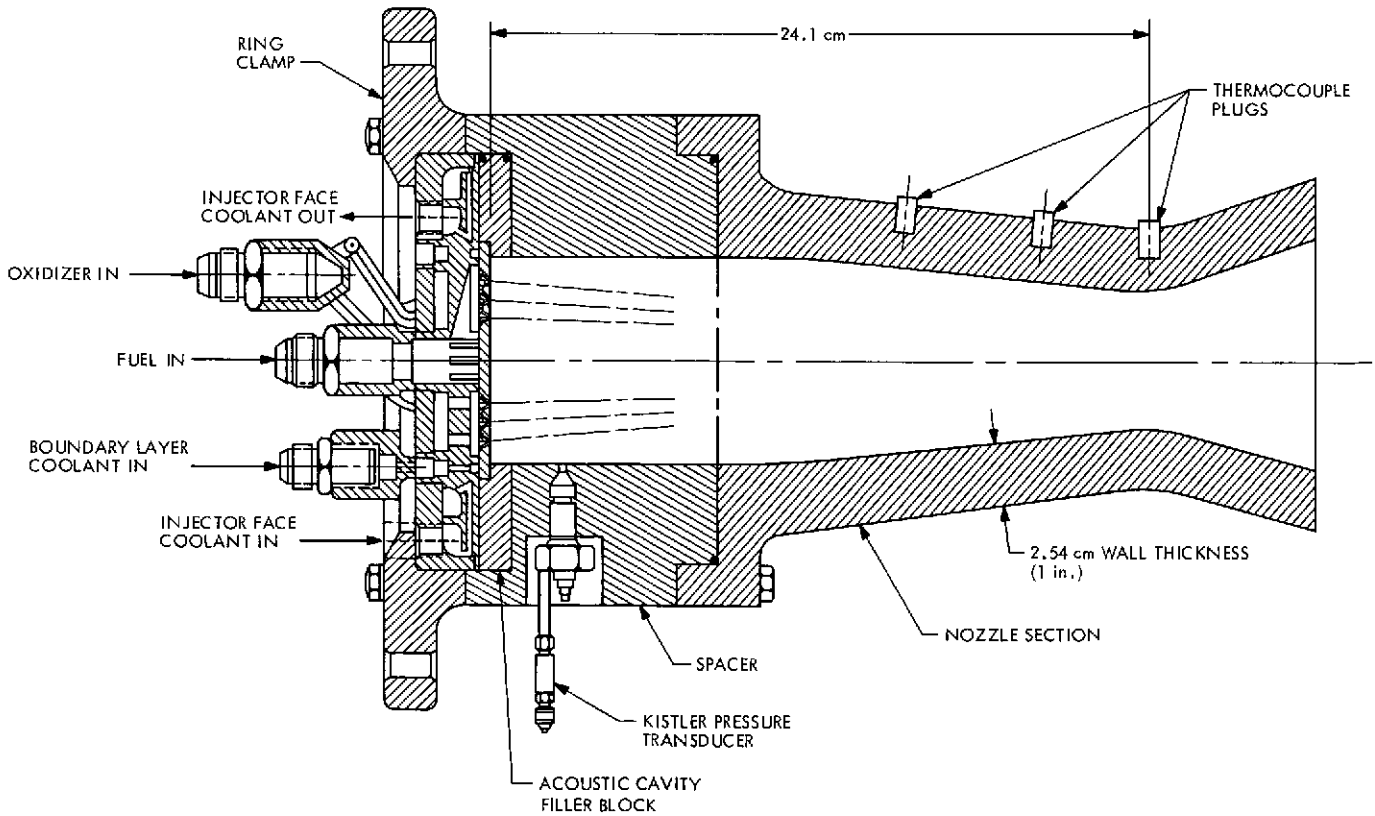

Fig. C-1. Thrust chamber configuration

Table C-1. Thermocouple plug installation dimensions (see Fig. C-2)

Station	L		R_i		h		x		L/R_i	x/L
	cm	in.	cm	in.	cm	in.	cm	in.		
1	2.73	1.078	3.43	1.350	1.53	0.603	1.525	0.600	.798	.557
2	2.81	1.108	2.97	1.170	1.57	0.619	1.565	0.616	.946	.557
3	2.77	1.091	2.54	1.00	1.57	0.619	1.565	0.616	1.091	.565

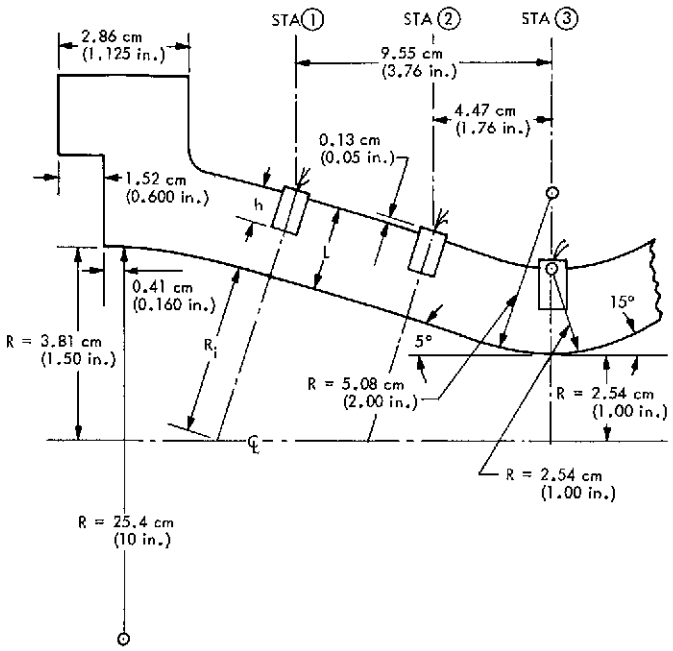

Fig. C-2. Thermocouple plug installation in nozzle

Following the steps outlined in Procedure II, the time-space mean wall temperature is estimated as 444°K (340°F). The thermal properties of copper at this temperature are given in Table C-2.

The time on the test-time scale corresponding to a given Fourier Number for convective heat transfer can be determined from the relationship

$$(t - t_0) = \frac{L^2}{\alpha} Fo$$

The value of L given for the throat-plane thermocouple plug in Table C-1, and the value of thermal diffusivity α given in Table C-2, are used to calculate the test time corresponding to $Fo = 0.60$, 0.80, and 1.00, as shown in lines 1 and 2 of Table C-3. The thermocouple plug temperature response record, Fig. C-4, is then used to determine the corresponding temperature rise and the rate of

Table C-2. Mean thermal properties of copper used in sample problem data analysis (T = 340°F)

Property	Value
ρ	8.91 g/cm³ (0.3220 lbm/in.³)
c_p	0.416 joule/g K (0.0958 Btu/lbm °F)
k	1.472 W/cm² K (0.00501 Btu/in. s °F)
$\alpha = \frac{k}{\rho c_p}$	1.408 cm²/s (0.1624 in.² s)

temperature rise at the test times corresponding to the selected Fourier Numbers. These quantities are also entered in Table C-3. This completes the collection and placing into usable form of the experimental data. The remainder of Table C-3 illustrates how these experimental data are used, in conjunction with the prepared analytically based charts, to determine the effective hot gas temperature and heat transfer coefficient.

The heat flux is calculated using the heat flux ratio from Fig. 30, as shown in Step 3 of Procedure II and in lines 6 and 7 of Table C-3. The heat flux determined in this manner is essentially independent of Fo and Bi and depends mostly on the measurement of the rate of temperature rise at the $x/L = 0.55$ position within the wall.

The next step in the analysis of the test data is to calculate the quantity

$$\left[\frac{2\alpha}{L^2}\frac{(T_x - T_0)}{\left(\frac{dT_x}{dt}\right)}\right]_{\text{test}}$$

at each Fourier Number, and to compare this value with the analytically calculated value at the same value of Fo, so that the matching value of Bi can be determined. This is done for the data at each of the three values of Fo in lines 8 and 9 of Table C-3.

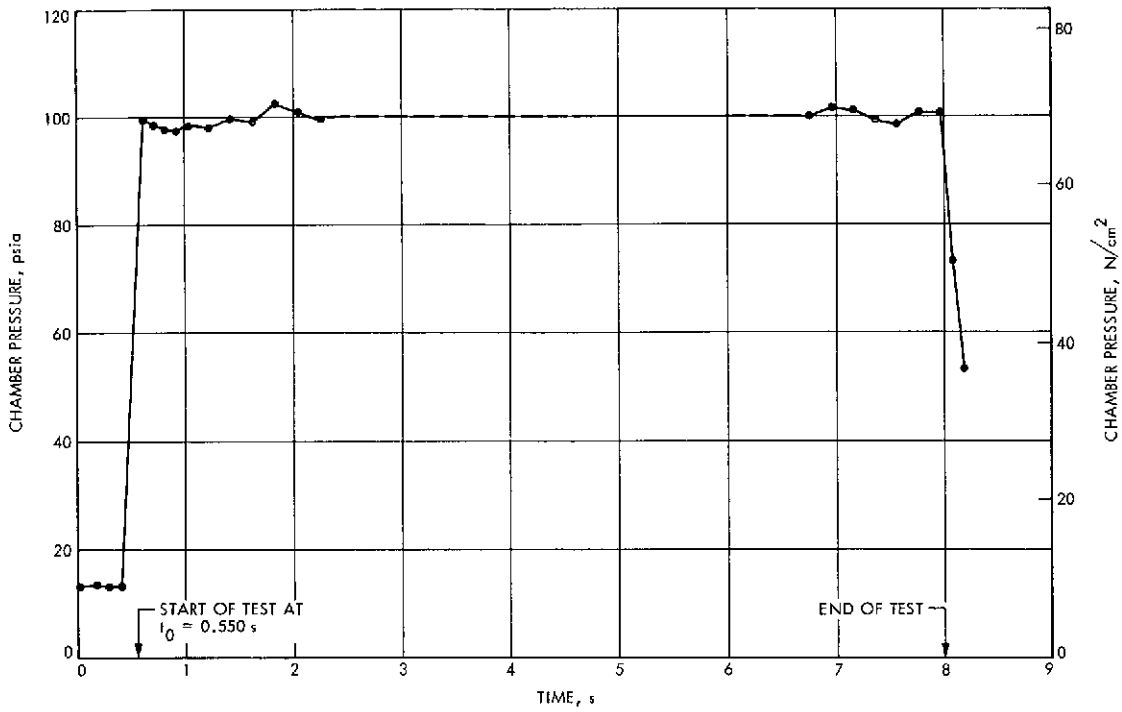

Fig. C-3. Combustion chamber pressure, rocket engine test

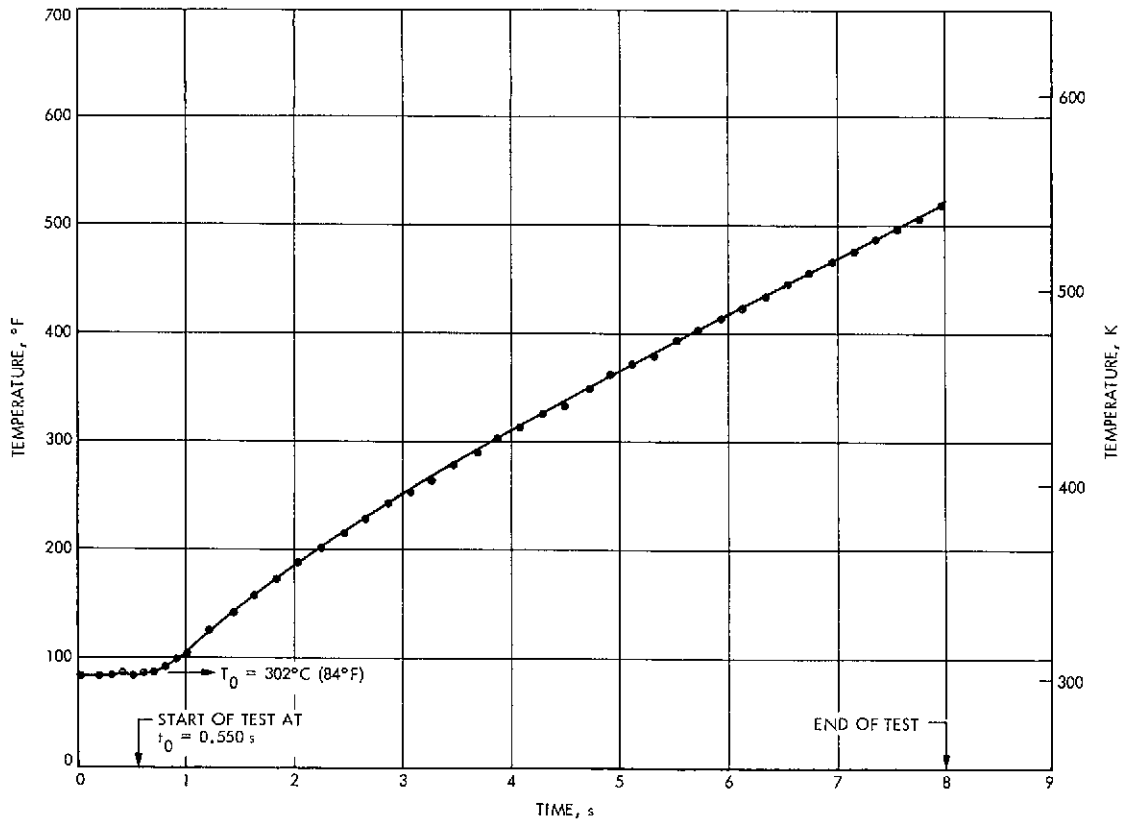

Fig. C-4. Temperature response of thermocouple plug located at nozzle throat plane

Table C-3. Calculation of heat flux, hot-gas temperature and gas heat transfer coefficient from thermocouple plug test data at selected Fourier Numbers[a]

Line No.	Parameter	$Fo = 0.60$	$Fo = 0.80$	$Fo = 1.00$
1	$(t_{test} - t_0) = \frac{L^2}{\alpha} Fo$, s	4.405	5.870	7.340
2	t_{test}, s	4.955	6.420	7.890
3	$T_{(x/L)=0.565,\,test}$, K (°F)	456 (361.5)	499 (438.5)	541 (514.0)
4	$(T_x - T_0)_{test}$, K (°F)	410 (277.5)	452 (354.5)	495 (430.0)
5	$\left(\frac{dT_x}{dt}\right)_{test}$, K/s (°F/s)	29.7 (53.40)	28.7 (51.62)	28.3 (50.95)
6	$\left[\frac{q}{\rho c_p L\left(\frac{dT_x}{dt}\right)}\right]_{chart}$ (from Fig. 30)	1.55	1.55	1.55
7	$q = \left[\rho c_p L\left(\frac{dT_x}{dt}\right)\right]_{\substack{test \\ (x/L)=0.565}} \times \left[\frac{q}{\rho c_p L\left(\frac{dT}{dt}\right)}\right]_{\substack{chart \\ (x/L)=0.55}}$, W/cm² $\left(\frac{Btu}{in.^2\ s}\right)$	470 (2.88)	439 (2.69)	435 (2.66)
8	$\left[\frac{2\alpha}{L^2}\frac{(T_x - T_0)}{\left(\frac{dT_x}{dt}\right)}\right]_{test}$	1.417	1.870	2.30
9	Bi (from figure number noted)	0.80 (41)	0.60 (42)	0.43 (43)
10	$h = \frac{k}{L} Bi$, W/cm² K $\left(\frac{Btu}{in.\ s\ °F}\right)$	1.080 (0.00367)	0.814 (0.00277)	0.580 (0.001975)
11	$\left[\frac{(T_x - T_0)}{(T_g - T_0)}\right]_{(x/L)=0.55}$ (from figure number noted)	.220 (31)	.230 (32)	.220 (33)
12	$\left[\frac{(T_x - T_0)}{(T_g - T_0)}\right]_{(x/L)=1.00}$ (from figure number noted)	.379 (36)	.354 (37)	.304 (38)
13	$(T_g - T_0)$, K (°F)	956 (1260)	1111 (1540)	1340 (1955)
14	T_g, K (°F)	1002 (1344)	1160 (1624)	1389 (2039)
15	$(T_w - T_0)$, K (°F)	521 (477.5)	558 (545.0)	586 (595.0)
16	T_w, K (°F)	569 (562)	605 (629)	632 (679)
17	$(T_g - T_w)$, K (°F)	691 (783)	809 (995)	1011 (1360)
18	$q = h\,(T_g - T_w)$, W/cm² $\left(\frac{Btu}{in.^2\ s}\right)$	469 (2.87)	451 (2.76)	438 (2.68)

[a]Given data for Table C-3 calculations:

$L = 2.77$ cm (1.091 in.)

$L/R_i = 1.091$

$x/L = 0.565$

$t_0 = 0.55$ s

$T_0 = 302$ K (84°F)

The gas heat transfer coefficient is now calculated from the Biot Number, using the equation

$$h = \frac{k}{L} Bi$$

The values of gas heat transfer coefficient are shown on line 10 of Table C-3.

The next step is to use the prepared charts to look up the temperature ratio at $x/L = 0.55$ and at $x/L = 1.00$ (the hot wall) for each value of Fo and its corresponding value of Bi; these quantities are shown on lines 11 and 12 of Table C-3.

Now the actual calculation of the gas temperature and the hot-wall temperature can proceed. The gas temperature is calculated by dividing the measured temperature rise at the thermocouple plug thermocouple junction by the temperature ratio for the $x/L = 0.55$ position as determined from the chart. Thus

$$(T_g - T_0) = \frac{(T_x - T_0)_{\text{test, } (x/L)=0.55}}{\left[\dfrac{(T_x - T_0)}{(T_g - T_0)}\right]_{\text{chart, } (x/L)=0.55}}$$

and

$$T_g = [(T_g - T_0) + T_0]$$

Similarly, the hot-wall temperature is calculated by multiplying the measured temperature rise by the ratio of the temperature ratios at the hot-wall and the midwall positions. Thus

$$(T_w - T_0) = (T_x - T_0)_{\substack{\text{test} \\ (x/L)=0.55}} \left\{ \frac{\left[\dfrac{(T_x - T_0)}{(T_g - T_0)}\right]_{(x/L)=1.00}}{\left[\dfrac{(T_x - T_0)}{(T_g - T_0)}\right]_{(x/L)=0.55}} \right\}_{\text{chart}}$$

and

$$T_w = [(T_w - T_0) + T_0]$$

From these results, the driving temperature difference for heat transfer, $(T_g - T_w)$, can be determined. The temperature calculations for the sample case are given in lines 13 through 17 of Table C-3.

The surface heat flux corresponding to the heat transfer coefficient and to the gas and wall temperatures determined above is calculated from the basic equation

$$q = h(T_g - T_w)$$

which can be written in terms of the measured and charted quantities as

$$q = \frac{k}{L}(T_x - T_0)_{\substack{\text{test} \\ (x/L)=0.55}} \left\{ Bi \left[\frac{1 - \left[\dfrac{(T_x - T_0)}{(T_g - T_0)}\right]_{(x/L)=1.00}}{\left[\dfrac{(T_x - T_0)}{(T_g - T_0)}\right]_{(x/L)=0.55}} \right]_{\text{chart}} \right\}$$

This heat flux is given on line 18 of Table C-3, and the values are seen to be acceptably close to the primary values of the heat flux given on line 7 of this table.

The results of this sample problem data analysis can be reviewed to evaluate the validity of the procedures: It is believed that the rocket motor operation was such as to establish steady state combustion almost instantaneously at the start of the test, with constant gas temperature and a heat transfer coefficient which decreases gradually as the wall temperature increases (see below). The properties of OFHC copper are relatively constant over the range of plate temperature covered by the test. Thus the assumptions basic to the analysis are fairly well satisfied.

The heat flux calculations agree, as they should, and seem to be of the right magnitude for the propellant and motor configuration being tested. There is no reason to consider the heat flux data to be in error by more than the percentage error in the measurement of the rate of temperature rise and in the evaluation of the average physical properties of the material.

At increasing values of the test time and Fourier Number, the apparent Biot Number decreases rather than remaining constant. While this may be partly due to the real effect of the hot-gas heat transfer coefficient decreasing slightly as the wall temperature increases, due to changes in gas density and viscosity with change in the average film temperature, it is more likely associated with high uncertainty ratios for determination of Bi in the range of Fo and Bi corresponding to the test conditions: in the range of $Fo = 1.0$ and $Bi = 0.50$, the

percentage uncertainty in Bi as determined by the methodology described here is approximately five times the sum of the percentage uncertainties in the Fourier Number and in the ratio of temperature rise to rate of temperature rise. Since the Bi uncertainty ratios decrease with increasing Fo, and since the accuracy of the evaluation of both Fo and of the ratio of temperature rise to rate of temperature rise should be expected to increase with increase in Fo, it is to be expected that the final Biot Number on line 7 of Table C-3 is a better value than the preceding values, although this final value may have an uncertainty of as much as $\pm 50\%$.

The apparent Biot Number variation during the test, and its uncertainty, are transmitted directly to the gas heat transfer coefficient, and, through the intermediate temperature ratio charts, this effect is felt in the determination of the gas temperature and the hot wall temperature.

The apparent gas temperature is seen to increase during the test, though even the final calculated value of 1388 K (2039°F) is lower than the steady combustion temperature which could be expected from the propellant used for the test.

The conclusion to be drawn from the analysis of the test data as given in Table C-3 is that the heat flux is probably determined with good accuracy, but that there is considerable uncertainty in the gas heat transfer coefficient and the hot-gas temperature. The fact that the gas temperature seems to be approaching a reasonable anticipated value as the test duration increases indicates that an increased test duration would have been desirable, within the limit imposed by the maximum allowable increase in inner wall temperature. This is consistent with the analytical study, which showed that Biot Number determination accuracy at $Fo = 2$ is much improved over a similar determination at $Fo = 1$.

NASA — JPL — Coml., L.A., Calif.